3D Motion Compensation for an Offshore crane

Assessing the feasibility for wind turbine maintenance

J.R. Buijs

Delft University of Technology

TU Delft

3D Motion Compensation for an Offshore crane

Assessing the feasibility for wind turbine maintenance

by

J.R. Buijs

in partial fulfillment of the requirements for the degree of

Master of Science
in Offshore and Dredging Engineering

at the Delft University of Technology,
to be defended publicly on Monday November 20, 2017 at 2:30 PM.

Student number:	4106326	
Project duration:	January, 2017 – November, 2017	
Thesis committee:	Prof. dr. ir. A. P. Van 't Veer,	TU Delft, Chairman
	Dr. ir. P. R. Wellens,	TU Delft, Supervisor
	Dr. ir. M. J. B. M. Pourquie	TU Delft
	Dr. ir. J. F. J. Pruijn	TU Delft
	Dr. ir. A. Nuttall,	Huisman Equipment B.V., Supervisor

This thesis is confidential and cannot be made public until November 20, 2019.

TU Delft

Acknowledgements

This thesis has been submitted in partial fulfillment of the requirements for the degree MSc. at Delft University of Technology. For 10 months, I have had the occasion to work on this very interesting and innovative subject. The past period was intense but also satisfactory, which motivated me through the project.

At first I would like to thank my thesis committee from Delft University of Technology, under supervision of Professor Riaan van 't Veer. Not only did you form an essential part of my graduation procedure, but I also enjoyed our discussions throughout the project. Special thanks to Peter Wellens, whom I became to know not only as an intelligent engineer, but also as a warm personality and meanwhile, friend. Our meetings were diverse and efficient, and you have motivated me throughout this project for which I am thankful.

Thanks to Huisman Equipment, for giving me the opportunity to work on a diverse and innovative topic within the offshore industry. The view during my walk from the office to the car was a daily surprise with heavy equipment and astounding technology. Thank you, Eric Romeijn, for your feedback and endless knowledge on cranes. Thanks to the R&D department for their support. Thank you Ashley Nuttall for being my daily supervisor. I have come to know Ashley as a unique problem solver with a very wide knowledge on technology. Combined with an open personality, you have supported me very well during this thesis project.

Finally I would like to thank my family, friends and Anne for their support during the past 10 months. Very soon, I will make up for the time lost while working on my thesis.

J.R. Buijs
Delft, November 2017

Abstract

Within the offshore industry, cranes form a key element for many operations. When working offshore on a floating vessel, the vessel will be subjected to wave induced motions and with a moving crane tip, a suspended load can start to swing. When the motions of the load become too large, the operation is interrupted. This means that offshore lifting operations can only be performed in mild weather conditions, limiting the operational window of the vessel. Alternatives such as jack-ups, function as a fixed platform to which the crane is attached, therefore eliminating the effect of waves on the workability of the vessel. Within the offshore wind energy industry, jack-ups are used for installation and maintenance of wind turbines. They offer large deck space and increased workability with respect to regular heavy lifting crane vessels. While the number of installed turbines is increasing, so is the need for servicing and maintenance. Nowadays, wind turbine maintenance is performed with jack-ups. However, due to their slow transit speed and time-consuming jacking process, an alternative is suggested with which maintenance can be performed. With this alternative, maintenance can be performed from a floating vessel resulting in reduced downtime and operational costs. For this, a motion compensated crane which can compensate for the motions of the vessel is required. Within this study, the mechanical feasibility of a motion compensated crane for wind turbine maintenance is assessed. The analysis is split into five different modules by which three different crane concepts are evaluated. The crane concepts used within this study are a Pedestal Mounted Offshore Crane, a Hybrid Boom Crane and a new concept which is currently under development.

To determine the compensating motions that are required to keep the crane tip in position, a Frequency Domain analysis is used. Vessel RAOs are directly coupled to the crane motions, using transformation matrices under the assumption of small displacements. For an operational period of 30 minutes, maximum expected responses of the crane motions are determined. From the lay-out of the cranes drive system, the current motion compensating performance is estimated with the use of workability graphs. For the PMOC it can be concluded that the luffing motion is the limiting factor for all design cases which limits its workability to H_{sig} = 0.8m. By increasing the capacity of the drive system, only minor improvements could be realized as a result of the increased inertia of the drivetrain which has a large impact on the workability performance. Even though the HBC performs slightly better than the PMOC, the performance of the new concept is much better than both other cranes.
The influence of crane stiffness on the motion compensating performance was investigated by separating deflections resulting from gravitational loads and dynamic effects. It was found that the deflections of the crane tip by gravitational loads have to be incorporated in the motion compensation control. Also, the natural frequencies of a crane design that follows from the conventional design method, are found to coincide with frequencies at which energy is present in the response spectrum of the compensating motions. By using a dynamic amplification factor, the required stiffness of the structure can be determined from the response spectrum. Therefore, the design philosophy should focus on stiffness as well as strength.

From the results that are obtained within this study it can be concluded that both the Pedestal Mounted Offshore Crane and the Hybrid Boom Crane are not feasible for 3D motion compensation of the crane tips motions when the operation of wind turbine maintenance is concerned. The main explanatory reason is the additional capacity of the drive system that is required to obtain a workability of $H_{sig} = 3m$. The new concept is found capable of compensating for $H_{sig} = 3m$ without excessive power usage. For all crane concepts, the stiffness of the design is not sufficient to prevent the crane from large dynamic amplifications by resonance. Therefore, the stiffness of a wind turbine maintenance crane is to be increased to obtain a feasible design.

Contents

List of abbreviations

PMOC	Pedestal Mounted Offshore Crane
HBC	Hybrid Boom Crane
MCCC	Motion Compensated Crane Concept
WITC	Wind Turbine Installation Crane
LCOE	Levelized Cost of Energy
OWF	Offshore Wind Farm
ALS	Accidental Limit State
OECD	Organisation for Economic Co-operation and Development
EWEA	European Wind Energy Association
DOF	Degree of Freedom
SWL	Safe Working Load
DC	Design Case
WMS	Wave Monitoring System
HPU	Hydraulic Power Unit
AHC	Active Heave Compensation
PHC	Passive Heave Compensation
HLCV	Heavy Lifting Crane Vessel
DP	Dynamic Positioning
PID	Proportional Integral Derivative
MRU	Motion Reference Unit
IMU	Inertial Measurement Unit
RAO	Response Amplitude Operator
FD	Frequency Domain
TD	Time Domain
FEM	Finite Element method
MWh	Megawatt hour
TWh	Terrawatt hour
FMEA	Failure Mode and Effect Analysis
CTV	Crew Transfer Vessel
RPN	Risk Priority Number
AOPS	Automatic Overload Protection System
MOPS	Manual Overload Protection System

Nomenclature

α	Slewing angle	rad
β	Boom angle	rad
γ	Knuckle angle	rad
L_{boom}	Length of the boom	m
$L_{knuckle}$	Length of the knuckle	m
$L_{CoG,b}$	Distance from the pivot to the CoG of the boom	m
$L_{CoG,k}$	Distance from the pivot to the CoG of the knuckle	m
L_{buck}	Buckling length	m
r_{boom}	Moment arm of the CoG around the slewing axis	$[m]$
r	Moment arm of the boomhoist force around the pivot	m
$\eta_{falls,b}$	Number of falls of the boomhoist	-
$\eta_{falls,k}$	Number of falls of the knucklehoist	-
$center_{pivot}$	Distance between the slewing axis and the pivot of the boom	m
ω	Frequency	$[rad/s$
$\dot{\omega}$	Rotational speed	rad/s
$\ddot{\omega}$	Rotational acceleration	rad/s^2
K_p	Proportional term of the control parameters	-
K_d	Derivative term of the control parameters	-
$I_{boom,s}$	Moment of inertia of the boom around the slewing axis	$kg \cdot m^2$
$I_{m,s}$	Slewing moment of inertia of the boom at the the motor shaft	$kg \cdot m^2$
$I_{m,b}$	Luffing moment of inertia of the boom at the the motor shaft	$kg \cdot m^2$
$I_{cranehouse}$	Moment of inertia of the cranehouse around the slewing axis	$kg \cdot m^2$
I_{motor}	Inertia of the E-motor	$kg \cdot m^2$
$I_{drivetrain}$	Inertia of the drivetrain including the brakes, gearbox, drum and E-motor	$kg \cdot m^2$
I_{slew}	Total slewing inertia at the motor shaft	$kg \cdot m^2$
$I_{CoG,s}$	Inertia of the boom around its CoG for the slewing motion	$kg \cdot m^2$
$I_{CoG,l}$	Inertia of the boom around its CoG for the luffing motion	$kg \cdot m^2$
ω_s	Rotational speed of the slewing motion	$[rad/s]$
$\omega_{m,s}$	Rotational speed of the slewing motor	$[rad/s]$
i_p	Transmission ratio of the gearing-pinion system of the slewing motion	-
i_g	Transmission of the gearbox of the slewing E-motor	-
$i_{g,l}$	Transmission of the gearbox of the luffing E-motor	-
$i_{total,s}$	Total transmission of the slewing motion	-
T_s	Slewing torque by the inertia of the boom around the slew axis	$[Nm]$
$T_{m,s}$	Slewing torque by the inertia of the boom at the motor shaft	$[Nm]$
$T_{m,l}$	Luffing torque by the inertia of the boom at the motor shaft	$[Nm]$

F_{bh}	Total force in the boomhoist assembly	$[Nm]$
F_{wire}	Force in one of the boomhoist wires	$[Nm$
M_b	Mass of the boom	$[kg]$
M_k	Mass of the knuckle	$[kg]$
M_{load}	Mass of the load	$[kg]$
$D_{drum,b}$	Drum diameter for the boomhoist	$[m]$
$D_{drum,k}$	Drum diameter for the knucklehoist	$[m]$
C_b	Factor between inertia of boom around pivot and E-motor	-
C_k	Factor between inertia of knuckle around tip of main-boom and E-motor	-
η_p	Efficiency of the gearing pinion system for the slewing motion	-
η_s	Efficiency of the sheaves for the luffing motion (per sheave)	-
η_d	Efficiency of the drivetrain including the gearbox and E-motor	-
$\eta_{slew,b}$	Efficiency of the slew bearing by static friction	-
$\eta_{t,slew}$	Total efficiency of the slewing motion	-
$\eta_{t,luff}$	Total efficiency of the luffing motion	-
$\eta_{t,knuckle}$	Total efficiency of the knuckle motion	-
H_{sig}	Significant wave height	m
H_{m0}	Significant wave height by spectral moment	m
H_{max}	Maximum expected wave height	m
m_0	Zero-th order spectral moment	m^2
m_2	Second order spectral moment	m^2
ζ	Water surface elevation	m
ζ_{an}	Amplitudes of regular wave components for the surface elevation	m
T_p	Peak period of the wave spectrum	s
T_2	Mean zero-crossing wave period	s
U_{10}	Time averaged wind speed at a height of 10 meters	$[m/s]$
S_ζ	Wave spectrum	-
f_{max}	Maximum factor for significant and maximum response	-
P_e	Probability of exceedance	%
A_t	Time signal of the target acceleration	$[m/s_2]$
V_t	Time signal of the target velocity	$[m/s]$
X_t	Time signal of the target position	$[m]$
A_{actual}	Time signal of the actual acceleration	$[m/s_2]$
V_a	Time signal of the actual velocity	$[m/s]$
X_a	Time signal of the actual position	$[m]$
F_{side}	Force by sidelead	$[Nm]$
E	E-modulus	$[Pa]$
δ_{tip}	Deflection of the tip	$[m]$
I_{xx}	Moment of inertia around the x-axis	$[m^4]$
I_{yy}	Moment of inertia around the y-axis	$[m^4]$
$F_{buck,max}$	Maximum buckling force	$[Nm]$
K_{wire}	Stiffness of wire rope	$[N/m]$
$K_{assembly}$	Stiffness of a wire assembly	$[N/m]$
ρ_{beam}	Density of the beam used for the equivalent boom model	$[kg/m^3]$
ω_n	Natural frequency	$[Hz]$

List of Figures

List of Tables

1 Introduction

1.1. Background

Within the offshore industry, cranes form a key element for many operations. Installation of structures, transfer of equipment and maintenance of structures are some of the activities in which an offshore crane is needed. Many cranes that are used on vessels are operated in very calm wave conditions or used for harbour lifts. However, when working offshore on a floating vessel, waves present at sea will induce vessel motions and with a crane rigidly connected to the vessel, the crane tip will be subjected to motions. With a moving crane tip, the suspended load will move and can start swinging, causing interruptions during operation and consequently limiting the vessel's workability at sea. Alternatives, such as jack-ups, function as a fixed platform to which the crane is attached and eliminate the influence of waves on the operation.
Motion compensation is an existing technology within the offshore industry and is used on a large scale for transfer of people between a moving vessel and a fixed structure[16]. Within the industry, some initiatives of 3D motion compensation for cranes are starting to gain attention. At this moment, solutions already exist that allow a small sized offshore crane to be placed on a motion compensated base to achieve a compensated crane tip. Multiple operations such as small cargo transfer from a vessel to a fixed platform, or wind turbine, can be performed in heavier sea conditions compared to a system without motion compensation. However, offshore equipment specialist Huisman is aiming for a new application of motion compensation for offshore cranes which is related to maintenance activities in the offshore wind industry. First, the development of the offshore wind industry is elaborated on after which the application of motion compensation for wind turbine maintenance is explained.

Figure 1.1: Jumbo Fairplayer - Heavy lift crane vessel.

1.1.1. Wind energy industry

The offshore wind energy industry is developing. Therefore, an increase is expected in the demand of wind turbine installation services and also, wind turbine maintenance. In the past couple of years, the total installed capacity of offshore wind power has grown steadily [27]. Technology is developing fast and innovative solutions are required to keep up with competition. Governmental financial support is still required to come to a profitable solution for exploiting companies but the Levalized Cost Of Electricity (LCOE) for wind power is decreasing fast, making it a stronger alternative in the current energy market. Whilst the world is re-evaluating its strategy with respect to the energy mix of the future, offshore wind is hot, especially in Europe. At the same time, the offshore oil and gas activities are slowing down and companies such as Huisman Equipment are looking for options to widen their product portfolio and services.
In 2016, EUR/MWh prices of Offshore Wind Farms (OWF) drastically decreased, which started with the tender of Borssele 1&2 in The Netherlands. A price of EUR 72/MWh was offered by DONG Energy, who won the tendering phase of this project. In september 2016, a new record of EUR 64/MWh followed by Vattenfall for a 350 MW nearshore wind farm in Denmark. In november, the winning bid for the Danish Krieger's Flak project was EUR 49.90/MWh and in December the Borssele 3 & 4 tender in the Netherlands was won by a consortium of Shell, van Oord, Eneco and Mitsubishi at a price of EUR 54.5/MWh. Fast decreasing prices for offshore wind in both OECD- and emerging markets, will be the primary drivers for development of wind power in the short to medium term [27].
Global demand for wind power increased and in 2016 the combined on- and offshore wind power marked 12.6% growth in cumulative capacity reaching a total market capacity of almost 500 GW at the end of 2016. The total global installed wind capacity is shown in the left part of figure 1.2 for the period between 2001 and 2016. When only offshore wind is concerned, the same increasing trend is observed. In 2015 the annual onshore wind market in the EU decreased by 7.8 % while the total installed offshore power more than doubled compared to 2014 [24]. The right side of figure 1.2 displays the development of installed capacity of offshore wind between 2011 and 2016.

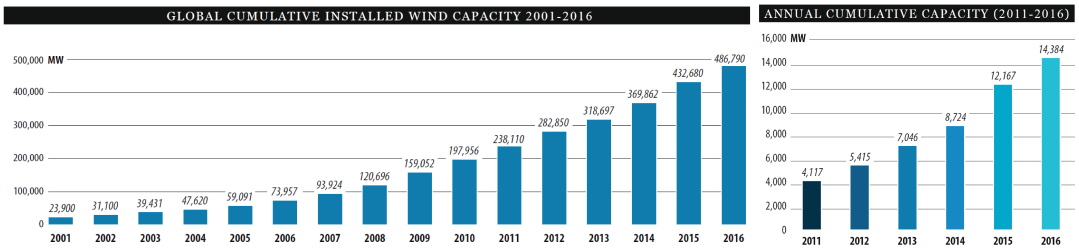

Figure 1.2: Growth of total installed offshore wind capacity between 2011 and 2016 [27].

With advancing technology and new opportunities for floating wind turbines in deeper water, market growth is expected to continue. According to WindEurope, offshore wind is expected to produce 7% to 11% of the EU's electricity demand by 2030 (totalling 3225 TWh) [13].
As described, the LCOE of Offshore wind has decreased in the last couple of years. The European Wind Energy Association (EWEA) expects a further decrease in the coming years. The main reason for the rapid decrease of the past years are changes in financing costs of projects, turbine technologies, supply chain capability and competitive auctions, all besides the learning effect of producing in greater volumes. Decreasing financing costs can be linked to the reduction in perceived risk of OWF's and the innovations in turbine technology are related to greater power output of turbines and higher reliability without increasing the cost per MW of capacity. Figure 1.3 illustrates the latest projects and future outlook for LCOE of offshore wind energy. With these market perspectives, many companies are eager to involve themselves in the offshore wind industry and new developments are important for the succes of the industry.

1.1.2. Maintenance and repair of wind turbines

Together with the growth of installed capacity of offshore wind, a growth in demand for servicing and maintenance can be expected. Within the 20-year operating period of a wind turbine, many of its components need regular servicing which requires a Crew Transfer Vessel (CTV) and some minor equipment. However, in the 20-year operating period it occasionally happens that the wind turbine suffers a critical failure. Turbine-blade and gearbox-drive replacements are not uncommon in the offshore wind industry, and require a difficult lift-

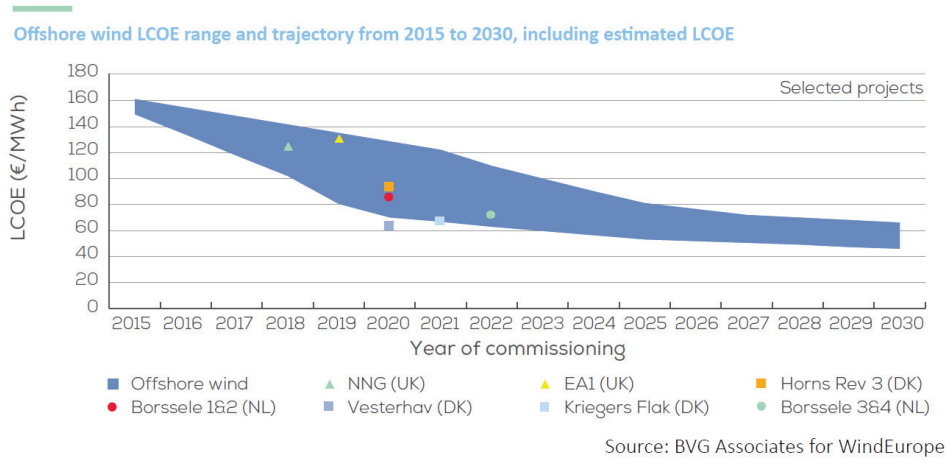

Figure 1.3: Offshore wind LCOE range and trajectory outlook from 2015 to 2030.

ing operation at sea. At present, most of the replacement work is done by jack-up vessels. These vessels provide a steady base for lifting operations because with the use of four legs that are attached to the vessel, they can elevate the hull above the water line. By doing this, the workability of the vessel is not limited by vessel motions resulting from wave loads anymore. However, the jacking system is very slow and the positioning of the jack-up is limited by previous footprints in the seabed. A footprint is created by the large load on the soil beneath the jack-up leg when it raises itself above the water line and when the vessel returns for maintenance it cannot place its legs at the same spots by regulation. Also, jack-ups generally have a lower transit speed than a construction vessel and together with the time consuming jacking process, a reduction in downtime is possible when a quicker vessel can be used. Another interesting development is the fact that different companies are investigating opportunities for floating wind turbines such as Statoil with its Hywind program [29]. One of the main advantages of a floating wind turbine is its ability to be placed in deep water. For bottom founded structures, increasing water depths quickly drive up the price of the foundation by which floating solutions become economically interesting. An accompanying disadvantage of a floating turbine is the fact that a jack-up cannot be used in deep water and therefore assistance for installation, service and maintenance, has to be done from a floating vessel. 3D tip compensation can contribute to the workability of offshore maintenance operations from a floating vessel and therefore offers market potential in the nearby future.

To be able to provide service and maintenance for offshore wind turbines, the crane used for the lifting operation must be able to reach large heights. The biggest turbines currently installed reach a nacelle height of approximately 105 meters (Vestas V164 8.0 MW [32]). Although components are always growing, the weights of a wind turbine blade and a gearbox are not very large and for this reason, the design load of the crane for this operation is estimated at 240 mt.

1.1.3. Huisman Equipment B.V.

Huisman Equipment is a specialist in large offshore equipment including many different types of cranes. Huisman has successfully introduced new concepts within the offshore market and wants to continue being a lead innovator. Whereas active heave systems are already capable of compensating the vertical motions of a crane tip, a 3D motion compensated crane-tip is suggested to allow floating replacement operations of turbine blades & gearboxes which is a typical innovation that fits Huisman's existing track record. Currently maintenance is performed with the use of jack-ups which are expensive and a floating solution could lead to benefits such as reduced downtime and reduced operational costs. Reducing the total costs of maintenance is interesting for offshore wind farm operators and therefore Huisman sees market potential in the development of a motion compensated crane. Huisman would be the first to develop a crane specifically designed for this operation by which they can expand their product portfolio, increase revenue and strengthen their position as an innovative manufacturing company.

1.2. Problem statement

While active heave systems can compensate for vertical motions of a load, a new system is to be developed to compensate crane tip motions in the horizontal plane to be able to 3D compensate the crane tip's motions. Irregular North Sea wave conditions will cause a vessel to move in all its 6 Degrees of Freedom and mainly the heave, pitch and roll motion will induce large displacements, velocities and accelerations at the crane tip. Standard offshore cranes, suitable for the replacement of wind turbine components, are capable of handling the induced loads but the crane tip motions restrict the workability of the operation because they will cause load swinging. A motion compensated crane could increase the workability of a floating solution for wind turbine maintenance and therefore the feasibility of 3D motion compensation of the crane tip is to be assessed. Within this study, the scope is limited to the mechanical aspects of the maintenance crane which leads to the following research goal:

Assess the mechanical feasibility of 3D motion compensation of an offshore crane for wind turbine maintenance operations.

The feasibility assessment is split in the following subgoals:
- Determine the operational context
- Determine the compensating motions of the crane
- Determine the workability of the crane for the current drive system
- Determine the effect of the stiffness of the crane on the motion compensating performance
- Determine the risks of motion compensation for wind turbine maintenance operations

To assess the feasibility of motion compensation for an offshore crane, three different crane concepts are analyzed and compared. The crane concepts that are used within this study are a Pedestal Mounted Offshore Crane, a Hybrid Boom Crane and a Motion Compensated Crane Concept. Also, the wind turbine maintenance operations that are concerned within this study are specifically focused on replacements of wind turbine blades and gearboxes.

1.3. Thesis outline

In order to asses the mechanical feasibility of 3D motion compensation for the crane tip of an offshore crane, different analysis steps are identified which are combined into a framework. Figure 1.4 illustrates an overview of these steps. The framework can be used as a design spiral with which the level of detail increases with the number of rotations through the spiral. The first rotation is used to asses the feasibility which is the main goal of this study. The different modules, and also chapters of this thesis, are the following:

1. Operational context & design cases. **(chapter 2)**
The operation of wind turbine maintenance is described and a vessel is selected that suits the operation. For a representative load case, the RAOs of the vessel are calculated with the use of diffraction software. Also, environmental impacts are described and assumptions on the alignment of vessel and waves during the operation are made. The working principles of the cranes that are used within the study are explained and the crane concepts are scaled to suit the operation of wind turbine maintenance. The output of this module is a set of design cases for which the compensating crane motions can be calculated.

2. Compensation motions of the crane to keep the crane tip at a fixed position. **(chapter 3)**
The RAOs of the crane tip in the global coordinate system are determined by superposition. Using transformation matrices, the RAOs of the degrees of freedom of the crane can be determined whilst assuming small displacements. The crane is assumed to stay in its initial position and only displacements from this position are considered. First order ship motions are included in the compensating criteria whilst second order ship motions are very slow and not limiting the drive requirements. Frequency Domain irregular wave analysis is used to calculate maximum expected responses of the compensating crane motions for different design cases. These maximum responses are the output of this module.

3. Workability of the crane for motion compensation by limitations of the drive system. **(chapter 4)**
From the calculated crane motions needed to compensate the vessel motions, the required actuator power, speed and torque is calculated. By coupling the requirements for motion compensation to the properties of the cranes drive system, the limits for motion compensation are determined. The Frequency Domain analysis is used for changing wave conditions to translate the cranes performance into a workability for offshore operations including motion compensation which is the output of this module.

4. Effect of crane stiffness on compensation performance. **(chapter 5)**
The effect of the stiffness of the crane on the motion compensating performance is quantified by determining the static- and dynamic response of simplified crane models. Whilst the initial crane design should be sufficiently strong for the offshore operation, the stiffness of the crane is of vital importance when wave induced motions are involved which can have frequencies near the eigenfrequencies of the crane. The natural frequencies of the crane, and their effect on the motions of the crane are the output of this module

5. Perform a risk assessment and estimate impact of different failure modes. **(chapter 6)**
With the use of an Failure Mode and Effect Analysis, possible failure modes are analyzed and their impact is estimated. Mitigation strategies are proposed and the effect of assumptions made in previous modules is elaborated upon. Output of this module is an overview of the largest risks accompanying motion compensation.

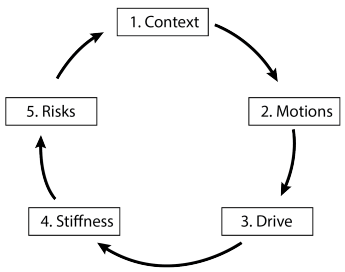

Figure 1.4: Schematic representation of the framework that is used within this study.

1.4. State of the art

Some innovative developments that relate to motion compensation for offshore cranes have been introduced in the near past. To determine which techniques are already present and which systems have successfully been developed, a state-of-the-art assessment is performed.

Heave compensation

In order to compensate for the vertical motions of the load induced by vessel heave, roll or pitch, heave compensation systems have been developed. Heave compensation can be done both passively and actively. Depending on the type of winch and the operation, a heave compensation system can be designed. Passive heave compensation (PHC) is generally used when lowering loads to the seabed and is purely based on the compression of gas without needing additional control. One of its main advantages is its low power demand and the fact that it can still operate during a black-out. Active heave compensation (AHC) is designed to control the vertical position of the load relatively to the seabed and compensates for small errors by inefficiencies in the passive system by an actively controlled cylinder. This system uses the real-time signal of the Motion Reference Unit (MRU) of the vessel. Active heave can be supplied for both hydraulic winches and electric winches [2]. In a motion compensated crane, AHC can be used to compensate for the vertical crane tip motions.

3D Motion compensation

Product already exist that can also effectively compensate vessel motions in all directions. Motion compensated platforms such as the Bargemaster platform offer the possibility to fix a regular land crane to the platform and use this base for motion compensation of the crane. These are however hybrid solutions and are not feasible for the load case of wind turbine maintenance because of the limited load capacity. Bargemaster is working on a fully motion compensated crane concept as well. The BM-T40 is a new design that is able to compensate sea-induced motions for a load up to 15mt at 10 meter radius [1]. MacGregor has recently introduced a three-axis motion compensated crane which can be installed on offshore service vessels. This crane can compensate vessel motions and lift 5mt at a 25 meter radius. The crane is hydraulically controlled at its base by cylinders and makes use of a telescopic boom [10]. Using a different approach, some concepts have been proposed with which motion compensation is performed at the tip of the crane. This way the heavy crane components do not have to be controlled actively and only the motions of the tip are compensated locally. Ulstein is developing such a system that can be retro-fitted on existing cranes. The main disadvantage of this system is that its capacity to compensate large translational movements is very limited and the system is only capable of handling weights up to 7mt [3]. Oceaneering International has successfully built a motion compensated crane which can lift containers from one moving vessel to another moving vessel. Unique is its possibility to compensate for the movements of the load receiving vessel. This development is part of a US Navy program (Sea Power 21) to create a floating port. The crane is designed for container transfer purposes only and the design is very heavy and robust, therefore this system is not suitable to scale up to perform construction work at heights that are rquired for wind turbine maintenance.

Delta parallel robot

A Norwegian research team investigated the use of a Delta parallel robot as crane head to compensate for ship motions in three axes at the location of the crane-tip. They modelled the full kinematics of the crane system, with the robot as its head. By the use of PID controllers, motions that result from the model of a supply boat vessel are compensated. The disturbances on the system from the elements are translated and rotated to the crane head frame of reference for use in the compensation procedure. A lifting height of approximately 25 meters was used in the simulations Workspace limits were reached for Hs > 3.0 meters (Hs - Significant wave height) where compensation efficiency starts to reduce for the crane tip position used. The effect of different crane tip positions on the system is not discussed within this research [31].

Anti-sway control
Active control of a cranes degrees of freedom that manipulate the tip position in the horizontal plane has been used to reduce the effect of payload pendulation [28]. While the crane operator controls the movement of the crane, an active controller can use fractions of the velocities and accelerations of the operators input to damp out oscillations by moving the crane into the direction of the load sway to dissipate energy from the system. The fractions at which the controller interferes can be adapted to the sea state. Another method that was tested to dissipate energy from the pendulum in order to damp out swaying motion is the use of the winch to vary the length of the hoist cable over time. This approach resulted in a very slow motion damping of the motions and turned out not to be usable for motion compensation [28].
Two different approaches for anti-sway are described by Ragunathan (2011) and Parker (2007). Input shaping and filter techniques can smoothen the input command and suppress load oscillations, this method is mainly used for one DOF (Degree of Freedom) land cranes. This system helps to compensate for sway that is generated by operation but it is not able to reduce sway generated by external disturbances [26]. Another approach uses the patented Active Rider Block Tagline Control System to suppress the load from swinging by the use of an extra winch that is attached to the main hoist, in between the crane tip and load [23]. This system cannot be integrated with AHC (Active Heave Compensation). In existing literature, very little research has been done done to incorporate both an active heave compensation system and anti-sway control in a combined control method.
For a motion compensation system, an interactive control interface has to be established as the crane operator must still be able to move the load using the regular crane controls whilst the active compensation module interferes with the signal to the crane actuators.

Coupling between load and vessel motions
For offshore operations, classification authorities set design constraints and rules and standards. DNV-GL is one of the renowned names in the industry and in Recommended Practice RP-H103, 'Modelling and Analysis of Marine Operations', DNV describes the rules and standards regarding lifting operations. It states that for light lifts less than 1-2% of the displacement of the vessel, the motion characteristics of the vessel (at the crane tip) are not affected by the lifted object [5]. Vorhölter et. al. have investigated this statement in their research 'Design Study of Floating Crane Vessels for Lifting Operations in the Offshore Wind Industry' and compared three different crane concepts. It was found that it is necessary to perform analyses with full coupling between the load motion and the motion of the vessel, even for small (2%) load cases when the crane does not have additional measures to control the motion of the load like tuggers or active motion compensation [9].
Within this study a relatively small load is concerned and when the active motion compensation system would fail, load swing induced vessel motions can be expected.

Estimation of ship motions
To be able to successfully compensate for vessel motions, active control of the offshore crane must be used. An important point to consider for such systems is the time delay between the sensors and actuators, which diminishes performance. In 2010, Küchler investigated the influence of delays (by data processing and trajectory generation) in a vertical motion compensation system and came up with a vessel motion prediction algorithm which he combines with the controller in order to decrease the effect of delays on the system [19]. The AHC uses prediction of vertical motion and an inversion-based control strategy. To allow the system to compensate, trajectory tracking of the load in an earth-fixed coordinate system is required. Since the position of the load cannot be measured exactly by flexibilities in the rope, the position and velocity are estimated using an observer based on the force measurement at the winch. An IMU has three accelerometers and three rotation sensors. To obtain the relative position of the ship the signals are integrated and to reduce errors like sensor noise, bias and misalignment, signal conditioning can be used. In 1998, Godhaven has proposed an algorithm for accurate estimation of the heave motion based on accelerometers, taking into account the mean wave height, dominating wave frequency, sensor noise, bias, and misalignment of the accelerometers [8]. In 2003, Johansen proposed a new strategy for active control in offshore crane operations while lowering a load through a moonpool [17]. Wave synchronization reduces the hydrodynamic forces on the load by minimization of variations in the relative vertical velocity between payload and water using a wave amplitude measurement. This system is combined with Active Heave Compensation to obtain accurate control.
With regard to vessel motion prediction, there are different strategies which can help to anticipate on expected vessel motion. In his paper on Active Control of Offshore Cranes, Küchler decomposes the measured motion signal into periodic components. From this decomposition he predicts the behavior of the vessel. It

is shown that vertical motions of the load of up to 4 seconds ahead are predicted in good accordance with the measurement [19].
In 2010, Danneberg presented an entirely different approach [15]. By measuring remote wave profiles and propagating them in time and space, he was able to estimate the ship response in real time. The system uses a WMS (Wave Monitoring System) and by linear propagation it is used to predict the wave field at the vessel location at the time the recorded wave train will reach it. Wave profiles in a distance of 1-2 km ahead of the vessel can be determined with the Wave Monitoring System. When the wave field and the vessels characteristics (RAOs) are known, the resulting vessel motion can be calculated. The estimation of ship motions provides the opportunity to synchronize the operation to the wave conditions. A critical part of the operation, such as the moment when the blade is connected to the nacelle, can be timed to a window of low expected vessel movement. This window can significantly contribute to the workability, as the window that is selected will lead to the best motion compensating performance of that sea state.

2

Operational context

This chapter defines general conventions and elaborates on the operation of wind turbine maintenance to ensure the reader understands the interpretation of the problem and the boundaries under which the problem has been elaborated on. The working principle of the three different crane types that are included in this feasibility study are explained and concepts are formulated for the operation of wind turbine maintenance. Also, design cases have been defined to generate structure among results from different modules and at the same time compare the impact of different crane positions on the motion compensating performance.

2.1. Description of the load & operation

Within this study, the operational focus is on the replacement of heavy wind turbine components that cannot be lifted with the service crane of the wind turbine itself. Mainly, a turbine gearbox- or turbine blade replacement are considered. Nowadays the heaviest gearboxes weigh approximately 86 tonnes and the turbine blades used for some of the largest offshore wind turbines (8 MW) weigh approximately 25 tonnes [14] [25]. On top of the weight of the wind turbine component, the weight of the lifting frame is to be added and because the offshore wind power industry is developing rapidly with increasing turbines sizes and therefore weights, the design SWL for motion compensation of the crane is aimed at 240mt, by which room for growth is accounted for.

Currently maintenance activities are performed by a jack-up. The jack-up will approach the wind turbine to a location from where it can perform the lifting operation and the jack-up will lower its legs in order to raise itself above the water level. In figure 2.1 an example of a wind turbine blade installation is shown where it can be seen that the jack-up is elevated above the water-line.

Figure 2.1: Installation of a wind turbine blade by a jack-up.

For current wind turbine blade installation operations, the operational window is limited to a maximum wind speed. There are no strict guidelines from authorities such as DNV up to what wind speed may be operated. The operators installing the blades, base their decisions on sensor data such as wind speeds, wave heights and wave periods, weather forecasts and experience. In general a maximum mean wind speed of approximately 11 m/s can be assumed up to which installation of turbine blades is possible and with higher wind speeds the operation will be terminated. More advanced systems exist in which the lower block of the crane is fixed to the boom to keep it steady. High Wind has tested their BoomLock system in wind speeds up to 15 m/s [21]. Section 3.1.1 elaborates further on wave conditions that can be expected at different wind speeds. The wave conditions that can be expected at these wind speeds will be the wave conditions that the motion compensation system must be able to compensate for in order to be competitive with a jack-up vessel.

2.2. Environmental conditions

During an offshore lifting operation, such as the floating replacement of wind turbine components, the vessel will be subjected to different types of loading mechanisms. Not only the vessel will experience loads but both the crane and the load can experience environmental loads as well. Three main environmental loads are described.

Wave Loads

Wave loads on a vessel will lead to vessel motions and can be split in two parts, namely being first order wave loads and second order wave loads. First order wave loads represent the sum of a contribution from each individual wave component in a sea state and excite the vessel's first order motion. Second order wave loads are quadratic with the wave amplitude and represent the contribution from each pair of wave components in a sea state [18]. For this study only the first order wave loads are included. Whilst a DP system or spread mooring set-up will maintain the vessel's position, second order wave loads are not to be compensated by the crane directly. Furthermore, the second order wave loads have a much longer period than first order wave loads and for this reason the limiting motions for the motion compensation system will come from first order loads. A side-note has to be made that relates to the accuracy of the station keeping system. When the station keeping system allows large amplitudes by second order drift loads, the compensating mechanism of the crane will have to incorporated these when the system is limited to a maximum stroke for compensation.

Current loads

A less fluctuating type of load is the current load. Current can have big impact on a vessel's station keeping performance and can be the main reason to choose a specific heading during the installation of wind turbine components. Most of the time, a vessel will choose its heading such, that it points it's bow into the direction of the current. This study does not incorporate the effect of current loads on the motion compensation system as the vessel that is used has a DP system and these loads are controlled by the DP system. Although the loads are not included, this load phenomena does reflect its presence in this study. Because the heading of the vessel is strongly influenced by the current, this mechanism will dictate the choice of heading. Whilst wind waves and currents are not always perfectly aligned, waves approaching the vessel at an angle must be concerned. To asses a realistic situation a maximum offset between the heading of the vessel and the waves approaching the vessel, of 30° to both sides is used in all calculations, keeping in mind that the requirements would be different when all angles are considered. In figure 2.2, the wave load condition is shown where the offset angle of wave loads is 30° with respect to head seas.

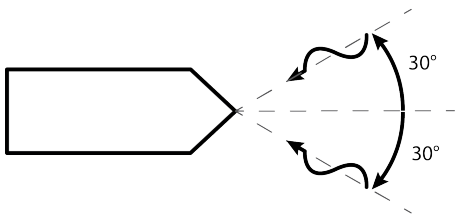

Figure 2.2: Angle between head seas and a 30°offset for the incoming waves.

Wind Loads
All objects above water will experience wind loads including the vessels hull, accommodation and deck equipment (for example a crane). Wind loads on the vessel can be small with respect to other loading mechanisms however, the suspended load in a crane can be strongly bothered by wind induced swinging motions which is the main limitation for turbine blade installation operations. The additional loads of the wind induced swinging motions of the load on the crane are not incorporated in this study. Also, the crane will experience wind loads, however it is assumed that the effect of these wind loads on the drive system is very small for the wind speeds at which turbine maintenance can be performed. For this reason, wind loads are not incorporated in the design requirements of the drive system.

2.3. Definition of vessel- & crane motions

The motion of a ship at sea has six degrees of freedom in the steadily translating coordinate system. Any ship motion is build up from these six components. The six ship motions are defined by:

- Three translations of the ship's center of gravity, in the ships x-, y-, and z-axes:
  - Surge in the longitudinal x-direction, positive forwards

$$x = x_a * cos(\omega t + \epsilon_{x\zeta}) \tag{2.1}$$

  - Sway in the lateral y-direction, positive to port side

$$y = y_a * cos(\omega t + \epsilon_{y\zeta}) \tag{2.2}$$

  - Heave in the vertical z-direction, positive upwards

$$z = z_a * cos(\omega t + \epsilon_{z\zeta}) \tag{2.3}$$

- Three rotations about these axes:
  - Roll about the x-axis, positive right turning

$$\phi = \phi_a * cos(\omega t + \epsilon_{\phi\zeta}) \tag{2.4}$$

  - Pitch about the y-axis, positive right turning

$$\theta = \theta_a * cos(\omega t + \epsilon_{\theta\zeta}) \tag{2.5}$$

  - Yaw about the z-axis, positive right turning

$$\psi = \psi_a * cos(\omega t + \epsilon_{\psi\zeta}) \tag{2.6}$$

Figure 2.3 displays the six vessel motions and also the three motions of a regular PMOC, the slewing, luffing and hoisting motions of the crane. The luffing motion is used to control the radius of the crane and while the radius increases, the overturning moment by the load will increase. Therefore, the Safe Working Laod (SWL) of the crane decreases for larger radii. The slewing motion is used to move the load away from the deck and the hoisting motion is used to control the vertical position of the load.

The global axis system that is referred to within this study is fixed to the earth, while local axis systems are fixed to for example the vessel CoG or the crane tip. Throughout this study, different local axis systems are referred to and in figure 2.4, the definition of different local axis systems is displayed.

2.4. Vessel

The vessel selected for this study is the Jumbo Fairplayer. The Jumbo Fairplayer originally is Heavy Lift Crane Vessel (HLCV) which is used for transport of heavy equipment. The vessel is equipped with two Huisman cranes and has a DP2 system. Companies find RAO data very sensitive and therefore, this is not widely available for different vessels. Because the evaluation of different crane concepts and their limiting factors is the main goal of this study, the optimal vessel design is not a focus point. The Fairplayer is a 144 meter long vessel and represents the characteristics of a stable monohull, for these reasons it is used in this study. The main characteristics of the vessel can be found in table 2.1. Ansys AQUA is used to calculate the RAOs of the vessel for a load case that represents the context of the operation, these RAOs can be found in appendix C.

Jumbo Fairplayer			
Length [m]	144	Breadth [m]	26.7
Depth [m]	14.1	Transit speed [knots]	17
Displacement [Te]	20120	Deadweight [Te]	10700

Table 2.1: Vessel specification Jumbo Fairplayer

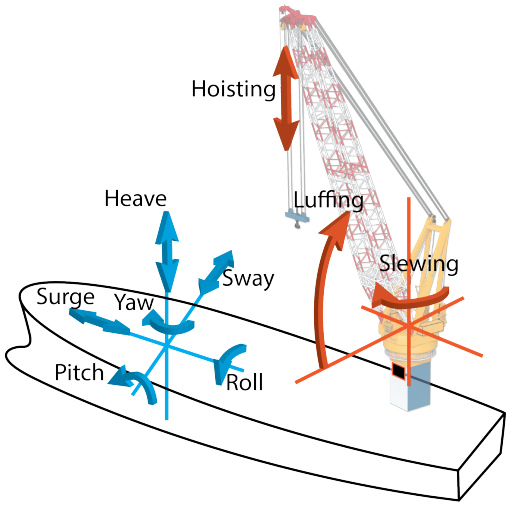

Figure 2.3: Definition of the vessel motions and degrees of freedom of the crane.

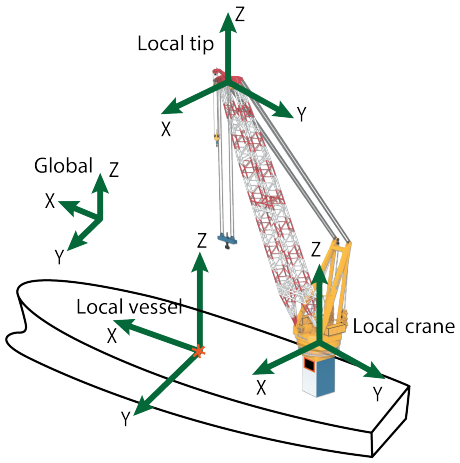

Figure 2.4: Definition of different axis systems.

2.5. Cranes

For the feasibility assessment of wind turbine maintenance from a floating vessel with a motion compensated crane, three crane types are compared. Huisman has built many types of crane throughout its history, and from these different designs, two are selected to be included in the analysis. These two crane types distinguish themselves by a different kinematic model. The third design is a concept which is currently under development within Huisman Equipment B.V..

2.5.1. Pedestal Mounted Offshore Crane

The Pedestal Mounted Offshore Crane (PMOC) is currently the most common crane used for installing offshore wind turbines. This crane type can be used for various tasks including loading/unloading, installation work, pipe transfer, deck handling and subsea installation. A PMOC mainly consists of a steel crane house, which is bolted to a pedestal via the slew bearing, and a boom. The slew bearing will have to withstand all the overturning moment from the load, while still being able to rotate the crane. In figure 2.6, the position of the slewing system can be observed. The boom can be of lattice- or box girder type and uses various hoist tackles to control the boom position and the lower blocks. The boomhoist is used to control the boom angle which is the angle between the boom and the horizontal. The boomhoist runs from the top of the cranehouse to the tip of the boom and usually consists of multiple falls which can also be seen in figure 2.5. All main equipment

such as - winches, electrical cabinets and/or Hydraulic Power Units (HPU) - is placed inside the cranehouse to protect it from the harsh marine environment and ensure optimal life time performance. This way reliability is increased and required maintenance is reduced to a minimum. PMOC's can be equipped with active & passive heave compensation which can compensate the vertical displacement of the load by motions of the vessel. These cranes are either electro-hydraulically driven or fully electrically driven. In the research, all cranes are fully electrically driven as most customers favour this type of drive system because of maintenance purposes.
In figure 2.5, the green arrows indicate the degrees of freedom of the crane which it will use for motion compensation. These are the slewing motions and the luffing motion, combined with the AHC system for compensation in the vertical direction. By using these degrees of freedom, the entire crane will move with respect to the vessel, while the crane is compensating for the vessel motions.

The main reason why this crane type is used in the comparison for the feasibility of motion compensation is the fact that it is the most common crane type in the offshore wind industry. It is to be investigated whether minor adjustments of the crane and its drive system could lead to a feasible motion compensating crane for wind turbine maintenance.

Figure 2.5: A 300 mt Huisman Pedestal Mounted Offshore Crane. The degrees of freedom of the crane are illustrated with the green arrow.

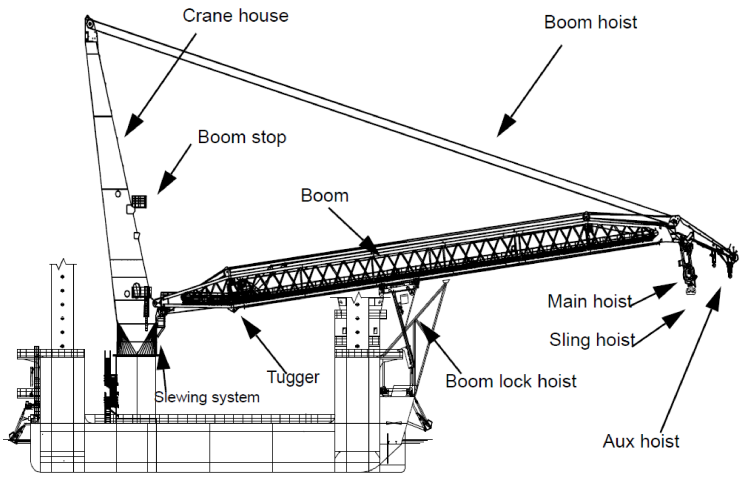

Figure 2.6: General overview of a PMOC on a jack-up with terminology.

2.5.2. Hybrid Boom Crane

The second concept that is used in the comparison for motion compensation is the Hybrid Boom Crane (HBC). This crane concept is developed by Huisman Equipment and combines the key performance elements of a PMOC and a Knuckle Boom Crane (KBC). A PMOC is limited in its degrees of freedom to only three motions, and will have to lower its boom to create reach. The Hybrid Boom Crane combines high lifting capacities, with a better positioning feature and ability to hold loads at a larger outreach.

In figure 2.7, the degrees of freedom of the HBC are highlighted with green arrows. The HBC has 4 degrees of freedom with which it can compensate for vessel motions of which 3 are the same as those of the PMOC. The additional feature of the HBC is a knuckle boom/fly-jib (see figure 2.8) that can be controlled separately from the boom. In figure 2.7, the degrees of freedom of the HBC are highlighted with green arrows. An HBC can also be equipped with AHC or PHC.

A regular boomhoist configuration for a PMOC consists of multiple falls which make the luffing motion relatively slow. It is expected that the luffing motion will be one of the limiting factors for a PMOC crane when it will have to compensate for the vessel motions. For this reason, the HBC crane is interesting for the motion compensation analysis as the combined movement of the boom and the knuckle contribute to a displace-

ment of the tip in the length direction of the boom. Also, depending on the design, the geometry can be chosen such, that the load is not vertically displaced while the boom is lowered. Just as with the PMOC, the entire crane will be moving with respect to the vessel, while compensating for the vessel motions.

Figure 2.7: A 1000 mt Huisman Hybrid Boom Crane. The degrees of freedom of the crane are illustrated with the green arrows.

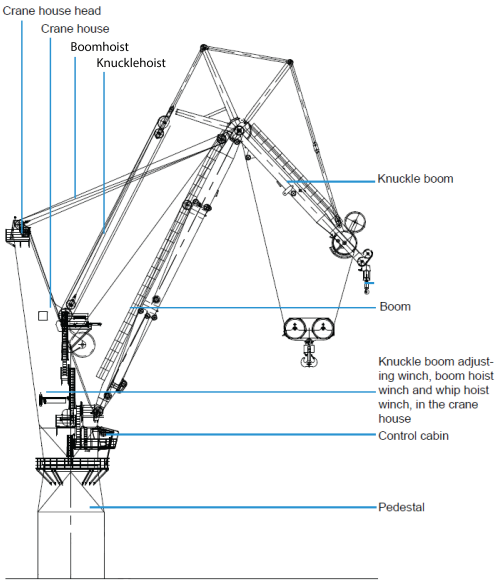

Figure 2.8: General overview of a HBC with terminology.

2.5.3. Motion Compensated Crane Concept

Specifically for the purpose of motion compensation for offshore wind turbine maintenance, a new concept is under development within Huisman Equipment. The purpose of this Motion Compensation Crane Concept (MCCC) is to compensate all crane tip motions in the horizontal plane with a skid-table that is attached to the top of the boom. Within this skid-table, the main hoist is suspended by a trolley that can translate in the horizontal plane. The skid-table is fixed to the mainboom, and the mainboom will not be moving with respect to the vessel. All compensating motions are to be performed by the skid table and an AHC system will assist in the vertical compensation of the load. An illustration of the MCCC is shown in figure 2.9 in which the green arrows indicate the degrees of freedom that will be used for motion compensation. This crane will also have a slewing and luffing system but these will only be used to bring the crane into the lifting position and not for motion compensation purposes during the operation.

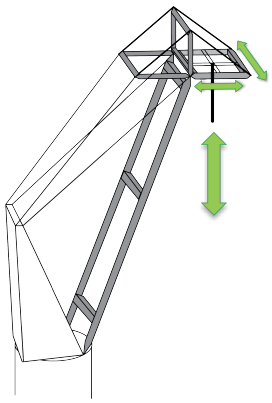

Figure 2.9: Sketch of the Motion compensated crane concept. The degrees of freedom of the crane are illustrated with the green arrow.

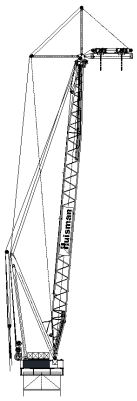

Figure 2.10: Detailed drawing of the motion compensated crane concept

2.6. Design cases

In order to effectively compare the crane concepts, different design cases are formulated in which the crane tip is located at different positions with respect to the CoG of the vessel in the horizontal plane. For all design cases, the load is modelled as a point mass that is suspended from the crane tip and by the assumption of good motion compensation, possible swinging motions are not accounted for.
The hub height of the turbine is a key parameter for the design of the wind turbine maintenance crane. Currently, the largest wind turbines have a hub height of approximately 105 meters [32]. An additional suspended wire length of 15 meters minimum is used to create enough clearance between the boom and the lifting frame of the turbine blade when the boom is nearly vertical. All together, a total lifting height of 120 meters measured from the sea surface would be needed. Wind turbines are expected to increase in size, and with larger rotor diameters, the hub height will have to increase as well. A growth margin of approximately 10 % is accounted for in the design criteria. The resulting tip height for all design cases that are described in this study, is 132 meters above the waterline.

When installing a wind turbine blade or gearbox, the distance between the vessel and the fixed structure, in this case the wind turbine, is to be maintained above a certain minimum. For one of the design cases (DC 1), the focus is to minimize the distance between the CoG of the vessel and the position of the hook and this will be limited by the minimum clearance. This clearance distance makes sure the floating unit and fixed structure will not come into contact while the floating unit is moving in waves. For a floating and a fixed structure in normal operation, the Accidental Limit State (ALS) clearance is 10 meters. A Limit State defined by DNV corresponds to a condition beyond which the structure, or a part of a structure exceeds a specific design requirement which in this case is the minimum clearance accounting for an accidental event or operational failure [6]. For a gearbox replacement, the vessel will have to approach the wind turbine up to the minimum clearance. For a turbine blade replacement, the substantial length of the blade can be used to maintain enough clearance with the wind turbine and keep the crane tip relatively close to the vessel's Center of Gravity (CoG) while the blade will be horizontally lifted. The slewing angle that is chosen for design case 1 is based on this limitation.

The mechanisms which the crane can use for motion compensation are split in three categories for the PMOC and HBC. Compensation along the x-axis of the local axis system at the tip of the boom (luffing), compensation along the y-axis of the local axis at the tip of the boom (slewing), and vertical compensation. The convention of the local axis system at the tip of the boom was already illustrated in figure 2.4. The boom angle, influences the cranes ability for effective compensation along the x-axis. When the boom is almost vertical a small luffing response will lead to a large displacement along the x-axis however, for a vertical boom the compensation by slewing is not very effective anymore because of the small radius. For the MCCC, the initial position of the crane does not influence the motion compensation performance of the crane. 4 design cases are used to compare and assess the motion compensating behavior of the cranes and also to gain insight into the advantages and disadvantages of different lifting positions.

Design Case (DC)	Crane type	X [m]	Y [m]	Z [m]	Slew angle [°]	Boom angle [°]	Knuckle angle [°]
1	PMOC	3.3	-27	135	-30	73	-
1	HBC	3.3	-27	133	-30	78	-65
1	MCCC	3.3	-27	135	-30	78	-
2	PMOC	-23	-46	135	-80	73	-
2	HBC	-23	-46	133	-80	78	-65
2	MCCC	-23	-46	135	-80	78	-
3	PMOC	-21	-58	130	-80	67	-
3	HBC	-21	-59	131	-80	73	-55
3	MCCC	-21	-58	132	-80	72	-
4	PMOC	-68	-1	135	-190	73	-
4	HBC	-68	-1	133	-190	78	-65
4	MCCC	-68	-1	135	-190	78	-

Table 2.2: Parameters that are used for the initial crane positions of the different design cases.

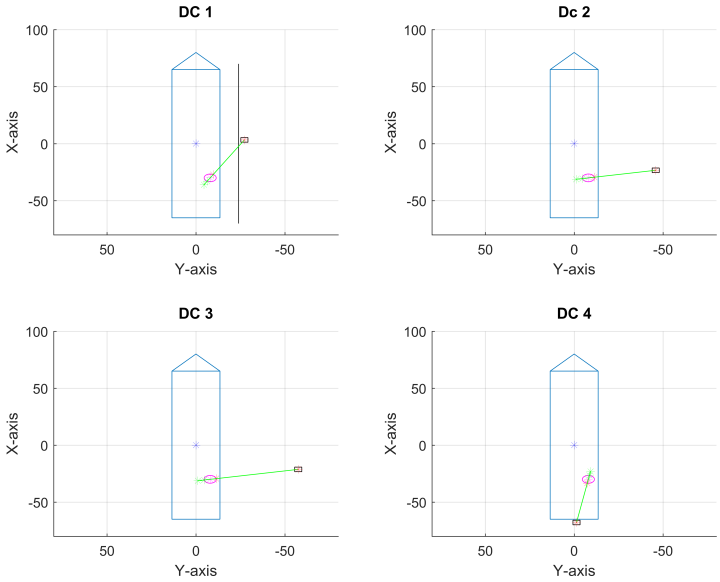

Figure 2.11: Four different design cases are formulated to gain insight into the advantages and disadvantages of different lifting positions.

Design case 1
To minimize the vertical motions of the tip, this design case positions the tip as close to the CoG as possible in the horizontal plane while maintaining the minimum clearance with the structure. The black line in the figure of design case 1 represents the minimum clearance. A maximum boom angle of 78°is used because while compensating, the boom angle may not exceed 83°for stability reasons.
Design case 2
In design case 2, the boom is positioned over the side of the vessel. Here the roll motion of the vessel is to be compensated by the luffing motion of the crane, whilst in design case 1 the roll motion imposes large slewing responses.
Design case 3
In design case 3, the boom angle is smaller, by which the cranes reach is larger. When the vessel cannot approach the structure very close, the horizontally projected length of the boom must be extended. This configuration will most probably decrease the performance of the luffing compensation, at the same time the slewing compensation will become more effective.
Design case 4
Depending on the operation, the operator might choose to lift over the stern of the vessel. Ship stability can be a motivation to use this lifting position, and also the ship can move away from the lifting location more quickly.

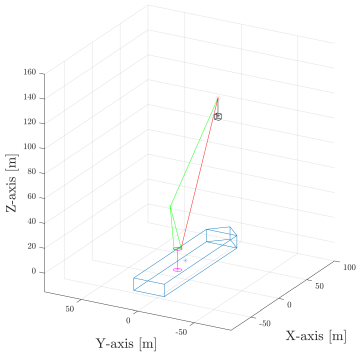

Figure 2.12: Matlab model of scaled PMOC.

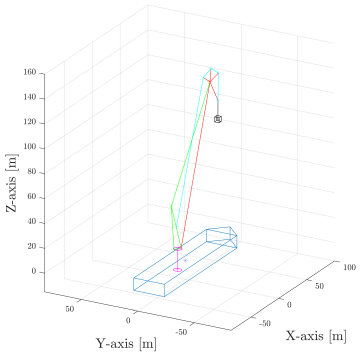

Figure 2.13: Matlab model of scaled HBC

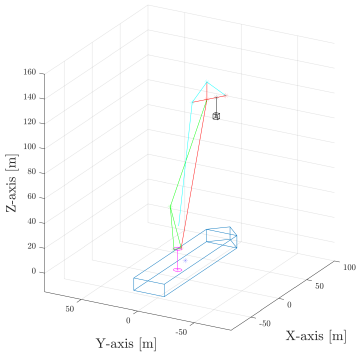

Figure 2.14: Matlab model of scaled MCCC

2.7. Sizing and scaling of cranes

The design cases formulated in the previous sections are based on the context of the operation. As stated, the tip position with respect to the vessel must be the same for all crane types to make a fair comparison in which the tip displacements that have to be compensated are the same. This means that the dimensions of all three cranes must be able to operate at the same lifting height. Within the previous designs of Huisman cranes, many cranes have equal properties when for example the maximum SWL is compared. However, the very high lifting height and relatively small load that is to be lifted, makes this operation a rare combination for which no specific designs exist.

In consultation with specialists at Huisman, three crane concepts have been developed for which the properties match the operation as good as possible. An initial design of a 600mt Wind Turbine Installation Crane (WTIC), which is in fact a PMOC, is used as a basis. This crane is built for the Neptune vessel of GeoSea and is designed for wind turbine installation from a jack-up. In figure 2.15 this crane is displayed next to a wind turbine with a hub height of 105 meters.

The same cranehouse position and pedestal height are used for all three cranes. For the PMOC concept, the length of the boom is increased to 120 meters so that it can lift the load to larger heights. The slew bearing is not changed because it has sufficient overturning moment capacity for the new load condition. The drive system is upgraded because the longer boom allows the load to generate larger forces on the drive system. The number of falls in the boomhoist is increased so that it can sustain the load that is imposed during the lowering of the boom into its transit position (horizontally attached to the vessel).

For the HBC, the boom of the PMOC is elongated to 132 meters and a fly-jib of 18 meters is attached to the top of this main boom. The mass of the fly-jib imposes larger slewing torques for which extra capacity is installed. Also the force in the boomhoist increases for small boom angles because of the mass of the fly-jib. For this, additional falls are installed. The number of falls for the fly-jib adjustment winch is determined by the maximum load capacity of the wire ropes and the overturning moment of the fly-jib at its most horizontal position. The geometric specifications of the MCCC followed from technical drawings by other departments within Huisman. The crane specifications used can be found in appendix D.

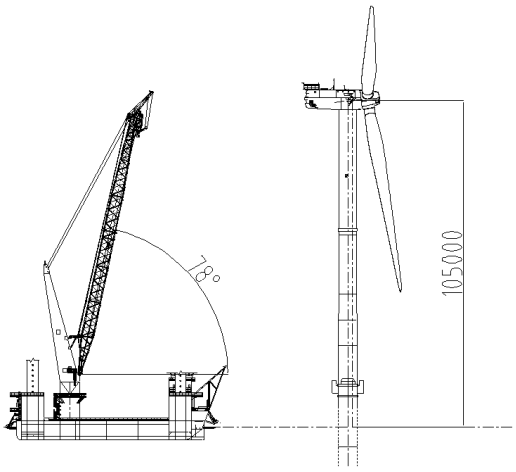

Figure 2.15: The original PMOC that is used as a reference case.

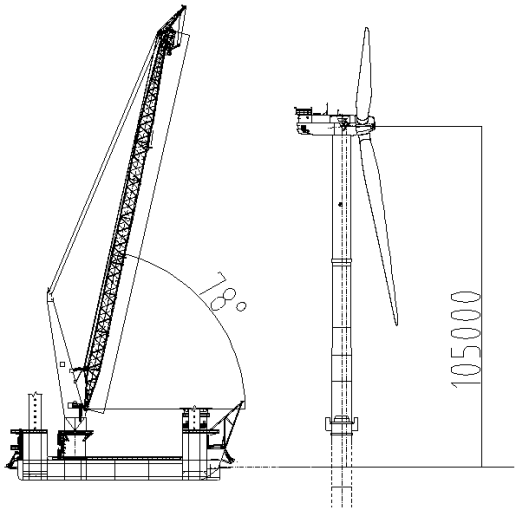

Figure 2.16: The scaled PMOC that is used in the analysis for motion compensation.

2.8. Discussion

In this first module of the framework that is used to assess the feasibility of motion compensation for wind turbine maintenance, the operational context is defined which results in a starting point for the motion analysis. The details as to what vessel headings will be used during the motion compensation operation are set to a maximum wave angle offset of 30°during the installation operation. The Jumbo Fairplayer (144m) is used for all design cases, representing a stable HLCV basis. The three different crane concepts that are used and compared in the framework (PMOC, HBC, MCCC) are elaborated on and their working principle is explained. For the compensating motions of the PMOC and HBC, the entire crane will move with respect to the vessel. However, with the MCCC, the tip motions will be compensated by translations in the skid table.
For existing designs of the PMOC and HBC, the luffing motion is relatively slow. However to compensate for the vessel motions and keep the load in position, the luffing motion must be able to keep up with the vessel motions and it is expected that this will be a limiting factor of the motion compensating performance of the cranes. The HBC offers an advantage over the PMOC while it can support the luffing motion with the rotation of the knuckle and therefore, its performance is expected to be somewhat better. With the MCCC, the slewing and luffing motion of the crane will not be used for compensation but only translations of the skid-table are used to compensate for vessel motions by which the mass to be displaced is reduced.

Also, design cases are formulated to compare the three crane types for the specific operation of installing offshore wind turbine components at large heights (132m). The design cases are formulated such, that the different degrees of freedom of the crane (e.g. slewing and luffing) are coupled to different degrees of freedom of the vessel (e.g. pitch and roll). It is therefore expected that the different design cases will lead to different limiting mechanisms of the crane. In total, 4 design cases are used to compare and asses the compensation behavior of the cranes. This is done to gain insight into the advantages and disadvantages of different lifting positions. While it is expected that the luffing motion will be a limiting factor, the best system performance is expected for the design case in which the luffing motion is coupled to the vessel rotation that has the smallest amplitudes.
General concepts for all three cranes are formulated because no specific crane designs exist within Huisman that fit the purpose of this operation. An initial design of a 600mt wind turbine crane is used from which the general arrangement of the different crane concepts is derived in consultation with specialists within Huisman. The sizes of the cranes are altered to be able to compare them at the same lifting height and their drive systems are upgraded for these larger lifting heights.
The output of this module is a clear operational context by which results can be interpreted. Also, an equal base is formed from which different geometric crane concepts can be compared. In the next module the crane motions that are necessary to compensate for the vessel motions are calculated for each different concept.

3

Compensation motions

When the crane must compensate for the vessel motions it must use its degrees of freedom to keep the load in position. The goal of this chapter is to couple the motions of the vessel to the motions of the crane and determine the crane motions that are required for motion compensation in wave conditions that can be expected during maintenance of offshore wind turbines. The motion compensation system is of most importance when the load is near the structure and therefore, the crane motions that are calculated will be based on the displacement of the tip for the initial crane positions that are described in the design cases from chapter 2. When the compensating motions are known, these can be linked to the drive system to assess the performance of the crane which will be done in chapter 4.

3.1. Frequency Domain

Within ship hydromechanics, the motion behavior of ships can be evaluated by either a Time Domain (TD) analysis, or a Frequency Domain (FD) analysis. From these analyses, the ship motions can be estimated very well, which are required to determine the compensating motions of the crane. Time Domain analysis is a very powerful tool to calculate ship responses at a high level of detail. This method is generally used for very specific operational analyses and is time consuming. To asses the feasibility of motion compensation for wind turbine maintenance, there is a need for a more general analysis with which many different situations can be modelled and compared, such as changing wave headings, wave periods and wave heights. For this reason, a Frequency Domain analysis method is used.

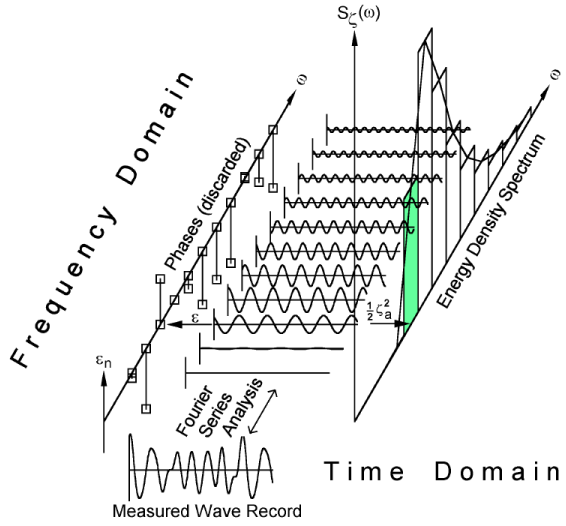

Figure 3.1: Transformation of a wave record in the time domain to the energy density spectrum in the frequency domain.

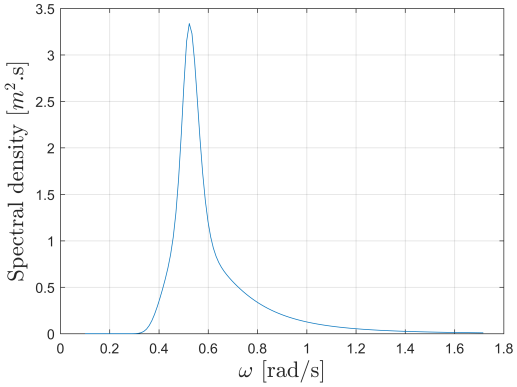

Figure 3.2: JONSWAP wave spectrum for a significant wave height of 3 meters and a peak period of 12 seconds.

3.1.1. Wave Conditions

To simulate wave conditions that represent local sea-conditions at the offshore wind farm, an irregular sea surface elevation must be used. An irregular sea surface elevation in the time domain can be seen as the sum of a number of regular wave components. The amplitude- and phase-spectrum that describe this time signal in the Frequency Domain follow from a Fourier analysis of the time record. In figure 3.1 the transformation from time domain to frequency domain is displayed schematically.
By experiments, equation's have been derived with which irregular wave conditions can be described in the Frequency Domain. For certain input parameters, such as the significant wave height and the peak wave period of the spectrum, an energy density spectrum of the waves can be calculated. The significant wave height is defined as 'The mean value of the highest one-third of the waves' and the peak wave period of the spectrum is the period at which the spectrum has the highest amplitude. Within this study, JONSWAP wave spectra are used because the maintenance activities are focused on the North Sea. In figure 3.2, a JONSWAP spectrum is displayed for a significant wave height of 3 meters and a peak period of 12 seconds. The y-axis represents the amplitude of the regular wave component of the frequencies on the x-axis. For a more detailed explanation of a wave spectrum, please consult appendix B. Deep water calculations are used whereas some OWF locations would not fulfill the requirements for deep water analysis. Bottom effects of the vessel motions are not accounted for.
The environmental conditions that are used for the design of a wind turbine maintenance crane should be generic and representative for different OWF's. Also, the wave conditions for which the maintenance crane should be able to compensate the vessel motions should be competitive with the use of a jack-up. For the installation procedure of a wind turbine blade with a jack-up, the operational window is limited to maximum wind speeds at which the blade starts to move too much by wind loads as describer earlier. For the motion compensating maintenance crane this same limitation will be valid. By the use of a wind wave model, wave conditions can be estimated depending on the wind speed and fetch distance where the fetch distance is the length of water over which the wind can blow to a specific OWF location. By using this model, wave conditions that can be expected at specific wind speeds are calculated and these are used as a requirement for the maintenance crane in order to be competitive with a jack-up. An alternative to using a wind wave model is using scatter diagrams that describe the local wave climate. However, these diagrams are not easy to obtain as the data is usually confidential.

At first, a reference location is selected. While the offshore wind industry is developing fast in the Europe/North-Sea region, the Deutsche Bucht OWF is chosen as a reference location. Deutsche Bucht is an OWF location north of The Netherlands and Germany, between Denmark and the United Kingdom (see figure 3.3). At this location, the distance to shore is known and also, 10-year average wind speeds (10 m/s) are available [22].

Figure 3.3: Reference location for wave conditions - Deutsche Bucht - witch a 1000 km distance marker.

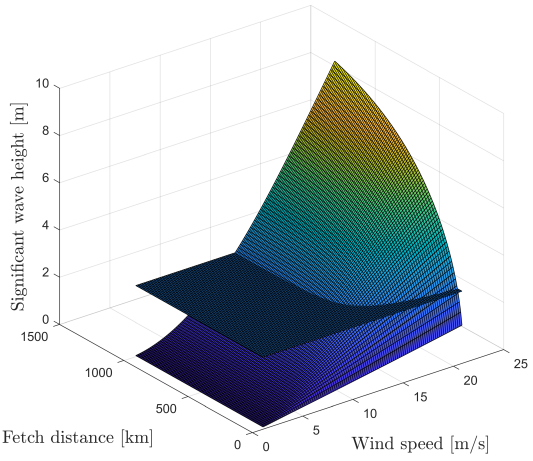

Figure 3.4: Significant wave height build up with increasing fetch and wind speed.

In the wind wave model, waves generated by wind are effected by the wind speed, fetch, time duration and gravitational acceleration. As L.H. Holthuijsen describes in his book [12], Pierson and Moskowitz determined relations that link the wind speed and wave height for wind induced waves for fully developed sea-states. Later on Young and Verhagen re-defined these relations to control the transition from young sea states to the fully developed sea state and these equations are used to estimate the significant wave height for a wind speeds that is limiting for the operation. Equations 3.1 to 3.3 are used to calculate the significant wave heights for different fetch distances and wind speeds, for which he parameters that are used are defined in table 3.1.

$$\tilde{F} = \frac{g \cdot F}{{U_{10}}^2} \tag{3.1}$$

$$\tilde{H} = \tilde{H}_{\infty} \cdot (tanh(k_1 \cdot \tilde{F}^{m_1})^p \tag{3.2}$$

$$\tilde{T} = \tilde{T}_{\infty} \cdot (tanh(k_2 \cdot \tilde{F}^{m_2})^q \tag{3.3}$$

Fetch parameters	
$\tilde{H}$	0.24
k1	0.000411
m1	0.79
p	0.572
T	7.69
K2	0.27e-6
m2	1.45
q	0.187

Table 3.1: Parameters used for the fetch calculations.

In figure 3.4, the increasing significant wave height for increasing fetch distances and wind speeds is plotted. The wind speed U_{10} that is used in equation 3.1 is the 10-minute average wind speed at a height of 10 meters. As mentioned in section 2.3, the maximum wind speed for the most advanced turbine blade installation methods is approximately 15 m/s, and 11 m/s for normal installations. When a fetch of 100 km is concerned, 15 m/s wind speed will lead to a 2.9 meter significant wave height and a peak wave period of ≈ 7 seconds. For a fetch of 1000 km and 11 m/s, a significant wave height of 3.0 meters can be expected. The peak wave period for this wave spectrum will be approximately ≈ 9 seconds. In Deutsche Bucht, a fetch distance longer than 1000 km is not expected because of the surrounding land.
Therefore, a design significant wave height of 3 meters is used so that the crane can operate in sea conditions that correspond to the maximum wind speed of the operation by which it can be a competitive alternative to a jack-up. The peak wave period of the wave spectrum (T_p) is set to 8 seconds. The horizontal plane in figure 3.4 corresponds to a significant wave height of 3 meters, the intersect between the horizontal plane and the surf plot are the limiting fetch distance and wind speed combinations for H_{sig}=3 meter.

3.1.2. Response Amplitude Operator

To calculate the motions of the vessel, Response Amplitude Operators (RAOs) are used which describe the effect that a sea state will have upon the motion of the ship. RAOs are transfer functions that consist of the parameters and are valid for one degree of freedom. They contains amplitudes that relates the amplitude of the vessel motion to the amplitude of the wave and also, phase shifts which define the time of the vessel motion relative to the wave. The RAOs used in this study are calculated by diffraction software (AQWA) and contain information at 50 different frequencies between 0.1 rad/s to 1.717 rad/s. Figures of the RAOs that are used within this study can be found in appendix C.

$$Response\ Amplitude\ Operator = \begin{cases} \frac{z_a}{\zeta_a}(\omega)\ amplitude\ characteristics \\ \epsilon_{z\zeta}(\omega)\ phase\ characteristics \end{cases}$$

3.1.3. Response Spectrum & Significant values

By using the RAOs of the vessel and the wave spectrum, the vessels motion response spectra in all six degrees of freedom can be calculated. This method is later on used to determine the responses of the crane motions as well.

$$S_{response}(\omega) = |RAO|^2 \cdot S_\zeta(\omega) = \sum_{n=i}^{N} A_i \cdot cos(\omega_i + \phi_i) \tag{3.4}$$

In equation 3.4, the absolute squared RAO is multiplied with the amplitude of the wave spectrum at every specific frequency in the spectrum. From this, a response spectrum can be obtained that describes the motion response of the vessel for one degree of freedom, that of the RAO that was used. Response spectra can be obtained for all degrees of freedom of the vessel motion. In figure 3.5 an example is shown of an RAO, wave spectrum and response spectrum and figure 3.6 schematically describes the calculation that is performed.
From the response spectra of the vessel motions, spectral moments can be calculated with which a significant response can be determined. The significant response of any vessel motion is calculated with the same method with which a significant wave height can be calculated from a wave spectrum. For this, equations 3.5 and 3.6 are used in which the zero-th order spectral moment (m_0) is used.

$$m_n = \int_0^\infty \omega^n E(\omega) d\omega \qquad for\ n = ..., -3, -2, -1, 0, 1, 2, 3, ... \tag{3.5}$$

$$H_{sig} \approx 4\sqrt{m_0} \tag{3.6}$$

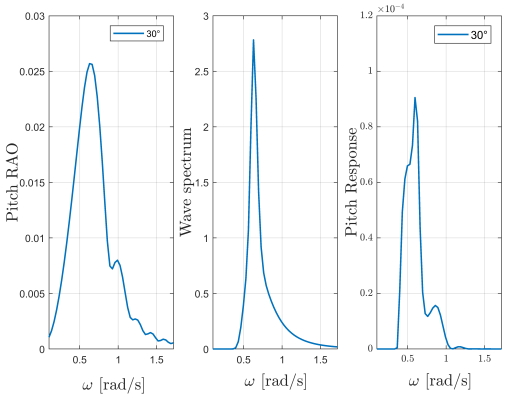

Figure 3.5: From left to right, pitch RAO, JONSWAP wave spectrum and resulting pitch response.

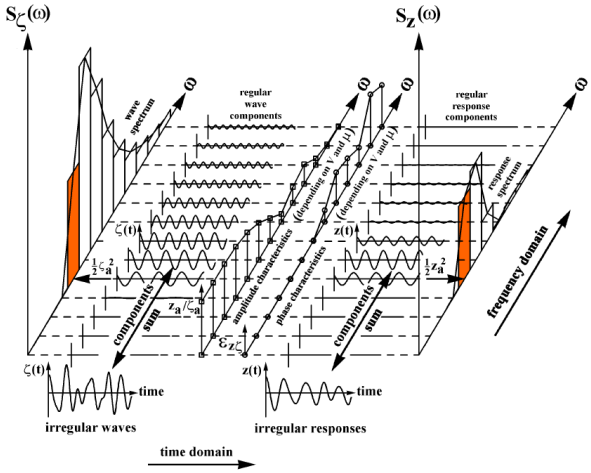

Figure 3.6: Wave spectrum, RAO and Response in the Frequency Domain.

3.1.4. Most probable maximum

When the significant response is obtained (equation 3.6), a maximum expected value can be determined in the same way that a maximum expected wave height is determined. Later on, maximum expected values for cranes motions are determined, which in their turn lead to the requirements of the drive system. In wave terminology, a 3-hour most probable maximum is a widely used parameter. The most probable maximum wave height is defined as follows:

"The maximum wave height that can be expected for a specific time period and significant wave, that has a probability of exceedance of 63%".

This means that there is still a chance of 63%, that a wave exceeds this most probable maximum wave height in a 3-hour period. To calculate the most probable maximum wave height, equation 3.9 can be used in which the significant response is used that was calculated by equation 3.6. The maximum expected wave height depends on the total number of waves that can be expected for a certain duration, and the probability of exceedance of the maximum estimate. The total number of waves for a specific duration is calculated with equation 3.8 in which the duration (D) and average zero-crossing wave period are used. The average zero-crossing wave period (T_2) is calculated with equation 3.7 in which both the zeroth-order- and second-order spectral moment are used. The probability of exceedance for the most probable maximum is 63% but maximum expected values can also be calculated for other probabilities of exceedance for which P_e in equation 3.9 is used. Equation 3.9 can also be written as equation 3.10 in which f_{max} represents the factor by which the significant response has to be multiplied to obtain the maximum expected value.

$$T_2 = 2\Pi \cdot \sqrt{\frac{m_0}{m_2}} \tag{3.7}$$

$$N = \frac{duration[s]}{average\ zero-crossing\ wave\ period} = \frac{D}{T_2} \tag{3.8}$$

$$H_{max} = \sqrt{\frac{1}{2} \cdot ln(N \cdot \frac{63}{P_e})} \cdot H_{sig} \tag{3.9}$$

$$H_{max} = f_{max} \cdot H_{sig} \tag{3.10}$$

There are no guidelines as to what probability of exceedance should be used, when maximum estimates are determined for specific offshore operations. One could argue that a most probable maximum response for a 3-hour period is not a correct design parameter because it is calculated with a probability of exceedance of 63%. On the other hand, the lifting operation might only take 30 minutes instead of three hours. For these reasons, parameters are selected that fit the operation of turbine maintenance and the impact of changing the duration and probability of exceedance on the maximum response is investigated. Whereas formula 3.10 can be used to obtain the maximum expected wave height from a wave spectrum, it can also be used to obtain the maximum expected response from a response spectrum of the crane motions. For a three hour duration and a probability of 63 % of a JONSWAP wave spectrum with a zero crossing period (T_2) of 9.5 seconds, the f_{max} factor will be 1.876.

Duration

To determine the maximum expected compensating crane motions during the operation, the duration of the operation is to be estimated. The focus of the motion compensation system is such, that it is only activated when the load is already in close proximity of the structure which reduces the duration of the motion compensating cycle. Also, necessary preparations will have been made in order to quickly secure the turbine blade to the structure. The shorter the operation, the less time there will be for something unexpected to happen. Therefore an estimate of 30 minutes is used, for the phase of the operation in which the load is close to the structure and the crane tip motions have to be compensated for in order to prevent a collision of the load with the structure. This duration will influence the maximum expected value of the compensating motions, which in their turn will influence the estimated performance of the cranes drive system. For every operation, the duration can be different and to illustrate the impact of a changing duration, this has been plotted in figure 3.7. In this figure it can be seen that for increasing durations the maximum factor f_{max} increases and espacially for shorter durations, large differences can be expected. However, from this graph it can also be

said that an increase of the duration from 30 to 60 minutes will have an impact on the maximum estimates that is smaller than 5%. The calculation of this maximum factor originates from the method to determine the maximum expected wave height from a wave spectrum. However, the same method can be used to determine the maximum expected crane response from the response spectrum of the crane motions. One note is to be made, in irregular wave analysis, a minimum duration of time signals must be used to ensure stationarity of the wave signal. By DNV-RP-C205, the interval for stationarity can range from 30 minutes to 10 hours [4] to which the analysis is limited.

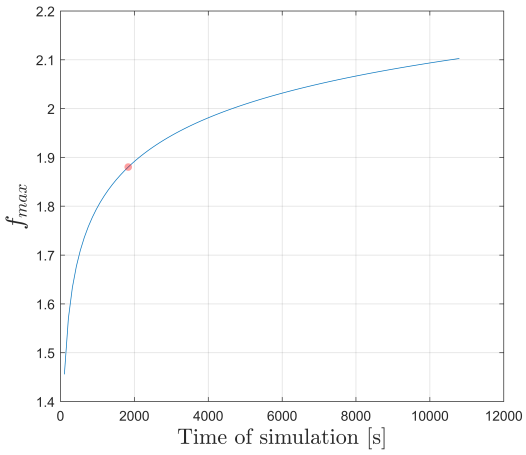

Figure 3.7: Increasing f_{max} versus increasing duration of the operation for a JONSWAP spectrum with a zero-crossing period of 9.5 seconds.

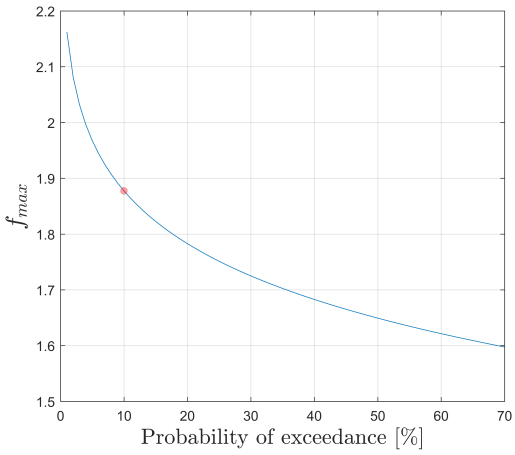

Figure 3.8: Decreasing f_{max} versus increasing probability of exceedance for a JONSWAP spectrum with a zero-crossing period of 9.5 seconds.

Probability of exceedance

For the probability of exceedance of the maximum response, a parameter has to be selected that fits the purpose of the operation as well. As figure 3.8 illustrates, the maximum factor f_{max} (same trend for maximum response) increases for lower probabilities of exceedance. While the 63 % of the most probable maximum seems to be too much, it is essential to realize what the will happen if the maximum expected response is exceeded and whether this is problematic. Depending on the phase of the operation, a slightly higher maximum response than designed for, would not directly lead to major issues because small motions of the load will not cause problems when the load is not near the structure. However, when the load is fixed to the structure and also still suspended by the crane, a potentially dangerous situation could present itself when the motions exceed the capacity of the drive system. To select a parameter for the probability of exceedance the same holds as with the duration, it is not one specific parameter which is correct and it is important to note that it can be different for each specific operation. Within this study a probability of exceedance of 10 % is selected. This means that during a 30-minute period, with average wave periods of 9 seconds, 20 individual waves will exceed the design value. The main reason why such a low probability of exceedance is selected is because when one single wave, or periodic crane motion, exceeds the limit of the drive system, the control system of the compensation mechanism can compensate for this error in the following waves because it will have spare capacity for the compensating motion. However, when multiple successive waves exceed the design limit, the error of the compensating system is expected to increase.

Now that a duration of 30 minutes - 1800 seconds is used together with a probability of exceedance of 10%, a maximum factor (f_{max}) by which the significant response is to be multiplied of 1.882 is obtained. When comparing this to the maximum factor of a three-hour, most probable maximum (1.875), it can be concluded that the difference is very small. For the chosen parameters, the small difference is a coincidence but when longer duration's, or smaller probabilities of exceedance are used, the f_{max} factor will increase and therefore the maximum crane responses will increase which leads to higher requirements of the motion compensation system. For the design of a motion compensated crane, the definition of the operation determines what probability of exceedance is logical to use. The impact of a larger wave than designed for can be assessed for different criteria. The position control system can fail, but in a worst case scenario the wind turbine can be

damaged by collision, and even the crane structure can fail which will lead to permanent damage and even injuries or loss of life. In chapter 6, the consequences of a larger wave than the design value are listed and based on the these impacts the risk factor for the largest wave can be altered.

3.2. Crane RAOs

By superposition, the RAOs of the vessel can be used to determine RAOs of the compensation motions of the crane to keep the crane tip in position. These RAOs will describe the relation between the crane response and the wave conditions under the assumption of a rigid crane structure. To be able to determine the motions in any arbitrary point and orientation with respect to the vessels Center of Gravity, the system is linearized. Because the motions of the ship, in wave conditions of H_{sig}=3 meters are small (< 5°), the small angle approximation is used. The error that is made by using the small angle approximation is estimated in appendix F.

The transformation from vessel RAOs to crane RAOs is done by multiple transformation matrices. These matrices are multiplied with the vector of the vessel motions ($\bar{r}_{Vessel}$) to obtain the compensating crane motions. From the RAOs of the vessel in its CoG, the RAOs at the crane-tip are determined by using the coordinates of the crane tip's position in the global axis system. From these crane-tip RAOs, the next step is to rotate the axis frame of the tip RAOs by the slewing angle to align one of the horizontal axes with the direction of the boom. In the final step, the RAOs of the compensating crane motions are obtained. These steps will be described in more detail within this chapter. In all calculations, RAO's are added as complex numbers. This way both the amplitude and phase information is retained. With equations 3.11 to 3.14 the transformation from amplitude- (A_{surge}) and phase (ϕ_{surge}) RAOs to the complex notation is described.

$$A_{surge} \qquad \phi_{surge} \tag{3.11}$$

$$RE_{surge} = A_{surge} \cdot cos(\phi_{surge}) \tag{3.12}$$

$$IM_{surge} = A_{surge} \cdot sin(\phi_{surge}) \tag{3.13}$$

$$CO_{surge} = RE_{surge} + i \cdot IM_{surge} \tag{3.14}$$

By applying linear superposition, a transformation matrix can be derived to relate the vessels motions to the motions of the crane tip, where the position of the crane tip is determined by X_{tip}, Y_{tip} and Z_{tip} in the global coordinate system.
The transformation matrix from vessel CoG to crane tip is:

$$\begin{bmatrix} RAO_{TipX} \\ RAO_{TipY} \\ RAO_{TipY} \end{bmatrix} = \begin{bmatrix} 1 & 0 & 0 & 0 & Z_{Tip} & -Y_{Tip} \\ 0 & 1 & 0 & -Z_{Tip} & 0 & X_{Tip} \\ 0 & 0 & 1 & Y_{Tip} & -X_{Tip} & 0 \end{bmatrix} \cdot \begin{bmatrix} RAO_{Surge} \\ RAO_{Sway} \\ RAO_{Heave} \\ RAO_{Roll} \\ RAO_{Pitch} \\ RAO_{Yaw} \end{bmatrix} = \boldsymbol{M}_{Tip} \cdot \bar{r}_{Vessel} \tag{3.15}$$

From the tip displacements, the compensating motions of the crane are approximated. For the PMOC, the slew angle α and the boom angle β (figures 3.9 and 3.10) can be controlled by the operator and together they determine the position of the crane tip in the horizontal plane of the global axis system. By changing the boom- and slew angle of the crane, the crane will be able to compensate for the tip motions and therefore the RAOs of the changing boom and- slew angle can be linked to those of the tip motions. The compensation mechanism is focused to compensate the tip motions in the horizontal plane with the boom itself and use the AHC system for vertical compensation. The vertical displacements that are a result of the compensating motions of the boom are coupled to the response of the AHC system. Additional transformation matrices are required to obtain the 'Slew', 'Luff' and 'Hoist' RAOs so that the RAOs of the vessel in its COG can be directly coupled to the compensating motions of the crane.

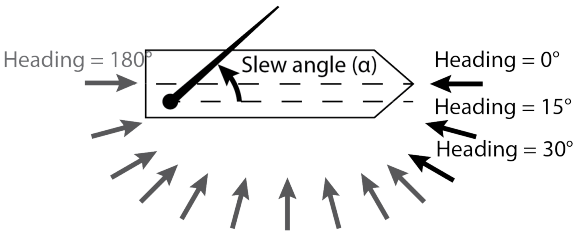

Figure 3.9: Conventions of the slewing position and the vessel headings.

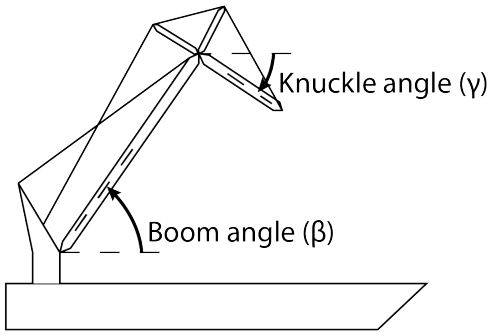

Figure 3.10: Conventions of the boom angle (β) and knuckle angle (γ) of a HBC crane. The convention of the boom angle is the same for the PMOC.

By equation 3.16, the local axis system at the crane tip is rotated around the Z-axis with the slewing angle. By doing this, the X-axis is aligned with the boom direction in the horizontal plane which can be seen in figure 3.11 where a slewing angle of -30 °is used corresponding to the slewing angle of design case 1.

$$\begin{bmatrix} RAO_{TipX'} \\ RAO_{TipY'} \\ RAO_{TipZ'} \end{bmatrix} = \begin{bmatrix} cos(\alpha) & -sin(\alpha) & 0 \\ sin(\alpha) & cos(\alpha) & 0 \\ 0 & 0 & 1 \end{bmatrix} \cdot \begin{bmatrix} RAO_{TipX} \\ RAO_{TipY} \\ RAO_{TipZ} \end{bmatrix} = \boldsymbol{M}_{Rotate} \cdot \boldsymbol{M}_{Tip} \cdot \bar{r}_{Vessel} \tag{3.16}$$

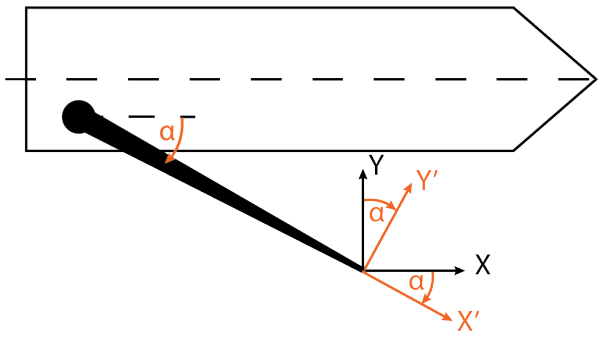

Figure 3.11: Rotating the axis system of the tip of the boom by a slew angle.

After aligning the boom and the X-axis of the local coordinate sytem, the 'Slew', 'Luff' and 'Hoist' RAO's are calculated with equation 3.17. These RAO's are calculated in $radians/m$ and can be used to calculate the crane response for different wave conditions. In equation 3.17, $center_{pivot}$ denotes the distance between the pivot and the slewing axis. In figures 3.12 and 3.13 illustrations are shown in which the different lengths, that are used in equation 3.17 are indicated. It is important to note that a multiplication of the matrices in a different order will lead to different results.

$$\begin{bmatrix} RAO_{Slew} \\ RAO_{Luff} \\ RAO_{Hoist} \end{bmatrix} = \begin{bmatrix} 0 & \frac{1}{cos(\beta) \cdot L_{boom} + center_{pivot}} & 0 \\ \frac{-1}{sin(\beta) \cdot L_{boom}} & 0 & 0 \\ \frac{-1}{tan(\beta)} & 0 & 1 \end{bmatrix} \cdot \begin{bmatrix} RAO'_{TipX} \\ RAO'_{TipY} \\ RAO'_{TipZ} \end{bmatrix} = \boldsymbol{M}_{PMOC} \cdot \boldsymbol{M}_{Rotate} \cdot \boldsymbol{M}_{Tip} \cdot \bar{r}_{Vessel} \tag{3.17}$$

Not only RAOs for displacements, but also RAO's for velocity and acceleration of the different motions have to be determined to continue with the drive calculations afterwards. These are obtained by differentiating equation 3.18 in which discrete regular waves are assumed by which the resulting $\dot{\omega}$ term is not incorporated, see equations 3.18 to 3.20.

$$x = A \cdot sin(\omega t + \phi) \tag{3.18}$$

$$v = \omega \cdot A \cdot cos(\omega t + \phi) = \omega \cdot A \cdot sin(\omega t + \phi - \frac{\pi}{2}) \tag{3.19}$$

$$a = -\omega^2 \cdot A \cdot sin(\omega t + \phi) = \omega^2 \cdot A \cdot sin(\omega t + \phi - \pi) \tag{3.20}$$

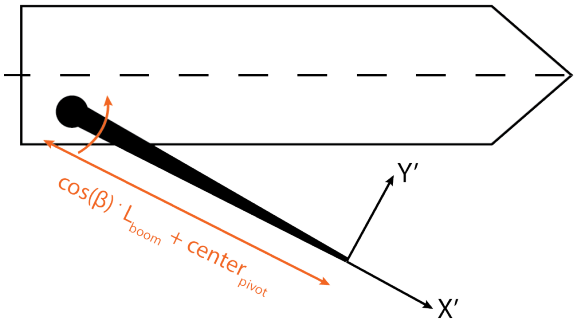

Figure 3.12: Determining the required slewing motion to compensate for the crane tip motions in the Y' direction of the local axis system at the crane tip.

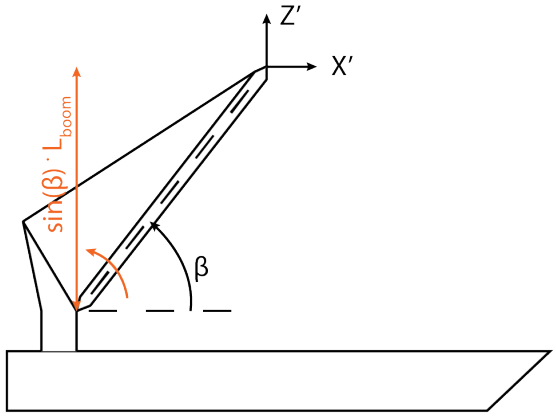

Figure 3.13: Determining the required luffing motion to compensate for the crane tip motions in the X' direction of the local axis system at the crane tip.

3.2.1. Hybrid boom modelling

To determine the compensating motions of the HBC, an extra degree of freedom is introduced. This type of crane can rotate the knuckle and with this rotation, manipulate lifting height and horizontal projected length of the boom in the local X' direction. It is necessary to choose a control strategy for the HBC as it can compensate motions along the X'-axis of the local coordinate system at the crane tip by 2 actions, rotating the boom, and rotating the knuckle. This control strategy will determine with what ratio the boom, and knuckle, are used for compensating tip motions. To couple these two compensating mechanisms, a constraint is introduced. The summed vertical displacement of the combination of individual boom and individual knuckle motion must be zero, which is a so-called 'level luffing' criterion (see figure 3.14). In this context, vertical displacement is measured in the local coordinate system of Center of Gravity of the vessel. The relation that follows from this constraint is derived in equation 3.21.

Relative vertical displacement of the crane tip is zero $\Delta Z = 0$

$$\begin{aligned} \Delta Z = 0 &= (sin(\beta + \Delta\beta) - sin(\beta)) \cdot L_{boom} + (sin(\gamma + \Delta\gamma) - sin(\gamma)) \cdot L_{knuckle} \\ = \frac{\Delta\gamma}{\Delta\beta} &= (sin^{-1}(sin(\gamma) + \frac{(sin(\beta + \Delta\beta) - sin(\beta)) \cdot L_{boom}}{L_{knuckle}}) - \gamma) / \Delta\beta \end{aligned} \tag{3.21}$$

Using this relation, a displacement of the tip along the x-axis in the local coordinate system at the crane tip, induces a rotation of both the boom and the knuckle. This relation is later on used in the transformation matrix for the HBC in equation 3.23

$$\begin{aligned}\Delta X_{tip} &= \Delta X_{By\ luffing} + \Delta X_{By\ rotating\ knuckle} \\ &= sin(\beta)\cdot L_{boom}\cdot\Delta\beta + sin(\gamma)\cdot L_{knuckle}\cdot\Delta\beta\cdot\frac{\Delta\gamma}{\Delta\beta}\end{aligned} \tag{3.22}$$

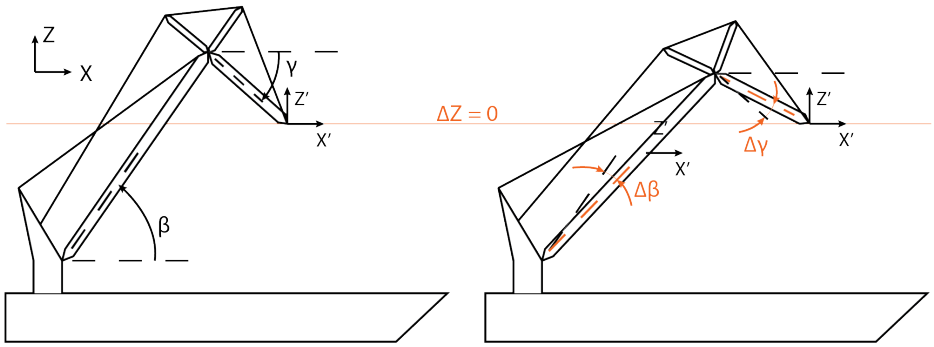

Figure 3.14: The rotation of the boom and knuckle are coupled and compensate for X'. The total vertical displacement of the crane-tip is zero in the local coordinate system of the CoG.

The initial tip RAOs are calculated in the same manner as done for the PMOC crane, even though there is an extra factor influencing the tip location (the length of the knuckle) which is included in X_{tip} in equation 3.15. A new transformation matrix is established to determine the crane RAOs. This new matrix (equation 3.23) replaces equation 3.17:

$$\begin{bmatrix} RAO_{Slew} \\ RAO_{Luff} \\ RAO_{Hoist} \end{bmatrix} = \begin{bmatrix} 0 & \frac{1}{cos(\beta)\cdot L_{boom}+pivot+cos(\gamma)\cdot L_{knuckle}} & 0 \\ \frac{-1}{sin(\beta)\cdot L_{boom}+\frac{\Delta\gamma}{\Delta\beta}\cdot sin(\gamma)\cdot L_{knuckle}} & 0 & 0 \\ 0 & 0 & 1 \end{bmatrix} \cdot \begin{bmatrix} RAO'_{TipX} \\ RAO'_{TipY} \\ RAO'_{TipZ} \end{bmatrix} \tag{3.23}$$

$$= \boldsymbol{M}_{HBC}\cdot\boldsymbol{M}_{Rotate}\cdot\boldsymbol{M}_{Tip}\cdot\bar{r}_{Vessel}$$

After determining the RAO of the boom motion (RAO_{Luff}), the RAO of the knuckle motion can simply be obtained by multiplying the boom rotation RAO with the conversion factor described in equation 3.21.

3.2.2. X-Y table modelling

For the Motion Compensated Crane Concept, the motions of the crane to compensate for the vessel motions are not very complicated. In this concept, the tip is the location of the suspended hoist rope within the X-Y frame. At this position, the motions in the horizontal frame are calculated with the tip RAOs that are rotated by the slewing angle. The boom of the crane itself will not be actively controlled while compensating, only for the initial positioning of the load. To obtain the motion RAOs of the X-Y compensating mechanism, equation 3.24 is used.

$$\begin{bmatrix} RAO_{Table_X} \\ RAO_{Table_Y} \\ RAO_{Table_Z} \end{bmatrix} = \boldsymbol{M}_{Rotate}\cdot\boldsymbol{M}_{Tip}\cdot\bar{r}_{Vessel} \tag{3.24}$$

3.3. Results & discussion

In this section, both the differences between lifting positions, and differences between crane types are elaborated on with the use of the calculated RAOs. For all three different types of cranes, RAOs and response spectra for all motions are obtained. From the response spectra, maximum expected responses are determined which function as input for chapter 4.

3.3.1. RAOs

The vessel RAOs that are calculated by ANSYS AQWA are known for 13 different vessel headings, ranging ranging from 0° to 180° with an increment of 15° (see figure 3.9). Therefore, the RAOs of the crane motions are also calculated for these 13 headings by the Matlab model that hase been developed. However, as described in chapter 2, only headings of +-30°are used for the motion compensation design criteria. The other headings are not used within this study but can be interesting in the future for workability estimates for specific wave conditions or failure mode analysis. Figure 3.15 displays the RAO of the slewing amplitude for design case 1. The first plot contains all headings, the second plot contains headings 0°, 15°, 30° and the third plot only contains the largest RAO of these three, in this case the one for an incoming wave angle of 30°. Throughout the research, not all heading RAOs will be plotted for clarity purposes, only the largest of the heading constraint.

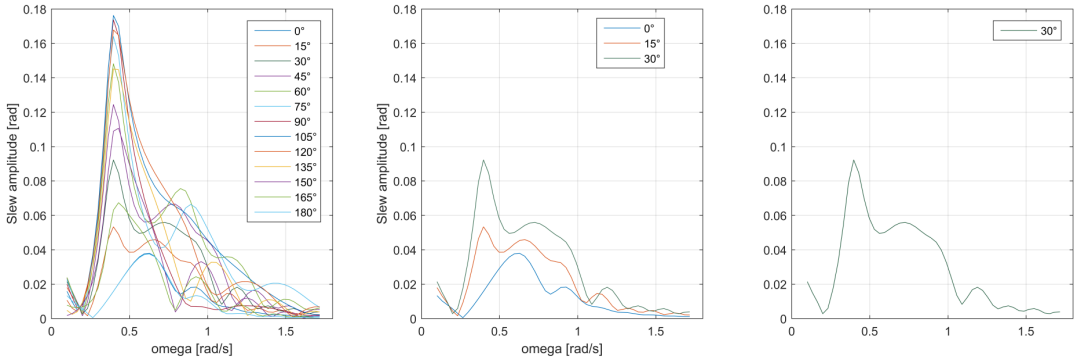

Figure 3.15: Example of the RAO of the slewing amplitude of the PMOC for design case 1 with different headings.

Pedestal Mounted Offshore Crane

Figure 3.16 contains the slewing, luffing and hoisting RAOs for the PMOC in all 4 design cases. As a result of the differences between the position of the tip in the design cases, changes in the crane RAOs are expected. When design case 2 and 3 are compared it is noted that their RAOs are almost exactly the same. This is explained by the slewing angle that is the same for both design cases. Only the luffing angle is slightly smaller for design case 3, which leads to a larger outreach from the vessel. Because the reach over the side of the vessel is larger, the slewing compensation mechanism is more effective which results in smaller slewing amplitudes. Also, interesting differences are observed between design case 3 and 4. In design case 3 the pitching motion of the vessel is compensated mainly by slewing the crane. Here vessels roll motion is strongly coupled to the luffing motion and the natural roll period of the vessel at 0.4 rad/s can be identified in the luffing RAO as it would be expected. In design case 4 this is the other way around, and the slewing motion has to compensate for the roll motions of the vessel. For normal, vessel shaped hulls, the roll motion is the most unstable degree of freedom. This means that for certain wave periods, a very large roll amplification can be expected. In the design of a vessel, the natural period of the roll motion can be adjusted by changing the vessels stiffness and inertia. Depending on the wave conditions at offshore wind farms, some vessels can have a large advantage above others when their natural roll period is larger than the average wave period. In operation, the crane should be lifting in a position in which the most effective compensation mechanism (either slewing or luffing for the PMOC) is coupled to the largest vessel motions that are expected for a specific peak wave period. The performance of the slewing motion and luffing motion can be assessed after they are coupled to the drive and structural requirements.

The hoisting motion is mainly related to the distance between the CoG of the vessel and the crane-tip in the horizontal plane. Design case 4 induces the largest vertical motions at the crane tip, which is explained by the distance between the tip and the COG of the ship.

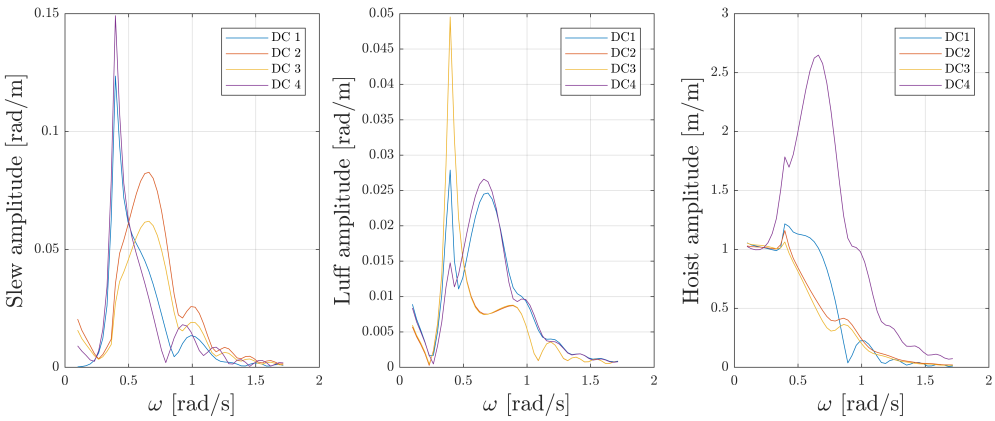

Figure 3.16: RAOs of the PMOC for different design cases with a maximum wave angle of 30°.

Hybrid Boom Crane

The RAOs of the HBC are displayed in figure 3.17 where generally the same crane response can be observed. The horizontal distance between the tip and the slewing axis is the same for both cranes. Therefore, it is expected that the slewing response will be the same for both crane types and this is indeed the case.

For a normal crane, the luffing motion is very slow because there are multiple falls in the boomhoist. The working principle of the boomhoist is explained in more detail in chapter 4. One of the main differences with the PMOC is the fact that the RAO for the luffing motion is significantly lower, although the displacements at the tip are the same. This is a result of the knuckle motion which is relieving the luffing motion of large amplitudes. The weight of the knuckle is much lower than that of the main boom and this will be advantageous for the drive requirements. The RAO of the knuckle is a factor of the luffing RAO because of the level-luffing assumption described in section 3.2.1, this explains the similar RAO shapes. For a changing knuckle angle, the relation between response of the luffing motion and knuckle motion will change (equation 3.21). The difference in knuckle angle between design case 2 and 3 is small and the effect on the luffing and knuckle RAO is present but very small as well. Another interesting difference with the PMOC RAOs is shown in the hoisting amplitude response. For the PMOC, the compensating luffing motion automatically compensates for vertical tip motion when it is compensating for vessel rotations. For example, when the slewing angle is zero (as in figure 3.13), a pitching motion of the vessel will induce a positive displacement along X', and a negative displacement along Z'. When the crane uses its luffing motion to compensate for X', it wil automatically generate a positive displacement along Z'. The level-luffing criteria of the HBC actually imposes larger hoisting amplitudes because the vertical component that is linked to the compensation along the length of the boom with the PMOC is eliminated. Depending on the capacity of the heave compensation system, the level-luffing criterion might not be the best relation to use when the luffing motion and knuckle motion of the HBC are coupled.

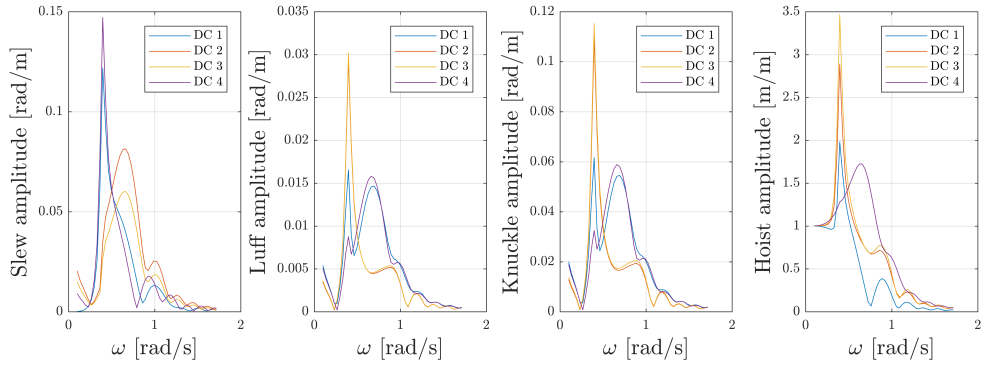

Figure 3.17: RAOs of the PMOC for different design cases with a maximum wave angle of 30°.

Motion Compensated Crane Concept
For the MCCC crane, the RAOs are practically the tip RAOs although they are rotated around the slewing axis by the slew angle of the crane. The RAO in Y-direction can be compared to the slewing RAO for the PMOC and HBC. In figure 3.18 the RAOs for all 4 design cases are shown. From these RAOs, design case 1 proves itself as the most optimal position when compensation motions are to be minimized, disregarding the wave periods that can be expected at the location of operation.

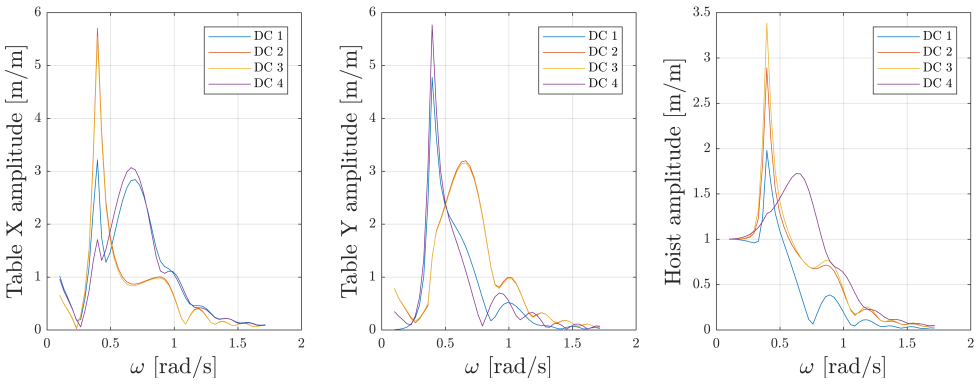

Figure 3.18: RAOs of the MCCC for different design cases with a maximum wave angle of 30°.

3.3.2. Responses & Maxima

Just as it can be done for wave heights, most probable maximum values can be determined for the crane motions. The response spectra of all crane motions follow from equation 3.4. Also, the significant value of the compensating motions follows from the integrated area of the response spectrum and is calculated with equation 3.6. For a significant wave height of 3 meters and a peak period of 8 seconds (following from section 3.1.1), maximum tip responses are calculated for design cases 1 to 4 with the use of equation 3.9. These are the tip responses in the local coordinate system at the crane tip. The maxima are calculated for a 30 min period with a probability of exceedance of 10% and because the maximum responses are linearly related to the maximum factor f_{max}, the sensitivity of these results is the same as that of f_{max}, see figures 3.8 and 3.7). The values displayed in table 3.2 are maximum amplitudes of the headings up to 30°.

Crane tip responses								
Maximum responses	Case 1	X	Y	Z	Case 2	X	Y	Z
Displacement $[m]$		5.62	2.27	0.77		2.39	5.67	1.81
Velocity $[m/s]$		4.31	1.63	0.60		1.94	4.25	1.43
Acceleration $[m/s^s]$		3.40	1.23	0.50		1.63	3.28	1.18
Maximum responses	Case 3	X	Y	Z	Case 4	X	Y	Z
Displacement $[m]$		2.32	5.56	1.87		5.73	1.63	3.22
Velocity $[m/s]$		1.88	4.16	1.49		4.34	1.22	2.45
Acceleration $[m/s^s]$		1.58	3.21	1.23		3.40	1.00	1.93

Table 3.2: Maximum expected response amplitudes of the crane-tip for a wave spectrum with Hsig=3 meters and Tp=8 seconds in a 30 minute period with a probability of exceedance of 10 %

The maximum responses indicate a larger pitching motion of the vessel than the rolling motion because the response in Y-direction is larger for design case 2 than that of the X-direction. When the RAOs for this specific situation are observed, it can be seen that for the peak wave period that has been used (8 seconds=0.78 rad/s), the pitching RAO of the vessel is close to its natural period and is also larger than the roll RAO of the vessel. Figure 3.19 displays the roll and pitch RAO in which the green marks indicate the peak wave period of 8 seconds.

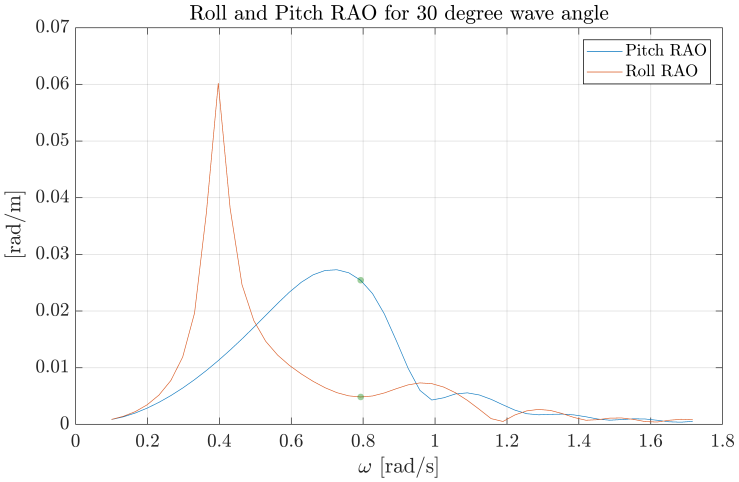

Figure 3.19: RAO of the roll- and pitch amplitude of the vessel for wave heading 30°.

The maximum expected response amplitudes of the crane motions for a 30 minute operational window are displayed in table 3.3 and 3.4. For the MCCC, the motion responses that the compensation mechanism has to handle are the same as the tip responses that are displayed in table 3.2.

PMOC crane responses								
Maximum responses	Case 1	Slew	Luff	Hoist [m]	Case 2	Slew	Luff	Hoist [m]
Rotation $[rad]$		0.059	0.049	1.611		0.147	0.021	1.095
Velocity $[rad/s]$		0.043	0.038	1.177		0.110	0.017	0.853
Acceleration $[rad/s^s]$		0.032	0.030	0.877		0.085	0.014	0.069
Maximum responses	Case 3	Slew	Luff	Hoist [m]	Case 4	Slew	Luff	Hoist [m]
Rotation $[rad]$		0.111	0.021	0.913		0.042	0.050	4.962
Velocity $[rad/s]$		0.083	0.017	0.711		0.032	0.038	3.772
Acceleration $[rad/s^s]$		0.064	0.014	0.577		0.026	0.030	2.960

Table 3.3: Maximum expected responses of the compensating motions of the PMOC for a wave spectrum with H_{sig}=3 meters and T_p=8 seconds in a 30 minute period with a probability of exceedance of 10 %.

HBC crane responses										
Maximum responses	Case 1	Slew	Luff	Knuckle	Hoist	Case 2	Slew	Luff	Knuckle	Hoist
Rotation $[rad]$		0.058	0.029	0.109	0.766		0.145	0.012	0.046	1.808
Velocity $[rad/s]$		0.042	0.022	0.083	0.598		0.109	0.010	0.037	1.431
Acceleration $[rad/s^s]$		0.032	0.018	0.066	0.498		0.084	0.008	0.031	1.176
Maximum responses	Case 3	Slew	Luff	Knuckle	Hoist	Case 4	Slew	Luff	Knuckle	Hoist
Rotation $[rad]$		0.107	0.013	0.049	1.887		0.042	0.030	0.111	3.217
Velocity $[rad/s]$		0.080	0.010	0.040	1.502		0.031	0.023	0.084	2.448
Acceleration $[rad/s^s]$		0.062	0.009	0.033	1.242		0.026	0.018	0.066	1.925

Table 3.4: Maximum expected responses of the HBC motions for a wave spectrum with H_{sig}=3 meters and T_p=8 seconds in a 30 minute period with a probability of exceedance of 10 %. The unit of the hoisting amplitudes is [m] instead of [rad].

The goal of this chapter was to determine the motions that the crane has to make to compensate for the crane tip motions that are a result of the vessel motions. In the tables above, the maximum expected crane motions are listed. When these motions are known, they function as input for the next module of the feasibility analysis. The values calculated in this chapter are specifically calculated for one single wave condition ($H_{sig} = 3m$, $T_p = 8s$) whereas the exact wave conditions will vary per installation location and changing weather conditions. The method used to estimate maximum crane responses can be used for any sea state.
In the 'Crane drive system' module, the drive system is analyzed and the performance of each crane in its current configuration is determined and compared.

4

Crane drive system

To determine the system performance of the crane, the motions calculated by the spectral analysis have to be coupled to the properties of the cranes drive system. Crane configuration, weights, gearing ratio's, inertia's and reeving diagrams are important to model the system correctly. All three different cranes have a different geometric lay-out and the performance of their motion compensating abilities is to be assessed. In the previous section, the location of the tip was the most important, at this stage the set-up of the drive system is important. To compare the different crane types, their performance is assessed by calculating their workability. Within these workabilities, different parameters of the drive system will be plotted such as the torque and power that are required for the compensating motions of the crane by which the limiting mechanisms of the crane can be identified. In this chapter it will be explained how these calculations are performed and afterwards the resulting workability for the PMOC, HBC and MCCC will be discussed.

4.1. General lay-out of the drive system

The slewing motion is identical for all three cranes. For the PMOC and HBC, the slewing motion will be used for motion compensation, the MCCC will not use slewing for compensation. In the design of all three crane, the cranehouse is mounted to the vessel by the slew bearing (see figure 2.6 for the position of the slew bearing). The slew bearing is designed such that it can withstand the overturning moment when the crane moves the load overboard and it is positioned at the base of the cranehouse. The slew bearing is one of the most critical, and also expensive, components of the crane. On the inside of the slew bearing, a gearing is constructed such that the slew motion can be powered by an electric or hydraulic motor (see figure 4.1). Multiple slewdrives can be combined where the limiting factor will be available space within the cranehouse. Within the slew bearing, an encoder measures the slew position, speed and acceleration of the slewing motion which is used to control the slewing motion.

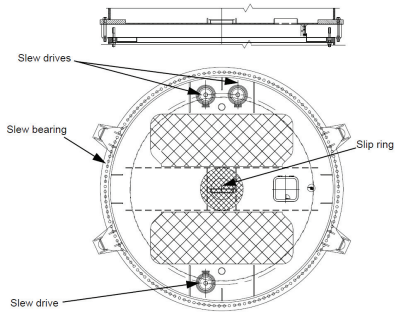

Figure 4.1: General configuration of the slewing system of the PMOC crane. A total of three slewmotors are used which are fixed to the pedestal.

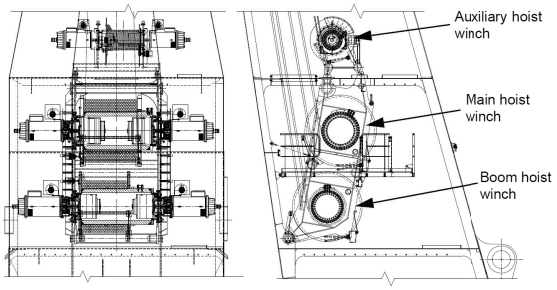

Figure 4.2: Winch lay-out within the cranehouse of an offshore crane.

The luffing motion of the crane is controlled by the boomhoist winch, which is positioned inside the crane-house as illustrated in figure 4.2. With the boomhoist winch, the length of the boomhoist can be adjusted, resulting in a luffing motion of the crane. For almost every offshore crane, the boomhoist has multiple falls to decrease the line pull in the steel wires, introducing a transmission ratio between the luffing motion and the rotating boomhoist winch. This transmission ratio depends on the number of falls that is used and can be schematically represented in a reeving diagram. An example of a reeving diagram is shown in figure 4.3. The number of falls that are used within a boomhoist configuration, and therefore the transmission of the boomhoist configuration, is part of an optimization process. When less falls are used, the wire diameter of the boomhoist wire will increase. Also the diameter of the guiding sheaves of the boomhoist configuration will increase, leading to higher costs and limitations in the design process. As stated earlier, the slow luffing motion is expected to limit the motion compensating performance of the crane and now that the working principle of the luffing motion is explained it can be said that the number of falls in the boomhoist configuration is a system parameter which cannot easily be reduced.

The rotation of the knuckle of the HBC is actuated by a winch as well. The same configuration as for the boomhoist is used, usually with less falls. The reason for this is that the overturning moment around the pivot is much larger than the overturning moment around the tip of the mainboom because the moment arm of the knuckle is smaller than that of the mainboom. Both the boom and knuckle position are directly controlled by their winches. A winch assembly consists of a drum, and a drive-train on both sides of the drum as illustrated in figure 4.4. The drive-train consists of an E-motor, gearbox, brake and cooling fan. All E-motors are controlled by invertors, which control the input frequency and voltage of the AC-motor.

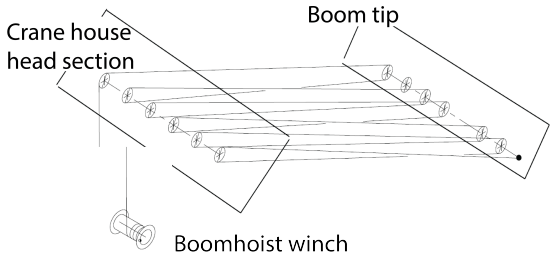

Figure 4.3: Example of a reeving diagram for a PMOC. For the PMOC in this study, a total of 15 falls is used in the boomhoist.

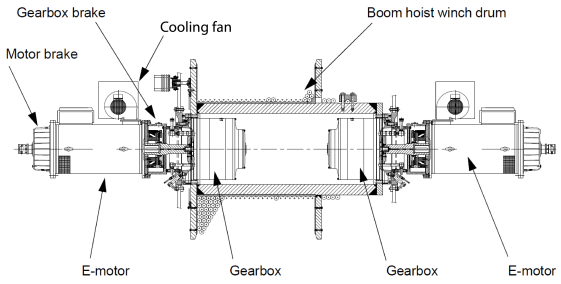

Figure 4.4: General assembly of a the drivetrain of a winch including the drum, E-motors, gearboxes, brakes and cooling fans.

4.2. Loads

To assess the motion compensating performance of the crane, the loads that are present during the motion compensating cycle are determined. In total, two different loading mechanisms are identified that have to be counteracted by the drive system of the crane. These two loads are gravitational loads and dynamic loads where the gravitational loads follow from the masses that are present within the system and the position of the crane and the dynamic loads follow from the compensating motions that the crane has to perform. Both of these loads will be changing while the vessel is moving in waves. The loading mechanisms will be discussed and later on combined so that the total load on the drive system can be estimated. In figure 4.5 an overview can be found of the different load components and the factors influencing them.

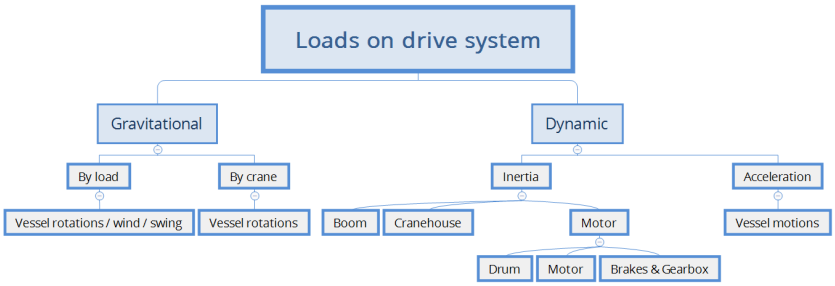

Figure 4.5: Overview of the load inducing mechanisms.

Gravitational load

The gravitational load will both act on the wind turbine component that is lifted by the crane and also on the crane itself. For the compensating mechanisms of the crane, these gravitational loads will not be constant during the motion compensating cycle. When there are no waves and the vessel has no heel or trim, the gravitational loads on the crane and the wind turbine component will only generate an overturning moment around the pivot by which the boomhoist is loaded. Because the vessel has no heel or trim, the slewing mechanism will not experience any effect of the gravitational loads on the crane. However, when the vessel moves with the waves and the crane compensates for these motions, the gravitational load on the boomhoist will change and also the slewing mechanism will experience loads that are a result of the gravitational forces on both the wind turbine component and the crane itself. Because the gravitational loads change with the vessel motions, these can be coupled to the RAOs of the vessel and a maximum expected value can be determined in the same way this is done for the maximum expected compensating motions of the crane. To do so, RAOs are calculated for the 'virtual' sidelead and offlead angle of the load. Within regular crane terminology, sidelead and offlead angles are defined such as illustrated in figure 4.6. Even though it is assumed that during the compensating cycle the load will not swing, there will be a sidelead and offlead angle as a result of the rotations of the boom while it is compensating. The virtual sidelead and offlead angles that are considered for the gravitational loads are illustrated in figure 4.7.

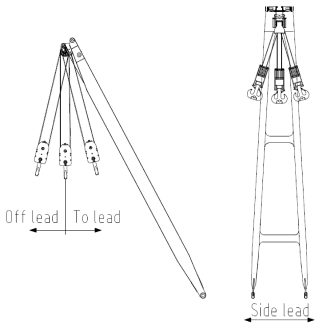

Figure 4.6: Sidelead and offlead of a crane.

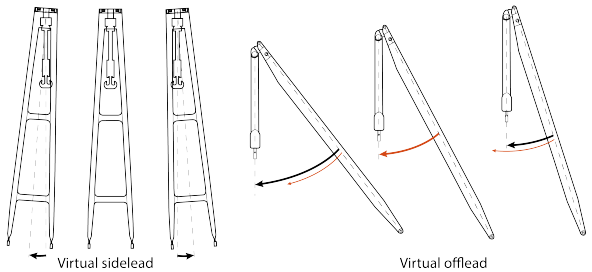

Figure 4.7: Virtual sidelead and offlead used for gravitational loads.

Dynamic load
The second, and also largest, loading component on the drive system of the crane is related to the inertia of the crane. To compensate for the vessel motions, the crane will have to perform compensating motions. It has already been described how the changing crane position will induce gravitational loading but to realize these compensating crane motions, an additional load on the drive system will be generated. This loading mechanism is referred to as dynamic loading and is also described by Newton's second law which states that to accelerate a mass, a force is required. The same hold for a rotational acceleration for which a torque is required to overcome the inertia of the crane and the drive system. The crane motions that are used for motion compensation have a rotational acceleration $\ddot{\omega}$ and with the use of equation 4.1, the dynamic loads on the drive system can be calculated. Whereas the drive system consist of different transmission ratios and different inertia components, the total inertia for the slewing motion, luffing motion, knuckle motion and skid table motions are calculated which are used to obtain the dynamic loads on the drive system.

$$T = I \cdot \ddot{\omega} \tag{4.1}$$

4.3. Inertia

The dynamic loads on the drive system are dependent on the inertia, and the acceleration of the crane. To determine the inertia's of the crane motions, the initial position of the crane is used. However, during the motion compensation cycle, the position of the crane changes and so does the inertia of the compensating motions. Therefore, the maximum response from chapter 3 are used to determine the maximum inertia of the compensating motions that will be present in the cycle. Also, a simplification is made with respect to the influence of the load on the inertia's of the crane. Because the focus of the compensation system will be to keep the load in position, it is assumed that the load will not have impact on the inertia of the compensating crane motions (see figure 4.8 for an example of compensation by slewing). In a situation where the load is kept in position perfectly, the drive system will not experience its inertia because it is not moved. Also, the length of the hoisting rope between the crane tip and the load will act as a horizontal spring between the tip movements and the possible load movements, the inertia of the load will have minor influence when small displacements are concerned. For possible load swing, the model that is used will not be able to correctly estimate the loads on the drive system. Additional sidelead angles will lead to an increase of the gravitational load, but also, the swinging mass will periodically influence the total inertia of the compensating motions.

For each of the compensating crane motions, the method by which the inertia is determined is explained and afterwards inertia distributions are discussed in which the influence of different components is quantified.

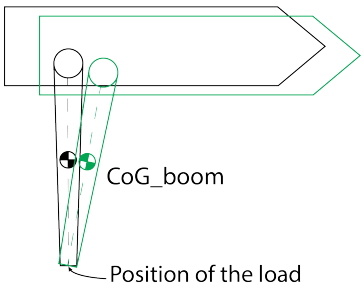

Figure 4.8: The load is assumed to stay in position during motion compensation and therefore the inertia of the load is not taken into account for the drive system calculations.

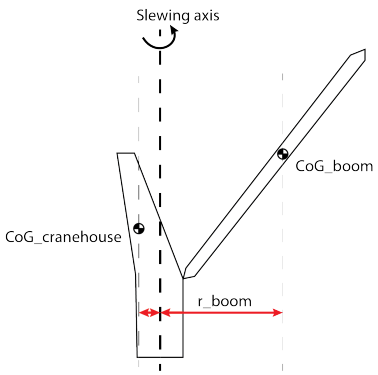

Figure 4.9: Rotational inertia of the boom and the cranehouse around the slewing axis.

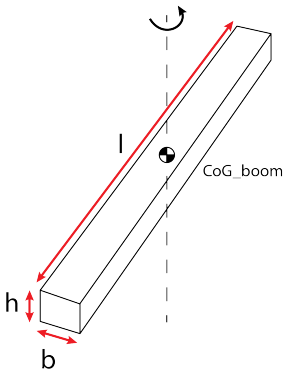

Figure 4.10: Rotational inertia of the boom around around its CoG for the slewing motion.

4.3.1. Slewing motion

To calculate the inertia of the slewing motion (I_{slew}), the mass of the boom is modelled as a point mass at the CoG of the boom and its inertia around the slewing axis ($I_{boom,s}$) is calculated with equation 4.3. This formula is a combination of the rotational inertia of the mass middle point of the boom around the slew axis, and the inertia of the boom around its CoG (equation 4.2, figure 4.10). In figure 4.9, the mass middle point of the boom is displayed and the distance r_{boom} is the moment arm around the slewing axis. This moment arm is a combination of the distance from the slewing axis to the pivot of the boom and the horizontal projected length of the boom which is dependent on the boom angle. During the motion compensating cycle, the boom angle changes while it is used for compensating the tip displacements. This means that the horizontal projected length of the boom changes as well and because r_{boom} is quadratically related to the inertia by equation 4.3, the maximum expected luffing amplitude during the compensation cycle from chapter 3 is used in the calculation of r_{boom}. By doing this, a conservative approach is taken because it is not known whether the maximum amplitude of the luffing compensation is present at the same time as the maximum slewing acceleration.
Not only the boom, but also the cranehouse has a rotational inertia around the slewing axis ($I_{cranehouse}$). For the cranehouse the distance between its CoG and the slewing axis is constant and equation 4.3 is used with the parameters of the cranehouse.
In addition to the inertia of the crane around its slewing axis, the inertia's within the drive system itself ($I_{drivetrain}$) will have to be overcome as well to accelerate the crane. Therefore, the inertia of the crane around the slewing axis is translated to the shaft of the slewmotor at which it can be added to the inertia of the drivetrain to obtain the total inertia of the slewing motion (I_{slew}). To do so, multiple transmission ratio's have to be used which is schematically illustrated in figure 4.11. The E-motor is fitted with a gearbox, and also there is a transmission ratio between the slew motor pinion (i_p) and the slewmotor gearbox (i_g) which is shown in figure 4.1. Equations 4.4 to 4.9 describe the relation between the slewing inertia at the slew-axis of the crane ($I_{boom,s}$) and the inertia of at the shaft of the E-motor ($I_{m,s}$).

$$I_{CoG,s} = \frac{m \cdot (b^2 + (cos(\beta) \cdot l)^2)}{12} \tag{4.2}$$

$$I_{boom,s} = M_b \cdot r_{boom}^2 + I_{CoG,s} \tag{4.3}$$

The inertia of the boom and crane house are translated to the motor axis by the following equations:

$$\omega_{m,s} = \omega_s \cdot i_p \cdot i_g \tag{4.4}$$

$$T_s = I_{boom,s} \cdot \omega_s \tag{4.5}$$

$$T_{m,s} = T_s \cdot \frac{1}{i_p \cdot i_g} \tag{4.6}$$

$$T_{m,s} = I_{m,s} \cdot \omega_{m,s} \tag{4.7}$$

$$I_{m,s} = I_{boom,s} \cdot (\frac{1}{i_g \cdot i_p})^2 \tag{4.8}$$

$$i_{total,s} = \frac{1}{i_g \cdot i_p} \tag{4.9}$$

The total inertia of the slewing motion is the sum of the inertia of the drivetrain and the inertia of the moving masses around the slewing axis.

$$I_{slew} = I_{drivetrain} + \frac{I_{cranehouse} + I_{boom,s}}{i_{total,s}^2} \tag{4.10}$$

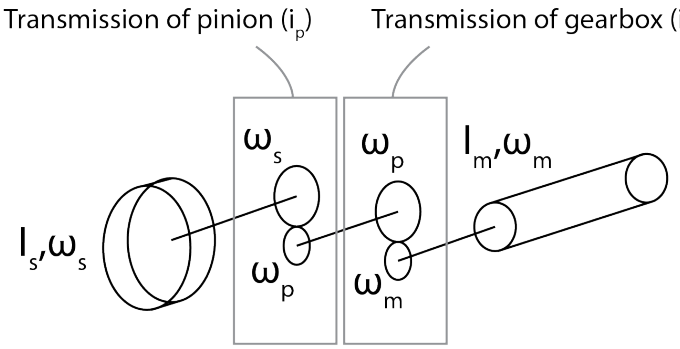

Figure 4.11: Overview of the transmission between the slewing motion and the rotations of the shaft of the slew motor.

4.3.2. Luffing motion

The inertia that is accompanied with the luffing motion is determined by modelling the mass of the boom as a point mass that is located at the CoG of the boom, just as this has been done for the slewing motion. The inertia of the luffing motion therefore consists of the point mass that is to be rotated around the pivot, and the inertia to rotate the boom around its CoG. For the luffing motion, the point mass has to be rotated around the pivot, which is done by changing the length of the boomhoist. The inertia of the boom around the pivot is also translated to the shaft of the E-motor of the boomhoist drive so that it can be added to the inertia of the drivetrain. Both the number of falls ($\eta_{falls,b}$) and the gearbox of the boomhoist drive ($i_{g,l}$) reduce the inertia that is experienced at the shaft of the E-motor of the boomhoist drive. A schematized representation of the luffing system is shown in figure 4.12.

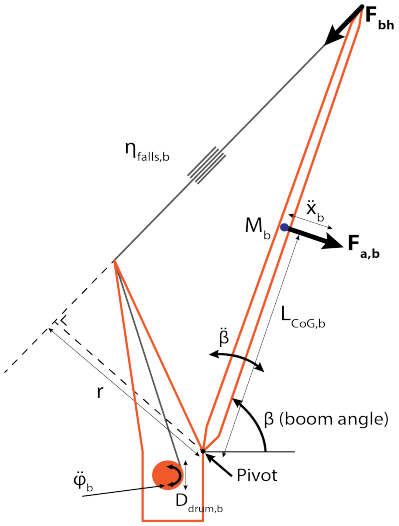

Figure 4.12: Schematic representation of the luffing motion.

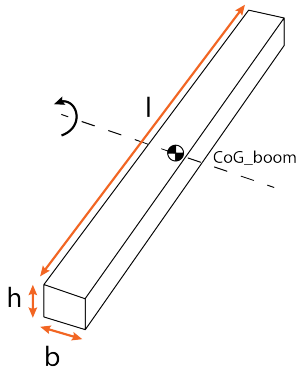

Figure 4.13: Inertia of the boom rotating around its CoG in the luffing motion

To translate the inertia of the boom around the pivot, to the shaft of the E-motor, a different method is used than that for the slewing motion. At first a sum of moments around the pivot is used (equation 4.11) to determine the force in the boomhoist (F_{bh}) as a result of the acceleration of the mass of the boom. By re-writing the parameters, the torque at the shaft of the boomhoist drive ($T_{m,l}$) is related to the force $F_{a,b}$ that is a result of the acceleration of the mass of the boom in equation 4.15. After this, a relation is obtained between the rotational acceleration of the boom ($\ddot{\beta}$) and the rotational acceleration of the shaft of the E-motor ($\ddot{\phi}_b$) in equation 4.16. Now that the torque at the shaft of the E-motor, and the rotational acceleration of the shaft

are related to the mass of the boom and the rotation of the boom, the inertia at the shaft of the E-motor as a result of the mass of the boom can be obtained.

$$\sum M_{pivot} = F \cdot L_{CoG,b} - F_{bh} \cdot r = 0 \tag{4.11}$$

$$F_{a,b} = (M_b + \frac{I_{CoG,l}}{L_{CoG,b}}) \cdot \ddot{x} = (M_b + \frac{I_{CoG,l}}{L_{CoG,b}}) \cdot \ddot{\beta} \cdot L_{CoG,b} \tag{4.12}$$

$$F_{bh} = \frac{F_{a,b} \cdot L_{CoG,b}}{r} \tag{4.13}$$

$$F_{wire} = \frac{F_{bh}}{\eta_{falls,b}} \tag{4.14}$$

$$\begin{aligned} &T_{m,l} = F_{Wire} \cdot \frac{D_{drum,b}}{2 \cdot i_{g,l}} = F_{a,b} \cdot \frac{D_{drum,b} \cdot L_{CoG,b}}{2 \cdot i_{g,l} \cdot r \cdot \eta_{falls,b}} = F_{a,b} \cdot C_b \\ &with \qquad C_b = \frac{D_{drum,b} \cdot L_{CoG,b}}{2 \cdot r \cdot \eta_{falls,b} \cdot i_{g,l}} \end{aligned} \tag{4.15}$$

The rotation of the boomhoist winch is related to the rotation of the boom by:

$$\ddot{\phi_b} = \frac{1}{C_b} \cdot \ddot{x} = \frac{1}{C_b} \cdot \ddot{\beta} \cdot L_{CoG,b} \tag{4.16}$$

$$F_{a,b} = (M_b + \frac{I_{CoG,l}}{L_{CoG,b}}) \cdot \ddot{x} = (M_b + \frac{I_{CoG,l}}{L_{CoG,b}}) \cdot C_b \cdot \ddot{\phi_b} \tag{4.17}$$

$$T_{m,l} = (M_b + \frac{I_{CoG,l}}{L_{CoG,b}}) \cdot C_b^2 \cdot \Delta\ddot{\phi_b} = I_{m,l} \cdot \ddot{\phi_b} \tag{4.18}$$

$$I_{m,b} = (M_b + \frac{I_{CoG,l}}{L_{CoG,b}}) \cdot {C_b}^2 \tag{4.19}$$

The factor C_b^2 is used as a reduction factor for the inertia of the boom around the pivot to the inertia of the boom at shaft of the E-motor of the boomhoist drive. To determine the total inertia of the luffing motion, the inertia of the boom ($I_{m,b}$) can be added to the inertia of the drivetrain in the same way this is done for the slewing motion (see equation 4.10).

For the luffing motion of the HBC, an additional mass is to be rotated around the pivot, being the mass of the knuckle. To incorporate this in the model, the same equations are used as for the PMOC but the mass of the knuckle is accounted for by translating it to the center of gravity of the boom. Therefore, M_b in equation 4.12 is replaced by $M_b + M_k \cdot \frac{{L_{boom}}^2}{{L_{CoG,b}}^2}$.

4.3.3. Knuckle motion

To determine the inertia of the knuckle motion, the same calculation method is used as for the luffing motion. Whereas the boom rotates around the pivot, the knuckle rotates around the tip of the mainboom. A schematized overview of the knucklehoist system is displayed in figure 4.14. The parameters used for the calculation of the inertia of the knuckle motion can also be found in figure 4.14. The moment arm of the boomhoist r is replaced by the moment arm of the knucklehoist r' and the distance $L_{CoG,b}$ is now defined by $L_{CoG,k}$. The mass of the knuckle (M_k) is modelled by a point mass that is located at the CoG of the knuckle. By using equations 4.11 to 4.19, the following relation is obtained:

$$C_k = \frac{D_{drum,k} \cdot \frac{L_{knuckle}}{2}}{2 \cdot r' \cdot \eta_{falls,k} \cdot i_{g,k}} \tag{4.20}$$

$$I_{m,k} = (M_k + \frac{I_{CoG,k}}{L_{CoG,k}}) \cdot {C_k}^2 \tag{4.21}$$

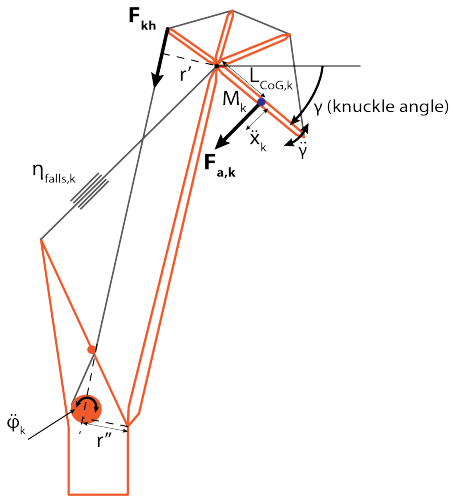

Figure 4.14: Schematic representation of the luffing motion.

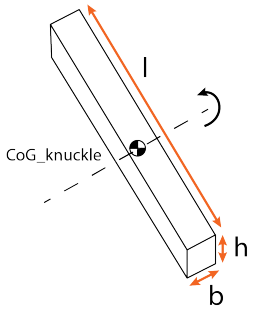

Figure 4.15: Inertia of the knuckle rotating around its CoG in the knuckle motion

4.3.4. X-Y table motions

For the MCCC, all tip motions will be compensated by the moving X-Y skid table. With this concept, the crane itself will not by moving to compensate for the tip motions, only the skid-table will move with respect to the crane. In figure 4.16 the compensating principle of the MCCC is graphically illustrated. In the left drawing, the MCCC is drawn in its initial position. In the middle drawing, the vessel is rotated by a roll angle of 2°. It can be seen that if the skid table does not compensate for the vessel motions, the positioning of the load will be lost. However, as can be seen in the right drawing, the compensating system will translate the lowering point of the load within the skid table so that the motions in the horizontal plane are compensated for. In the third figure it can also be seen that after the compensating motion of the skid table, the vertical position of the load is slightly lower for which the AHC system will have to compensate. From the working principle of the skid table it can be seen that there are no 'structural' masses that have to be accelerated to compensate for the motions in the horizontal plane. However, because the skid table does have to move within its frame, the E-motors within the skid table will have to generate a translating motion by which it will have to overcome the inertia of the E-motor itself. For this reason, only the inertia of the drivetrain is used for the dynamic loads of the MCCC.

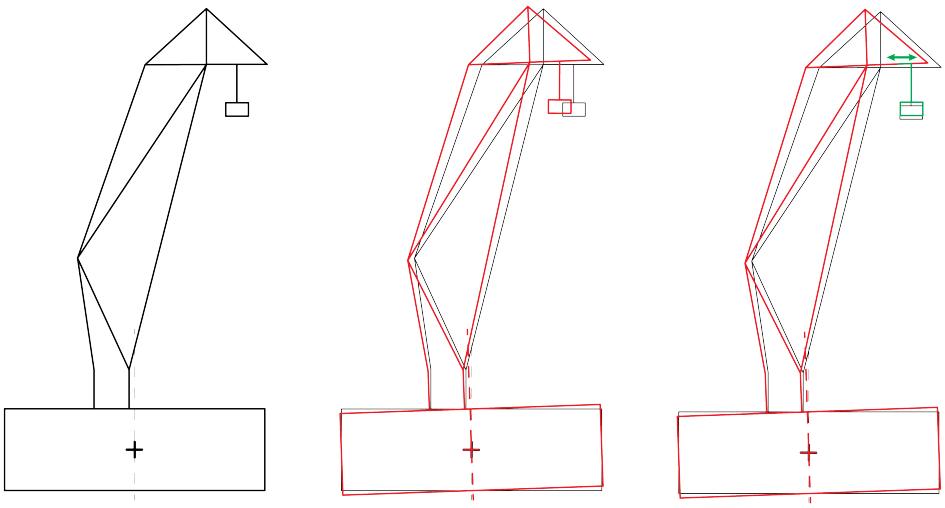

Figure 4.16: Compensation mechanism of the MCCC. The middle and right drawing represent a roll angle of the vessel of 2°.

4.3.5. Inertia distribution

For each of the crane concepts that is included in the analysis, the total inertia of the compensating motions has been determined by translating different inertia components to the shaft of the E-motor. Now that the different inertia components are known at the shaft of the E-motor, a comparison can be made as to what inertia components have a large impact on the drive system. In figure 4.17, different inertia distributions are shown for the slewing motion of the PMOC and HBC. From all distributions it can be concluded that the inertia of the cranehouse is of negligible size. The top figures, 4.17a and 4.17b, illustrate the inertia distributions of the PMOC and HBC for the initial crane position of design case 1. In figures 4.17c and 4.17d, the inertia distributions for the PMOC and HBC are plotted but then for design case 3. Design case 3 is used to illustrate the effect of the initial crane position on the inertia distribution of the slewing motion. Because the inertia of the boom around the slewing axis is calculated with equation 4.3 in which the horizontal distance of the boom is squared, an exponential increase of the boom inertia can be expected for smaller boom angles. While the inertia of the drive system is constant, the inertia of the boom comprises a larger part of the total inertia of the slewing motion.

With the use of these inertia distributions, the impact of a reduction of the inertia of different parts in the crane system can be estimated. For design case 3 it can be concluded that a reduction of the inertia of the boom would bring a better result on the total performance of the crane than a reduction of the inertia of the drivetrain. Therefore, these inertia balances function as an indicator as to what crane components should be improved to obtain a better performance.

However, the total loads on the drive system will be a combination of both the gravitational loads and dynamic loads. The inertia distribution does not say anything about this relation and therefore a reduction of the total inertia will not necessarily lead to a proportional increase of the cranes performance because a reduced inertia only reduces the dynamic loads on the drive system. The balance between the gravitational loads and the dynamic loads is elaborated on in section 4.4.

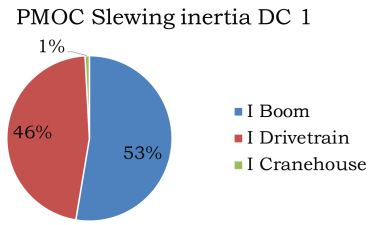

(a) Inertia distribution of the slewing motion for the PMOC in design case 1.

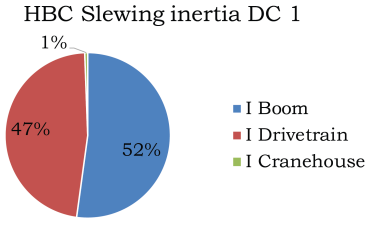

(b) Inertia distribution of the slewing motion for the HBC in design case 1.

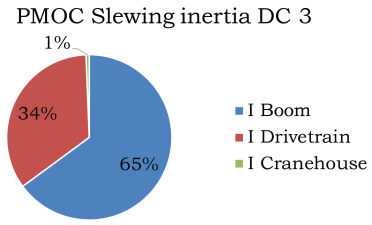

(c) Inertia distribution of the slewing motion for the PMOC in design case 3.

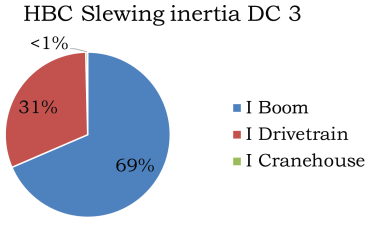

(d) Inertia distribution of the slewing motion for the HBC in design case 3.

Figure 4.17: Inertia distributions at the shaft of the E-motor for the slewing motion of the PMOC and the HBC cranes.

From the inertia distributions of the luffing motion of the PMOC and HBC (figure 4.18), it can be observed that the inertia of the drivetrain accounts for more than 90 % of the total luffing inertia. As a result of this, the differences between design case 1 and design case 3 are very small as the inertia of the boom has a minor influence on the total inertia. The reason why the inertia distribution of the luffing motion has a totally different balance than that of the slewing motion is explained by the fact that the luffing motion is subjected to much larger gravitational loads. Because the gravitational loads are large, the transmission ratio between the luffing motion and the shaft of the boomhoist motor is larger by which the torque that is experienced at the motor is reduced. However, because of this, the inertia of the luffing motion is also significantly reduced.

In a normal lifting operation, it is not required to accelerate the luffing motion of the crane very quickly. Because of this, the inertia distribution is not very important while the dynamic load will not be the limiting factor of the luffing mechanism. Now that motion compensation is to be realized, the accelerations of the luffing motion are larger than it is originally designed for and the inertia of the luffing motion will become more important. When the luffing performance is to be increased, it can be said that one should focus on reducing the inertia of the drivetrain to obtain the best result when the total transmission is not changed.

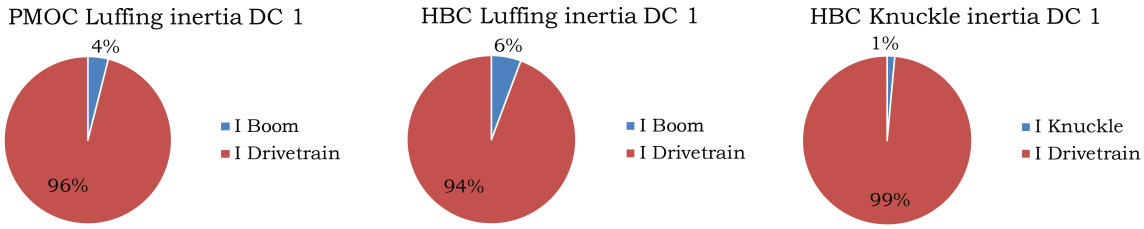

(a) Inertia distribution of the luffing motion for the PMOC in design case 1.

(b) Inertia distribution of the luffing motion for the PMOC in design case 1.

(c) Inertia distribution of the luffing motion for the PMOC in design case 1.

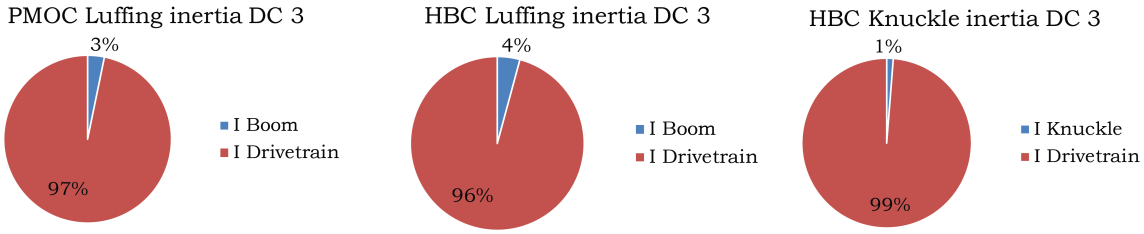

(d) Inertia distribution of the luffing motion for the PMOC in design case 1.

(e) Inertia distribution of the luffing motion for the PMOC in design case 1.

(f) Inertia distribution of the luffing motion for the PMOC in design case 1.

Figure 4.18: Inertia distributions at the shaft of the E-motor for the luffing and knuckle motion of the PMOC and the HBC.

4.4. Torque

For increasing wave heights, the vessel motions will become larger. When these vessel motions become larger, the loads on the drive system for motion compensation will become larger as well. To asses the motion compensating performance of the crane, different elements of the drive system will be plotted in a workability graphs of which one is the torque capacity of the drive system.

With the inertia's and crane motions, the total loads on the drive system can be calculated. Whilst the gravitational load is only relying on the rotations of the vessel, the dynamic load is depending on all vessel motions. So, by adding the maximum expected value of both, a phase difference between these maxima is not accounted for and therefore this could turn out to be a conservative estimate. However, because both the gravitational loads and the dynamic loads are a result of the vessel motions, the phase difference between both can be included in the calculations. To include this phase difference in the calculation, RAOs are determined for the gravitational torque and for the dynamic torque. These torque RAOs can afterwards be added with the complex notation, including their phase information and from the total torque RAO, a maximum can be calculated. The RAOs for the gravitational torque, and dynamic torque are listed in equations 4.22 to 4.25.

$$RAO_{T,dyn,slew} = \frac{RAO_{acc,slew,motor} \cdot I_{slew,motor}}{No._{slewmotors}} \tag{4.22}$$

$$RAO_{T,dyn,luff} = \frac{RAO_{acc,luff,motor} \cdot I_{luff,motor}}{No._{luffmotors}} \tag{4.23}$$

$$RAO_{T,grav,slew} = \frac{9.81 \cdot sin(RAO_{sidelead}) \cdot (M_{load} \cdot L_{hor,load} + M_{boom} \cdot L_{hor,boom})}{i_{total,s}} \tag{4.24}$$

$$\begin{aligned} RAO_{T,grav,luff} = & \frac{9.81 \cdot sin(RAO_{offlead}) \cdot (M_{load} \cdot L_{vert,load} + M_{boom} \cdot L_{vert,boom}) \cdot D_{drum,b}}{2 \cdot r \cdot \eta_{falls,b} \cdot i_{g,l}} \\ & + \frac{9.81 \cdot cos(RAO_{offlead}) \cdot (M_{laod} \cdot L_{hor,load} + M_{boom} \cdot L_{hor,boom}) \cdot D_{drum,b}}{2 \cdot r \cdot \eta_{falls,b} \cdot i_{g,l}} \end{aligned} \tag{4.25}$$

In figure 4.19, the amplitude and phase spectrum of both the gravitational slewing torque RAO, and the dynamic slewing torque RAO are plotted. From the phases of both RAOs it can be seen that for low wave frequencies, there is a phase difference between both loading mechanisms. However, the amplitudes at which the loading mechanisms have a different phase are relatively small and therefore the phase difference does not have a large impact on the total torque of the slewing motion. In fact, the phases of gravitational load and the dynamic load correspond very well for larger frequencies.

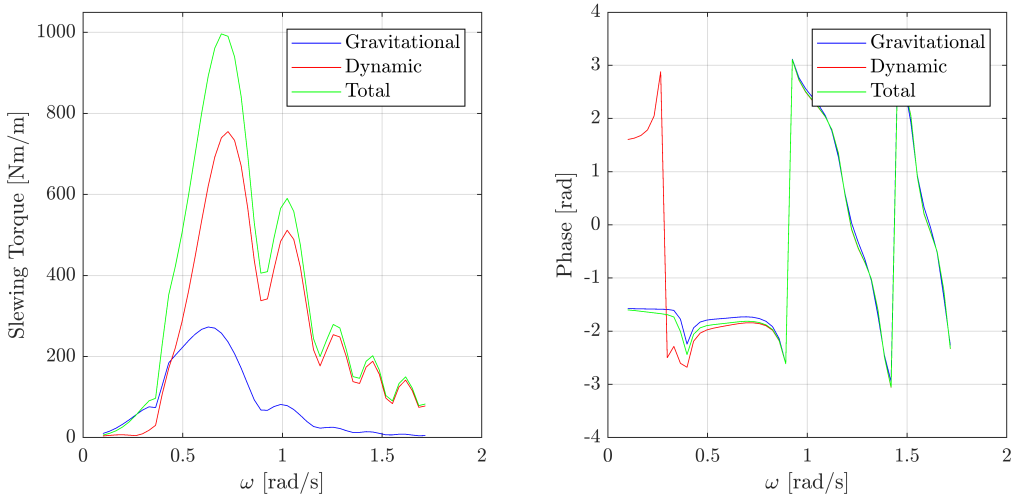

Figure 4.19: Amplitude and phase RAOs of the static-, dynamic- and total slewing torque of the HBC for design case 2 (heading 30°).

With the use of the total torque RAOs, the total torque can be estimated including the phase difference between both loading mechanisms. However, it is also interesting to see what the contribution of the gravitational loads and the dynamic loads are to the total loads on the drive system. This has been plotted in figure 4.19 from which it can already been seen that the ratio between gravitational load and dynamic load will change for different shapes of the wave spectrum.
For a peak period of 7 seconds, the slewing torque is dominated by the acceleration of the boom which can be seen in figure 4.20. However when the wave spectrum has a peak period of 15 seconds, the relation between the torque used by gravitational loads and by dynamic loads has an almost equal balance. This is explained by the RAO's of the vessel. For large wave periods, the accelerations of the vessel become lower, however the absolute rotations become larger. Therefore, for larger wave periods, the boom accelerations become smaller and the sidelead and offlead angles become larger, which can be seen in the balance of the torque requirement.

As one would expect from the inertia balance of the luffing motion, the balance of the luffing torque is dominated by the 'dynamic' acceleration torque. In figure 4.21 it can be seen that almost all of the torque, that is required from the drive system to compensate for the vessel motions, is 'dynamic' torque. Also, for an increasing peak wave period, the balance of the system gets better, which was already observed for the slewing motion as well.

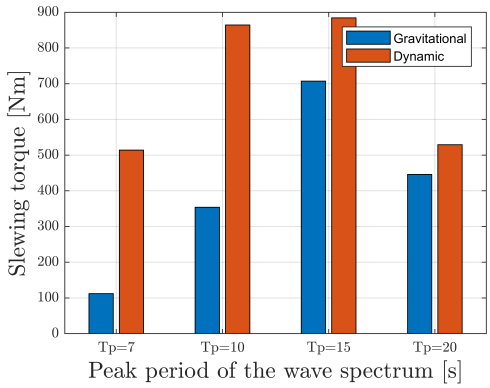

Figure 4.20: Distribution of the static and dynamic slewing torque for different peak periods of the wave spectrum and. Design case 1, wave heading 30°, and $H_{sig} = 3$ is used for this figure.

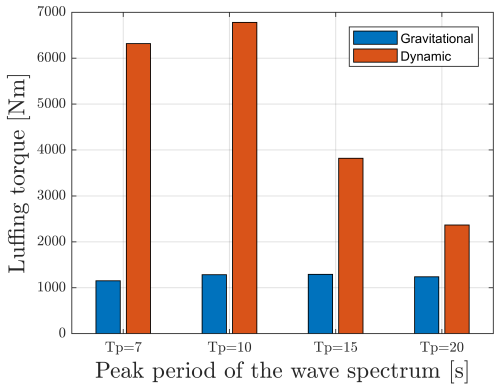

Figure 4.21: Distribution of the static and dynamic luffing torque for different peak periods of the wave spectrum. Design case 1, wave heading 30°, and $H_{sig} = 3$ is used for this figure.

Efficiency losses
Throughout the drive system of the crane, not all mechanisms are 100% efficient. Therefore, friction losses should be accounted for when the total required torque of the drive system is calculated. Only the most dominant friction losses are incorporated in the model. The friction losses that are calculated are used to increase the drive requirements after the total torque has been calculated. However, for a perfect result, the efficiency's should have been incorporated in the different steps of the torque inducing mechanisms for which they have an effect on the calculated torque. This has not been done for this model which leads to slightly conservative estimates. The reason why the estimates are conservative is the fact that the part of the total torque that is required to accelerate the E-motor, and the part of the total torque that is required to accelerate the crane components have a different efficiency. When the slewing motion is considered, the efficiency of the gearing pinion will not have an effect on the torque that is required to accelerate the slewmotor. While these efficiency's are combined to a total efficiency, also the torque that is required to accelerate the motor will be multiplied with the efficiency component of the gearing pinion.

The efficiency's that have been incorporated for the torque estimates are listed in table 4.1. The static friction of the slew bearing is an effect that is present when the slew motion is initiated. Because the acceleration will be the largest when the periodic motion changes direction, this friction is included. The sheave efficiency that is listed in table 4.1 is the efficiency per sheave. For this reason, the sheave efficiency in equations 4.27 and 4.28 is to be used to the power of the number of sheaves in the system (Sh_{luff} and $Sh_{knuckle}$). The efficiency of the drivetrain is assumed to be the same for all crane motions. For the maximum expected torques that are calculated, equation 4.29 is used to include the efficiency of the system.

$$\eta_{t,slew} = \eta_{slew,b} \cdot \eta_p \cdot \eta_d \tag{4.26}$$

$$\eta_{t,luff} = {\eta_s}^{Sh_{luff}} \cdot \eta_d \tag{4.27}$$

$$\eta_{t,knuckle} = {\eta_s}^{Sh_{knuckle}} \cdot \eta_d \tag{4.28}$$

$$T_{actual} = T_{max} \cdot \frac{1}{\eta_t} \tag{4.29}$$

Component	Efficiency	Symbol
Slew bearing	0.9	$\eta_{slew,b}$
Slewing pinion	0.98	η_p
Sheaves (per sheave)	0.99	η_s
Drivetrain	0.94	η_d

Table 4.1: Efficiency's that are included in the drive requirements.

4.5. Power

To be able to asses the drive system performance from a power perspective, the power that is required for the different compensating crane motions is to be calculated. To calculate the power of the compensating motions, the equation for the power of an angular motion is used (equation 4.30) for which the torque and velocity are have to be known. From the motion analysis in chapter 3 the maximum expected velocities of the crane motions are known and in section 4.4 the maximum expected torque that has to be delivered by the drive system is calculated. From these values, the maximum expected power can directly be estimated in the frequency domain. There is however a problem with this, because both the torque and the velocity of the crane motions follow from a frequency domain analysis, only a maximum expected value can be obtained. The specific moment in time when the maximum torque, or the maximum speed occurs, is unknown and this is expected to have a large impact on the maximum expected power. The reason for this is that there is a certain phase delay between the velocity and acceleration of the irregular crane motions which is not accounted for when the maximum expected values are used to determine the maximum power and therefore the maximum power that is calculated will be conservative. To illustrate the effect of the neglected phase delay, an example is described for regular waves.

For a perfectly sinusoidal motion of the crane, the phase difference between its acceleration and velocity would be exactly $\frac{1}{2}\pi$. When the power, which is necessary to realize this motion, would be calculated in the time domain, the velocity signal and acceleration signal can be multiplied. In the upper plot of figure 4.22, two regular waves are plotted which represent the time signal of the torque (wave 1) that is required for the sinusoidal crane motion and the velocity (wave 2) of that same crane motion. Multiplying these time signals will lead to the a resulting wave (wave 3) with a maximum amplitude of 3. In the lower plot, the same initial waves are plotted for the torque (wave 1) and velocity (wave 2), but now there is a phase difference of $\frac{1}{2}\pi$ between both. The multiplication of these waves will lead to a different time signal for wave 3 which has a maximum amplitude of only 1.5. With this example it can be seen that neglecting the phase delay can lead to conservative outcomes and especially for the velocity and acceleration signal, this is expected to make a large difference.

$$P = T \cdot \dot{\omega} \tag{4.30}$$

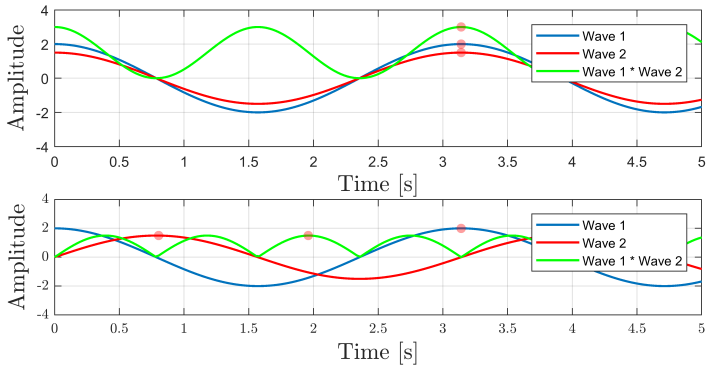

Figure 4.22: In the upper graph, two regular waves without a phase delay and the multiplication of both. In the lower graph, two regular waves with a phase delay of $\frac{1}{2}\Pi$, and the multiplication of both.

Because the calculated torque is a result of both gravitational loads and dynamic loads, the phase difference between the torque and the velocity will not exactly be $\frac{1}{2}\pi$. Instead of multiplying the maximum expected values from the frequency domain analysis, other approaches were investigated to calculate the power in the frequency domain. To account for the phase difference in the calculation of the maximum expected power, the RAOs of the torque and the velocity have to be combined and whereas the 'gravitational' torque and the 'dynamic' torque could be added and combined into a single RAO, this cannot be done for the power. The power is dependent on both speed and acceleration of the motion which would mean a multiplication of the RAOs, and that leads to a nonlinear calculation. Different options were explored within the frequency domain

which are described in appendix G. Unfortunately this did not result in a trustful outcome and therefore the power is estimated from time domain calculations in which the phase delay can be incorporated. To do so, the response spectra of the torque and velocity of all calculated crane motions are transformed to the time domain.

Time Series power estimation

Non-linear calculations can be performed in the time-domain but before time domain calculations can be done, the data from the frequency domain has to be transformed to the time domain. For a wave spectrum, the transformation from the frequency domain to the time domain is done by a superposition of all regular wave components from the wave spectrum. In figure 4.23 an illustration is given that demonstrates the transformation from the frequency domain to the time domain to obtain an irregular wave record. The amplitudes of the wave components in the time domain are determined by knowing that the area under the associated segment of the wave spectrum $S_\zeta \cdot \Delta\omega$ is equal to the variance of the wave component. For this, equation 4.32 is used. For the phase angles of the regular wave components from the spectrum, a set of uniformly distributed random values in the range between 0 and 2 Π is generated. To be sure that the method that is used to generate time series from a spectrum is correct, this is validated in appendix I.

$$\zeta(t) = \sum_{n=1}^{N} \zeta_{an} \cdot cos(\omega_n t + \phi_n) \tag{4.31}$$

$$\zeta_{an} = \sqrt{2 \cdot S_\zeta(\omega) \cdot \Delta\omega} \tag{4.32}$$

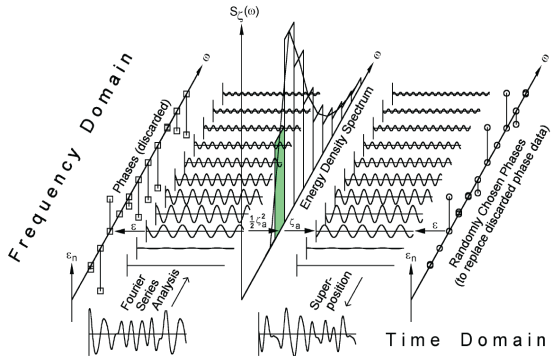

Figure 4.23: Transformation of the wave spectrum to a wave record in the time domain.

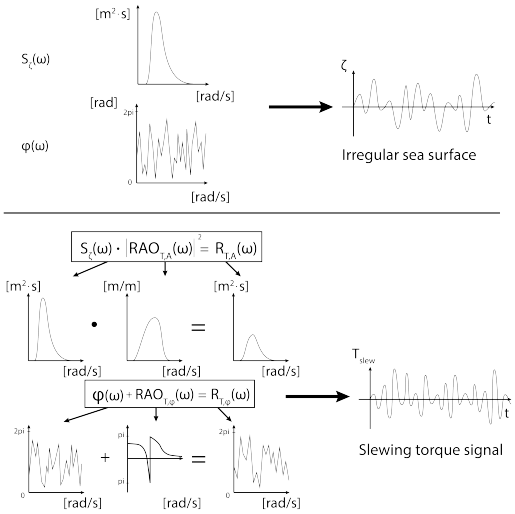

Figure 4.24: Transformation of the wave spectrum to a time record and transformation of the response spectrum of the slewing torque to a time record.

To obtain the time signals that are needed for calculating the power of the crane motions, this same transformation method is used to transform the response spectra of the crane motions to the time domain. In chapter 3.1.3 it was described how the response spectra of the crane motions can be obtained, by multiplying the wave spectrum with the RAO squared (equation 3.4). Instead of using the amplitudes and phases of the wave spectrum in equation 4.32, the amplitudes and phases of the response spectrum are used by which a time signal is generated of the response spectrum (see figure 4.24). The units of the response spectra can be different for torque, velocity etc. as the units of the RAOs are different. There is however one critical step in generating time signals of the response spectra that is not the same for generating a time signal of the wave elevation which has to do with the phases of the regular wave components. For a wave signal, the phases are random values. For the time signals of the response spectra the waves phases are still random values but the phases of the RAO have to be added to these random wave phases to obtain the phases of the response spectrum. This is an essential part of the procedure because for both the time signal of the torque, and the time

signal of the velocity, the same random wave phases are used for one single time representation. This way the phase difference between the torque and the velocity is maintained and the time signals can be multiplied.

Number of time series

Time signals of all response spectra can be obtained by using this transformation. After constructing time signals of the torque and velocity of any arbitrary crane motion these can be multiplied to obtain the time signal of the power of that motion. From these time series of the power, a maximum expected value can be determined. However, because the wave phases used, are uniformly distributed random variables, multiple representations of the time signal have to be made, as each time signal will be different. The maximum power, following from the time series is dependent on the random wave phase and to determine how many representations have to be made, it is investigated after which number of simulations this maximum converges. The convergence of the number of representations has been investigated by determining the maximum wave height of a wave spectrum and varying the number of time series that are used to determine this maximum. For the convergence of the maximum power from a time series, the same will hold as for the maximum wave height because the same calculation method is used with regard to the random wave phases. Because the values for maximum wave heights of a wave spectrum can also be determined in the frequency domain, these are used to validate whether the calculation method is correct instead of investigating the convergence of the power itself. For these maxima, the duration and probability of exceedance are parameters that must also be used in the time domain to obtain the same maximum expected value. The wave spectrum that is used to investigate the convergence has significant wave height of 3 meters and a peak period of 12 seconds and this was done for a duration of 1800 seconds and probability of exceedance of 10 %. In figure 4.25 one can see that approximately 50 simulations are enough to obtain a stable estimate, while a statistical offset remains for larger numbers of simulations. The statistical offset that can be seen in figure 4.25 is not something that would be expected from theory because an infinite number of simulations should eliminate the randomness of the process. However, influences such as the randomness of the random generator from Matlab and the influence of the discretization of the wave spectrum, are difficult to quantify and the offset of approximately 3% of critical importance for the application in which this is used, namely, assessing the feasibility of motion compensation for different crane concepts.

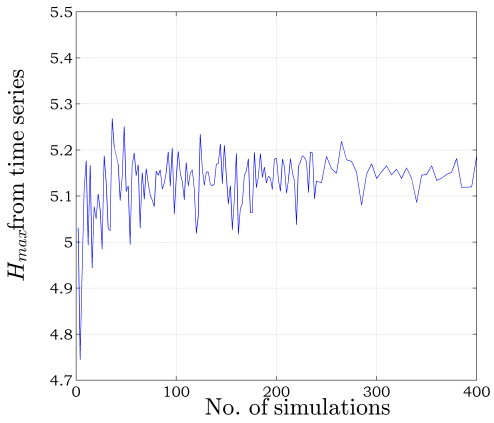

Figure 4.25: Convergence of the maximum estimate from a 3-hour time series with a probability of exceedance of 63 % for a wave spectrum with $H_{sig} = 3m$ and $T_p = 12s$ for an increasing number of simulations.

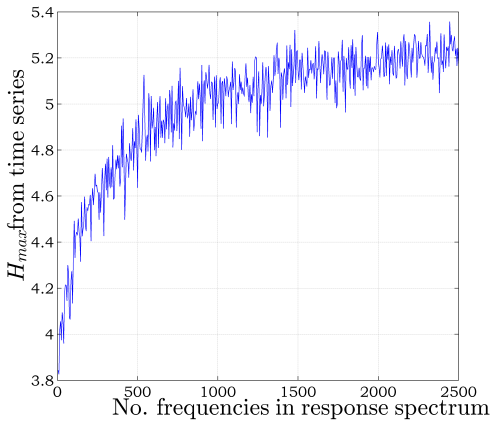

Figure 4.26: Convergence of the maximum estimate from a 3-hour time series with a probability of exceedance of 63 % for a wave spectrum with $H_{sig} = 3m$ and $T_p = 12s$ with an increasing spectral resolution.

Spectral resolution
In the response spectra, amplitudes of regular wave components are defined for 50 different frequencies because the RAOs are known for 50 different frequencies. The frequencies for which amplitudes are known range from 0.1 rad/s to 1.717 rad/s. The resulting spectral resolution of the response spectrum is 0.033 rad/s. A time representation is plotted for the response spectrum of the slewing torque. This response spectrum is plotted in figure 4.28c and the corresponding time signal can be seen in figure 4.28a. From this time signal it can be seen that the signal is not very irregular and does not correspond to a typical irregular sea surface elevation which is the source of the crane motions. This is a result of the limited number of frequencies in the response spectrum and to prove this, another time signal of the same response spectrum is plotted in figure 4.28b after interpolating the response spectrum to increase the spectral resolution. The response spectrum that is obtained after linearly interpolating for 1500 frequencies is displayed in figure 4.28d and for all interpolations it is afterwards checked that the zeroth order spectral moment of the spectrum is not changed.

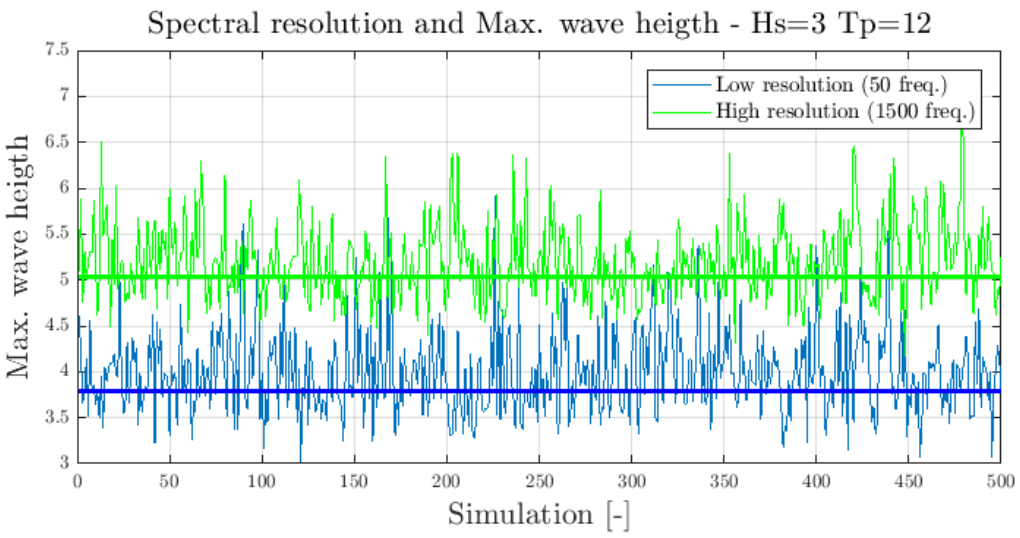

Figure 4.27: Maximum wave height from a wave spectrum with $H_{sig} = 3m$ and $T_p = 12s$ for different spectral resolutions. The bold horizontal green line and blue line indicate the maximum wave height with a probability of exceedance of 63%.

It was found that the maximum value that is estimated from the time series is significantly different for time signals with a low spectral resolution than that of time signals with a high spectral resolution which can also be expected from looking at figures 4.28a and 4.28b. In figure 4.27, the difference of the maximum expected wave height from the time signals for a low- and high spectral resolutions is shown. To investigate what the spectral resolution should be to obtain a representative maximum estimate, again a wave spectrum is used because the outcome of the wave spectrum can be verified by means of spectral calculations in the FD. Wave spectra with a frequency range between 0.1 rad/s and 1.717 rad/s are used with a total number of frequencies between 50 and 2500 by which the spectral resolution increases. This corresponds to spectral resolutions between 0.033 rad/s and 6.5e-4 rad/s. For all spectral resolutions, time representations of the sea surface elevation are calculated for the corresponding wave spectrum. From the time representations, the maximum expected wave heights are determined and these are plotted verses the number of frequencies in the wave spectrum. In figure 4.26 it can be seen that the maximum expected wave height that is estimated from the time series converges at approximately 1500 frequencies in the wave spectrum which corresponds to a spectral resolution of 1e-3 rad/s. For this convergence, a wave spectrum is used with a significant wave height of 3 meters and a peak period of 12 seconds and the maxima are determined for time series of 1800 seconds and 10 % probability of exceedance.

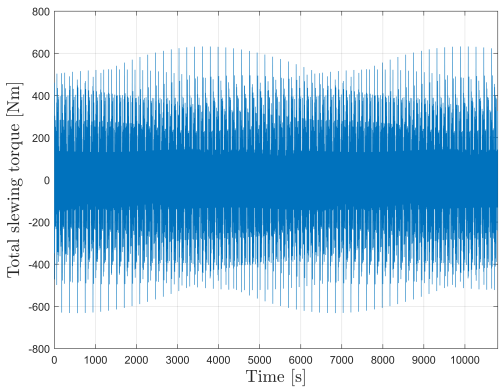

(a) Time signal of the required torque for motion compensation from the response spectrum with 50 frequencies.

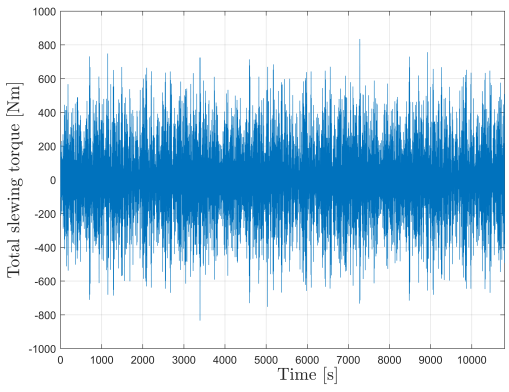

(b) Time signal of the required torque for motion compensation from the response spectrum with 1500 frequencies.

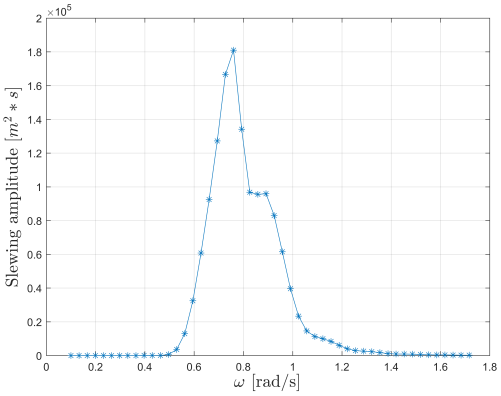

(c) Response spectrum that is used for the time representation of the torque before linear interpolation (50 frequencies).

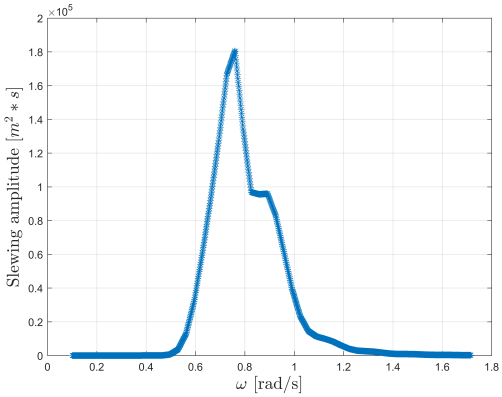

(d) Response spectrum that is used for the time representation of the torque after linear interpolation (1500 frequencies).

Figure 4.28: Time signals for different spectral resolutions of the same spectrum, before and after linear interpolation.

The sampling frequency that is used for the generation of time series also influences the maximum estimate. For all previous calculations a sampling frequency of 10 Hz is used to generate the time signals. Because the vessel motions are relatively slow, a sampling frequency of 10 Hz is expected to be sufficient and the maximum estimates from the time signals are not expected to change significantly for an increasing sampling frequency. To prove this, different simulations were performed with higher sampling frequencies but the maximum expected values from the time series did not change. Also, the method that is used for determining maximum expected values of a response spectrum by transforming it to the time domain is validated in appendix I.

At the stage where correct time series are produced, the torque and velocity can be multiplied to obtain the power signal of the motion. From this power signal, the maximum is estimated after multiple simulations and for this maximum, the same probability of exceedance is used as for the spectral estimated in the frequency domain. The power that is calculated for the different crane motions for different wave spectra is used to generate the workability graphs which will be discussed in section 4.7.1.

4.6. Position control

From the previous sections, maximum expected values can be determined for the stroke, torque, power, etc of different compensating motions. However, these maximum expected values are based on the maximum expected motions of the crane from the FD analysis. In this section, it is investigated what the limited torque and its probability of exceedance mean for the error of the position of the tip during a time simulation. It is expected that without delivering the maximum torque from a time signal, still a very accurate positioning system can be realized by the use of control systems with feedback loops and it is investigated what the effect of the limited capacity of the drive system is on the motion compensating performance of the crane.

In a situation, where the required torque for the crane motion exceeds the capacity of the drive system, the acceleration of the crane will be lower than the acceleration that would be required to perfectly compensate for the vessel motions. Because a probability of exceedance of 10% is used in previous calculations, there will be situations in which this happens. This means that the crane tip cannot be kept in position for a short period and an offset of the desired crane tip position will be the result. However, because the crane motions will be periodic, the maximum acceleration that is required for perfect compensation will only be required for a short period. This means that although the maximum acceleration that would be required to perfectly compensate for the crane tip's motions cannot be realized, the maximum acceleration that the system is able to realize can be maintained somewhat longer to compensate for its limitation. For this, a control system is used, which can be optimized to minimize the error of the tip position that is a result of the limited acceleration of the crane. For this, a time signal of the slewing torque is used that followed from the response spectrum of the slewing acceleration of the crane. This time signal is displayed in figure 4.29.

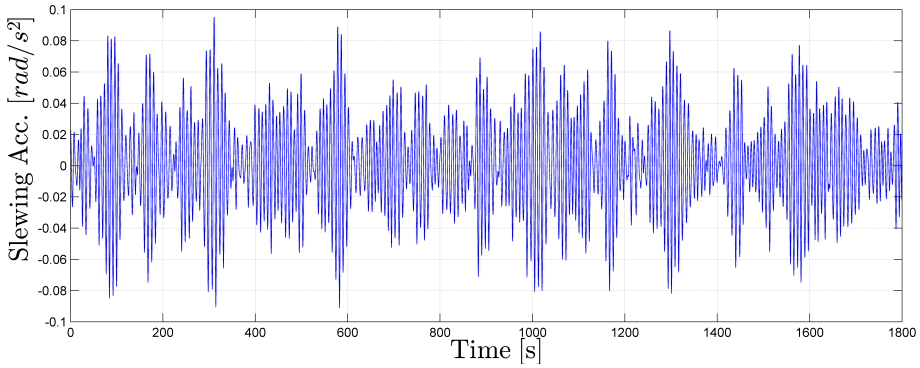

Figure 4.29: Example of a time signal of the slewing acceleration that is obtained from the response spectrum of the slewing acceleration for design case 1 for a significant wave height of 3 meters.

$$V_t(t) = V_t(t-1) + \frac{A_t(t) + A_t(t-1)}{2} \cdot dt \tag{4.33}$$

$$X_t(t) = X_t(t-1) + \frac{V_t(t) + V_t(t-1)}{2} \cdot dt \tag{4.34}$$

From the time signal of the acceleration of a motion, the velocity (V_t) and displacement (X_t) signal can be determined for which equations 4.33 and 4.34 are used. The same is done for the time signal of the slewing motion (figure 4.29) where an angular acceleration is concerned which leads to an angular velocity and a rotation after numerically integrating. These acceleration, velocity and rotation signals are referred to as the target signals. In the next step the maximum acceleration is limited, which simulates a situation in which the drive system runs into its maximum capacity while it is compensating for the crane tip's motions. Because the acceleration of the target signal cannot be followed exactly, the resulting velocity and rotation will drift and the position will be lost when the error is not compensated for. These time signals are referred to as the actual time signals and are calculated with equations 4.35 to 4.37.
At this stage a controller is introduced which will try to minimize the positioning error by compensating for the limited acceleration capacity of the system. The controller calculates the error between the target signal of the velocity and the actual velocity at every time step. It will compensate for this error with the control

parameter K_d. Also, it calculates the error between the target signal of the rotation and the actual rotation for which it compensates the acceleration with control parameter K_p. To determine these corrections, equations 4.38 and 4.39 are used. The actual acceleration signal is than adjusted with the correction of the velocity and the position. In figure 4.30 the same time signal is plotted as in figure 4.29 but now the maximum acceleration is limited by a constraint which only allows a maximum acceleration that is a fraction of 75% of the maximum acceleration that is present in this specific time signal (A_{max}). Three subplots are shown which are the acceleration, velocity and rotation of the slewing motion of the crane. The blue line represents the target signal whereas the red line represents the actual signal that can be realized by the drive system of the crane.

$$A_{actual}(t) = max\ (min\ (\ (A_t(t) + Acor, v(t) + Acor, x(t)),\ A_{max})\ ,\ -A_{max}\ ) \tag{4.35}$$

$$V_a(t) = V_a(t-1) + \frac{A_a(t) + A_a(t-1)}{2} \cdot dt \tag{4.36}$$

$$X_a = X_a(t-1) + \frac{V_a(t) + V_a(t-1)}{2} \cdot dt \tag{4.37}$$

$$Acor, v = V_a(t) - V_t(t) \cdot K_d \tag{4.38}$$

$$Acor, x = X_a(t) - X_t(t) \cdot K_p \tag{4.39}$$

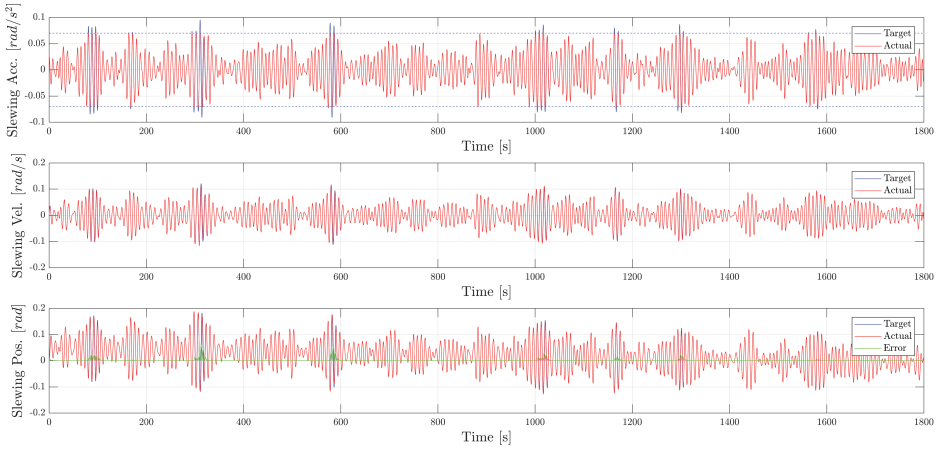

Figure 4.30: Time signals for the slewing acceleration, velocity and rotations. Target signals (blue) and real signals (red) resulting from a limited maximum acceleration are plotted. The resulting error in position is plotted in green.

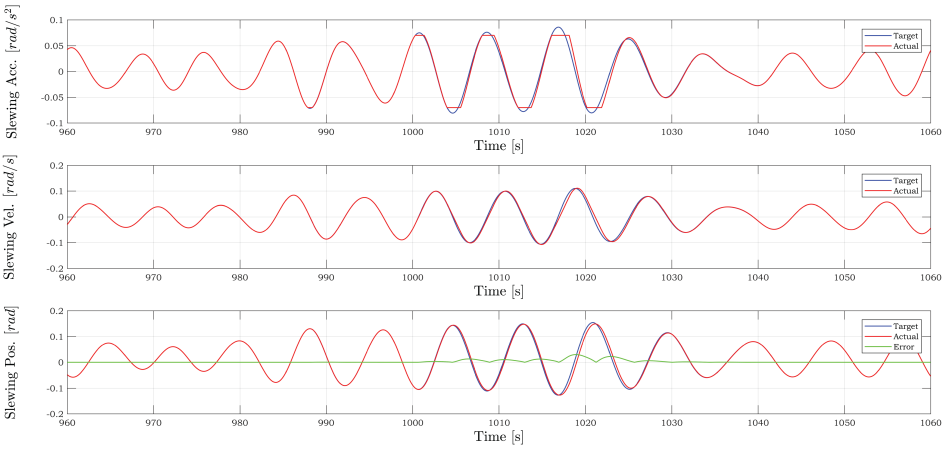

Figure 4.31: Zoomed time signals for the period between 960 seconds, and 1060 seconds for this specific time representation.

In this example, the actual signal of the slewing acceleration is modified by the influence of a simple controller which can be seen in figure 4.31. Again, the angular acceleration, velocity and rotation of the slewing motion are plotted and this figure illustrates the same signals as in figure 4.30 but is is zoomed to the period between 960 seconds and 1060 seconds. In the acceleration signal, it can be seen how the target signal exceeds the limits of the drive system, and the controller compensates for the error that is a result of the limited acceleration by maintaining the maximum acceleration a little longer. In the signal of the slewing position, the green line represents the error between the target angle of the slewing position and the actual angle of the slewing position.

For this example, a 75 % constraint on the maximum expected acceleration from the spectrum is used and from figure 4.31 it can be seen that the error will build up to approximately 0.03 radians. The accompanying error of the crane tip is also depending on the boom angle and for design case 1, an error of the slew position of 0.03 radians would mean a tip offset of 1.2 meters. When a constraint of 90 % is used on the acceleration signal of the slewing motion, the resulting error of the position of the crane tip reduces to 0.1 meters.

Random waves
However, for the application of such a position control system in the motion compensation system of an offshore crane this result cannot be used to estimate the positioning error. From the example it was shown that for the particular time signal used, a constraint that reduces the maximum torque requirements of the drive system by 90 % will lead to an offset of the crane tip which would be considered acceptable. However, because of the random wave phases that are associated to the wave spectrum, every time representation will be different and so, the maximum acceleration of the specific time signal and the resulting positioning error will be different. Therefore, the positioning error should be calculated for many simulations and from the maximum error of all those individual simulations, one can see what the actual impact of the limited maximum accelerating capacity of the drive system is.

At first, the error is estimated for the current maximum accelerating capacity of the drive system. This maximum has been calculated from the response spectrum for a duration of 1800 seconds and a probability of exceedance of 10%. To determine the positioning error for this maximum acceleration, many (500) time series are generated, and for all of these, the maximum error that is present in the time series of 1800 seconds is calculated. From these positioning errors, the absolute maximum of 500 simulations can be extracted, but also the positioning error with a 10 % probability of exceedance can be determined both of which can be found in figure 4.32. On the left side of this figure, the maximum acceleration of the time signal is plotted for every simulation and the green line indicates the maximum acceleration with a probability of exceedance of 10 %. On the right side of the figure, the maximum positioning error of the time signals is plotted where it can be seen that the absolute maximum error for these 500 simulations is approximately 0.75 meters and the 10 % exceedance error is 0.03 meters.

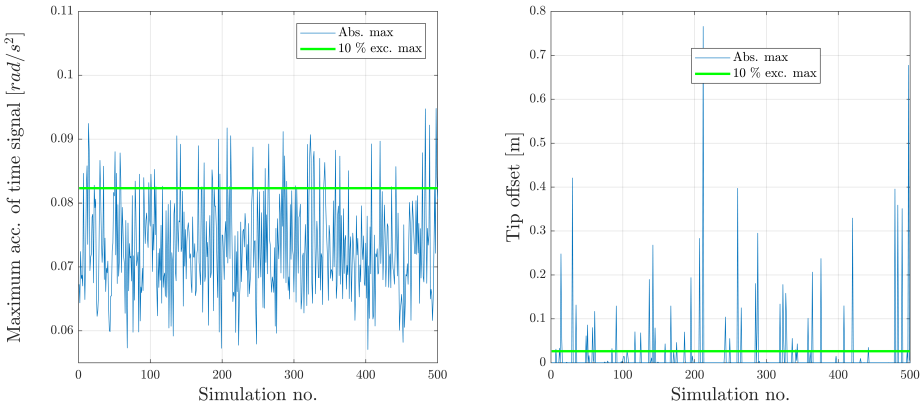

Figure 4.32: On the left side, the maximum acceleration of the time signal is plotted and for these time simulations, 100% of the maximum acceleration from the FD was used. On the right side the maximum error of the time series is plotted per simulation.

Now the same hypothesis is tested that was tested on the single time representation from the example in figure 4.29. The maximum accelerating capacity of the drive system is limited to 90% of the value that was used for the previous simulation. By doing this, it can be expected that more waves will exceed the limits of the drive system and the error of the positioning system will increase. In figure 4.33, the results that are obtained for the constrained drive system are displayed. On the left, the maximum accelerations of the time signals are plotted where the green line indicates the maximum acceleration with a probability of exceedance of 10% and the red line indicates the limited acceleration that follows from the constraint. On the right side of the graph, the maximum positioning errors of the time signals is plotted from which it can already be seen that these are much larger than for the situation without the constraint. The absolute maximum for these 500 simulations is approximately 5.4 meters and the 10 % exceedance error is 0.4 meters.

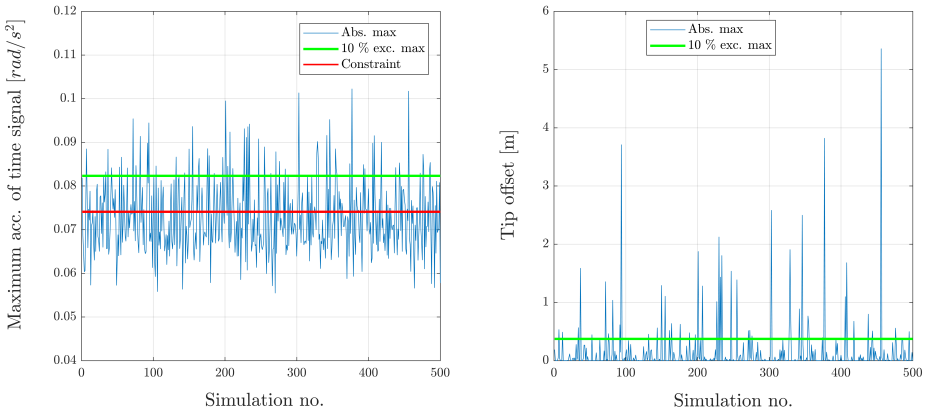

Figure 4.33: On the left side, the maximum acceleration of the time signal is plotted and for these time simulations, 90% of the maximum acceleration from the FD was used. On the right side the maximum error of the time series is plotted per simulation.

By limiting the maximum accelerating capacity of the drive system with a factor of 0.9, a new maximum acceleration is obtained. This same acceleration can also be obtained from the response spectrum for a different probability of exceedance which can already be expected from figure 4.33. It was found that the limiting factor of 0.9 corresponds to a probability of exceedance of approximately 35% for this situation. This explains the large increase of the positioning error because the probability that multiple successive waves exceed the limits of the drive system increases. Calculations were also performed for probabilities of exceedance of the maximum acceleration of 5%, and 20% and these results can be found at the end of appendix I. For 5% probability of exceedance, the 10% exceedance error is approaching zero and an absolute maximum of 0.45 meters was found from 500 simulations. For 20% probability of exceedance, a 10% exceedance error of 0.15 meters and an absolute maximum of 3.3 meters was found for 500 simulations.
In the section where the probability of exceedance to be used for the maximum expected values was selected, it was already suggested that for higher probabilities of exceedance, the error will increase rapidly and from these results this can be confirmed. However, it should be noted that these results only give an indication as to what happens when the waves exceed the maximum estimate. In these calculations, the parameters that were used for the control system are not changed and by using other, or changing, control parameters, different results can be obtained. Also, these calculations do not account for any flexibilities in the system whereas these will have an effect on the position of the crane tip. It can be concluded that a relatively low probability of exceedance should be used because the ability of the control system to compensate for the limitations of the drive system works very well for one single high wave but for multiple high waves the error will quickly increase.

In the previous elaboration, the controller that was used focuses on minimizing the positioning error of the tip. To do this, it measures the error between the target signal and the actual signal after which it can compensate for this error. However, to increase the performance of the controller, it would be beneficial if the controller already starts to build up a small margin on the positioning error when a large wave is approaching. This way the total error, that is a result of the wave that exceeds the limits of the drive system, is minimized. In the offshore industry, systems already exist that can predict vessel motions by the use of wave radar (Wave Measurement Systems). Such a system measures remote wave profiles and propagates them in time

and space to predict the wave field and estimates the ship response to the predicted waves [15]. From the predicted ship response, the accompanying crane response could be estimated by which the control system can prepare itself for large amplitudes of the acceleration of the crane. It is expected that this will improve the performance of the positioning system without increasing the required capacity of the drive system for which further research should prove what the impact will be.

4.7. Results & Discussion

4.7.1. Workability

As a result of previous sections, the required torque, power, speed and stroke can be calculated for any sea-state. The best way to gain insight into the limitations of the crane concepts when motion compensation is concerned, is to construct a workability graph that represents the cranes capability to compensate motions for different sea states. In such a workability graph, the performance of the crane is expressed in terms of significant wave height up to which the system can compensate, for different peak wave periods of the wave spectrum.

For vessel designs, scatter plots are used to assess their performance. In DNV RP-C205, worldwide scatter plots are given. The global range of periods included, is from T_p=5 seconds, to T_p=30 seconds. For the workability curves, a T_p range between 5- and 40 seconds is selected because some limitations are better visible for larger wave periods. In figure 4.34, all wave spectra that are used for the workability estimates are plotted.

To determine the workability of the crane, the relation between the requirements of the drive system and the wave height is used. For most of the crane properties, such as the torque, speed, and stroke of the crane, a linear relation with the wave height is valid because only linear RAOs are used. Only the power requirements of the crane are not linear, these are quadratically related to the wave height. With the use of these relations, the calculated drive system properties, can be divided by the significant wave height that functioned as input for the calculation. This way, the drive system requirement, for any significant wave height when other wave spectrum parameters do not change. Doing this the other way around, also the significant wave height up to which the system can compensate can be calculated for the current capacity of the drive system. By doing this for different sea states, the motion compensating performance of the crane cann be represented in a workability plot. In figure 4.35, such a workability plot is presented in which the y-axis represents the significant wave height up to which the system can compensate and the x-axis represents the peak wave period of the wave spectrum. For each property of the drive system, a line can be drawn which describes the limiting wave height up to which it can compensate for a specific peak wave period. By plotting multiple properties of the cranes drive system in the same workability graph, the limiting mechanism can be identified.

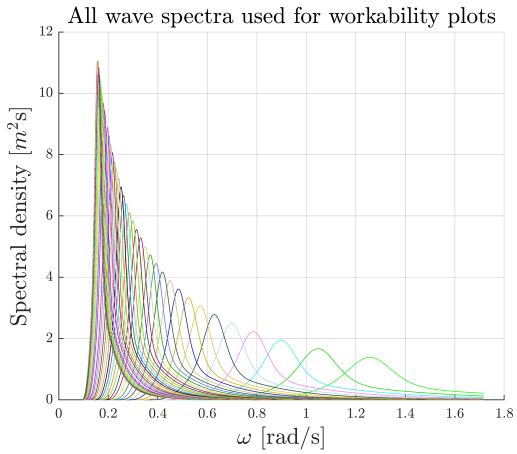

Figure 4.34: All wave spectra that are used for the workability analysis. The peak period of the spectrum is varied between 5 seconds and 40 seconds. For $T_p < 5$, not all energy of the wave spectrum is captured in this frequency range.

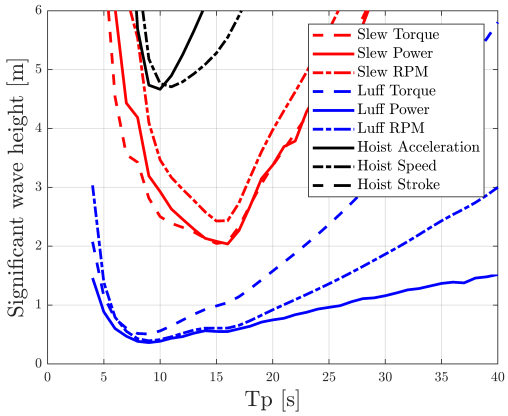

Figure 4.35: In this graph, the maximum significant wave height is plotted for which the drive system of the crane can compensate at different peak periods of the wave spectrum. By comparing multiple properties of the drive system, the limiting mechanism can be identified by the lowest line in the graph.

PMOC Workability

In figure 4.36, the workabilities that are calculated for the PMOC are displayed. These graphs are based on the design cases that are formulated in chapter 2 and the initial drive properties that are defined in appendix D. From the figure it can be seen that the luffing motion (blue lines) is the limiting factor for all of the different design cases and the crane can only compensate for a significant wave height of approximately 0.8 meter for T_p = 8s, in the most promising design case (design case 2). The poor performance of the luffing motion can be explained by the large transmission ratio between the actual rotation of the boom, and the rotations of the drum of the boomhoist winch. The total transmission from the boomhoist elongation to the rotation of the drum is considerable because of the 15 falls and for this reason the speeds and accelerations at the drum are large. Because the accelerations and the speeds at the drum are large, the inertia of the E-motor has a large impact on the resulting torque and power. From the inertia balance that was described in section 4.3.5 it was already observed that the inertia of the E-motor would be problematic. The question arises why the numerous amount of falls are used while it was shown that this negatively influences the performance of the drive system. At first, the falls reduce the line pull in the boomhoist assembly. This is important because otherwise the wire diameter would have to increase. An increased wire diameter will have a larger minimum bending radius by which the diameter of the sheaves will have to increase leading the a more expensive system. Another effect of a reduction of the number of falls is an increase of torque at the E-motor shaft because the total transmission is reduced. The inseparable issue of the luffing motion is the fact that the force to hold up the load is transmitted through the boomhoist. This force is included in the gravitational load that is calculated in section 4.4 and when the number of falls reduced, the gravitational torque on the drum increases. This will be discussed in further detail in section 4.7.2. The jagged lines of the power are a result of the statistical offset of the time domain calculations.

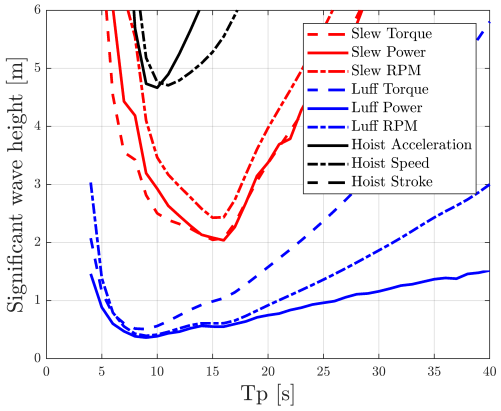

(a) PMOC workability DC 1

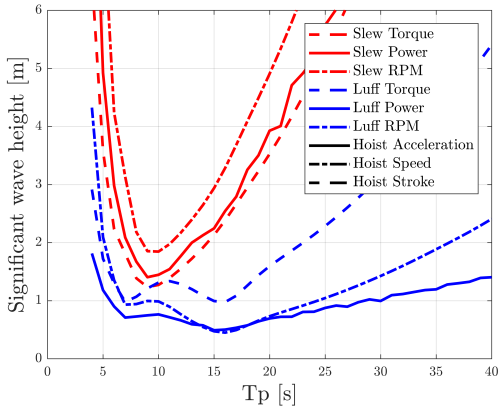

(b) PMOC workability DC 2

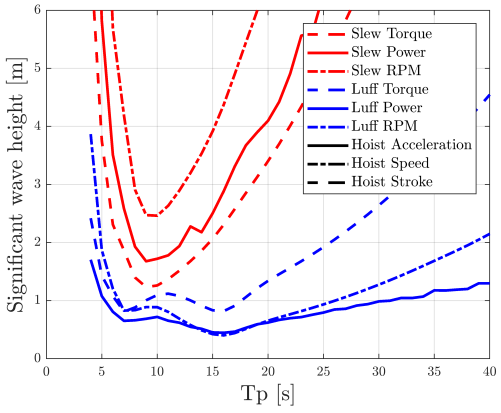

(c) PMOC workability DC 3

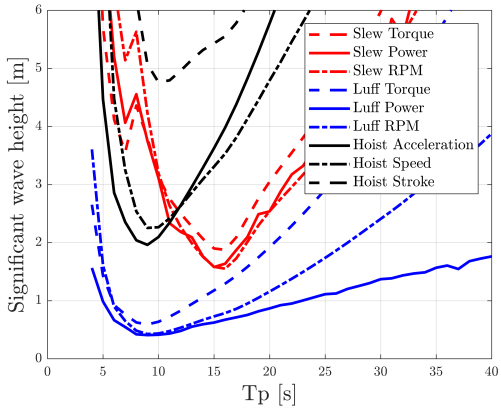

(d) PMOC workability DC 4

Figure 4.36: Workability graphs for the Pedestal Mounted Offshore Crane. Figures a-d are the workabilities for design case 1 to 4.

From the workability graphs it can also be seen that the performance of the slewing motion for design case 1 is much better than the luffing performance. However for design cases 2 and 3, the slewing performance decreases. This can be explained by the fact that in design case 2 and 3, the slewing motion is almost perfectly coupled to the pitching motions of the vessel and because only headings up to 30°are used, the pitching motion of the vessel is larger than the roll motion of the vessel. As one would expect from a general point of view, the degree of freedom of the crane with the best motion compensating performance should be linked to the degree of freedom of the vessel that generates the largest tip displacements in order to obtain the best workability performance of the total system. For the PMOC, this means that design case 2 would lead to the best compensating performance.

Concluding on the workability of the PMOC it can be said that the performance of the luffing motion is the limiting factor of the PMOC by which it can only compensate up to $H_{sig} \approx 0.8$m. By reducing the gearbox ratio of the luffing winch some improvement can be achieved in the balance between maximum torque and power by which also the limitation of the motor speed will decrease. However, it is expected that this effect will not increase the workability significantly. The slewing motion seems to be almost sufficient for effective compensation in design case 1 but reduces in design cases 2 and 3. The balance between torque and power of the slewing motion is good because both of these are limited to almost the same wave height.

HBC Workability

In the workability of the Hybrid Boom Crane, extra parameters are included which can be seen in figure 4.37. The extra degree of freedom that this crane type offers is combined with the luffing motion and by this the performance of the luffing motion increases. When the workabilities of DC 1 and DC 4 of the HBC are compared to the PMOC, it can be seen that the luffing performance of the HBC is approximately 1.5 times better than that of the PMOC. However, by inspecting the workability graphs of the HBC, it can also be concluded that the relation between the luffing motion and the knuckle motion is not optimal. The luffing motion runs into its limit before the knuckle motion does. This suggests that an alternate control strategy of the luffing and knuckle motion could increase the total performance of the crane. By comparing DC 2 and DC 3 it can be seen that the performance of DC 2 is slightly better than that of DC 3. This is explained by the different boom angle of the initial crane position. Because in DC 3, the boom angle is smaller, the boom angle rotation to compensate a tip displacement in the local x-direction is larger. In fact, the compensating mechanisms is less efficient. For very high boom angles, the efficiency would be optimal but than there will be no stability because in this position the boom is close to the point where it can fall back. The same is true for the PMOC and an accompanying effect of high boom angles is a reduction of the performance of the slewing motion.

The slewing performance of the HBC is almost equal to that of the PMOC which is remarkable. One would expect that the additional mass of the knuckle, at the tip of the mainboom, would impose a large additional inertia for the slewing motion. In fact this is the case, the relatively small mass of the knuckle generates a large inertia because of the distance between the slewing axis and the CoG of the knuckle. However, the inertia of the mainboom is smaller because its boom angle is 78° instead of the 73° boom angle from the PMOC in DC 1. At the same time, the installed torque and power for the slewing motion is larger for the HBC, because gravitational loads for heel are larger.

Observing the performance of the AHC, the PMOC offers much better vertical compensation performance. The luffing motion of the PMOC automatically compensates for a part of the vertical motions of the tip. When the vessel rolls to one side, the tip position is lowered and moved to the side. Because the PMOC compensates by rotating the boom, both the sideways translation and vertical translation are compensated for, even though the control is focused on the sideways translation. This works very well when the pivot of the boom is close to the CoG of the vessel as illustrated by the AHC performance of the PMOC in design cases 2 and 3. When the HBC compensates for the sideways motion, it uses the level luffing criterion to coupling the luffing and knuckle motion. This means that the horizontal compensation does not influence the vertical position of the tip in the local axis system. Because of this, all the vertical offset of the crane tip by the roll motion of the vessel is to be compensated by the AHC and this explains the difference between the PMOC and HBC. It can be concluded that for a more balanced design, the level-luffing criterion should not be used to couple the luffing and knuckle motion.

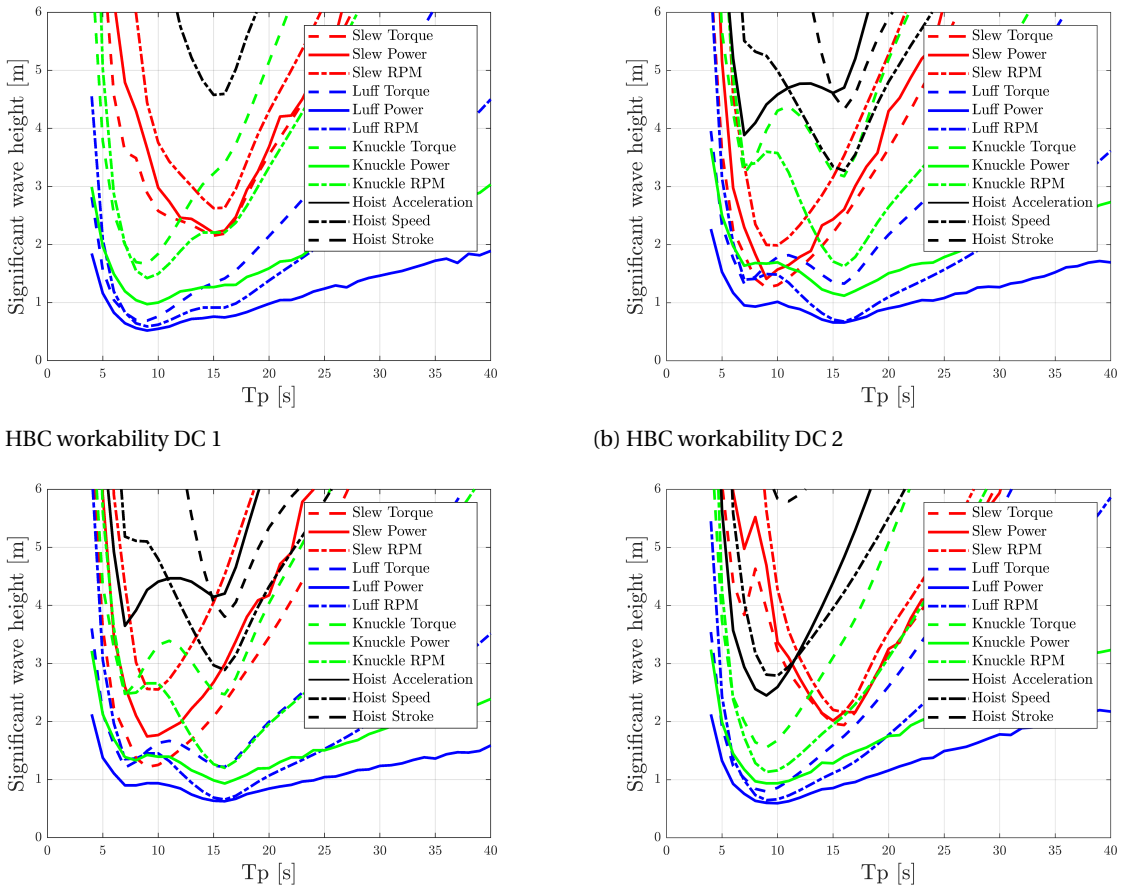

(a) HBC workability DC 1

(b) HBC workability DC 2

(c) HBC workability DC 3

(d) HBC workability DC 4

Figure 4.37: Workability graphs for the Hybrid Boom Crane. Figures a-d are the workabilities for design case 1 to 4.

MCCC Workability

The workability of the Motion Compensated Crane Concept is plotted in figure 4.38 for design cases 1 to 4. To calculate the workability of this concept, the drive system configuration was to be determined whereas this is not an existing crane concept. To do so, the capacity of the drive system was adjusted to be able to compensate for the target significant wave height of H_{sig} = 3m. Therefore, the fact that the crane concept can almost compensate for H_{sig} = 3m is not a surprise. However, it is important to note that the capacity of the drive system that is used for these graphs is much smaller than the capacity of the drive system of the PMOC and HBC. For both the X-compensation and the Y-compensation, E-motors are used that are approximately 2 times smaller than the E-motors that are used for the boomhoist of the PMOC and HBC. By this it can be said that the MCCC concept is much more efficient for motion compensation when the capacity of the drive system is concerned.

In the workability graphs of the MCCC, two additional lines are plotted that are not present in the workabilities of the PMOC and HBC. These are the X-Stroke and Y-Stroke of the motion compensation system. These strokes are the limitations of the skid-table because of its width and length. It can be seen that for design case 1, and design case 4, the Y-Stroke is limiting the workability and here the same holds as was described for the PMOC earlier. The crane's degree of freedom that has the best compensating performance should be used to compensate for the largest tip motions. Therefore, design case 2 and design case 3 give the best performance because here the tip displacements by the roll motions are the largest and they are coupled to the skid table direction with the largest stroke.

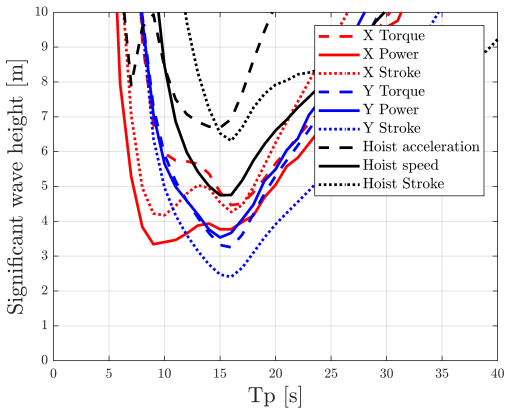

(a) MCCC workability DC 1

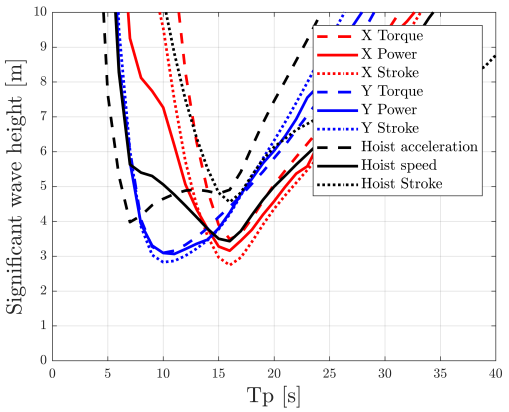

(b) MCCC workability DC 2

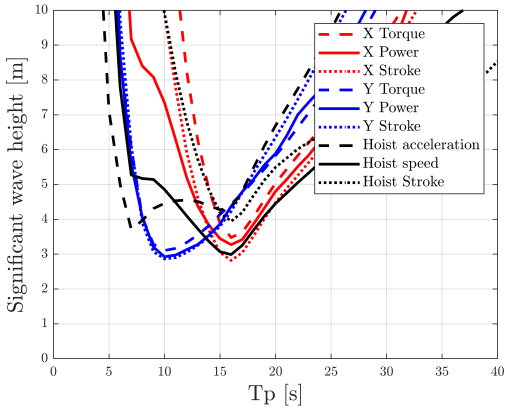

(c) MCCC workability DC 3

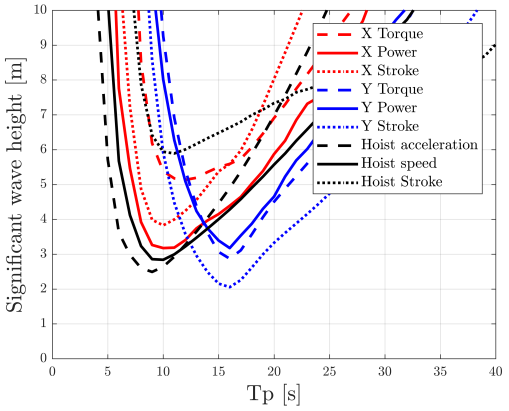

(d) MCCC workability DC 4

Figure 4.38: Workability graphs for the Motion Compensated Crane Concept. Figures a-d are the workabilities for design case 1 to 4.

4.7.2. Comparison & modifications of the drive system

From the workabilities that are calculated for the different crane concepts, it can be concluded that the MCCC offers the best motion compensating performance. For the drive system of the MCCC, only half of the capacity of the boomhoist from the PMOC and HBC was used by which it can be stated that the motion compensating principle of the MCCC is much more efficient. Not only does the MCCC perform better than the other concepts, it also is the only concept that reaches a workability of $H_{sig} \approx 3$m, which is required to be competitive with the use of a jack-up. The workability of the PMOC and HBC's for their initial drive systems are limited to $0.8m$ and $1.0m$ respectively. From these results it can be said that the MCCC is the most feasible concept from a workability perspective.

Although the workabilities of the PMOC and HBC for the current drive system properties are not sufficient to compete with the workability of the MCCC. By adjusting the properties of the drive system, an increased workability could be obtained and therefore different modifications of the drive system and their effect on the workability are investigated. Three adjustment are discussed:

- Reducing the total transmission ratio of the luffing mechanism by using another gearbox ratio.
- Installing E-motors with advanced cooling systems by which the motor inertia reduces.
- Increase the capacity of the drive system.

To investigate the impact of different modifications of the the system, design case 1 of the PMOC is used. In figure 4.39a the reference workability is plotted.

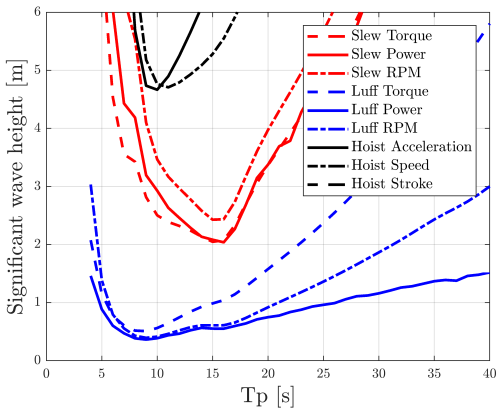

(a) Reference workability of the PMOC for design case 1 with the original drive system.

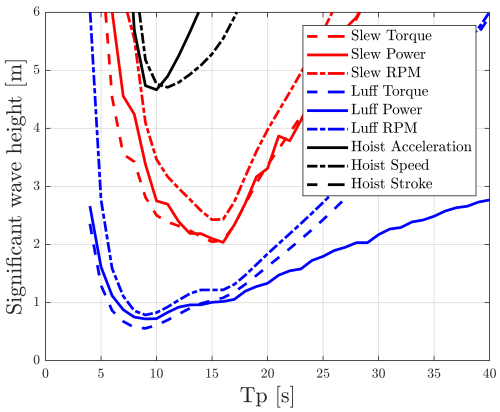

(b) Workability of the PMOC for design case 1 with a reduced transmission ratio of the luffing motion by using another gearbox in the drivetrain.

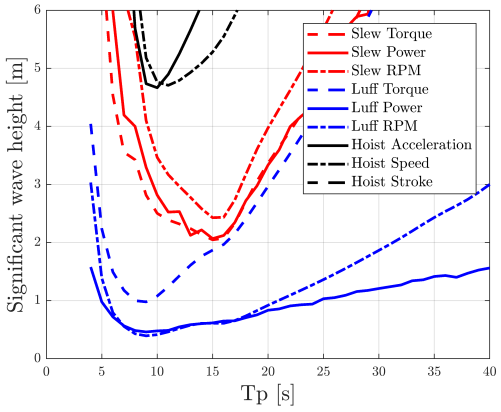

(c) Workability of the PMOC for design case 1 with a reduced motor inertia by using advanced cooling systems on the E-motor.

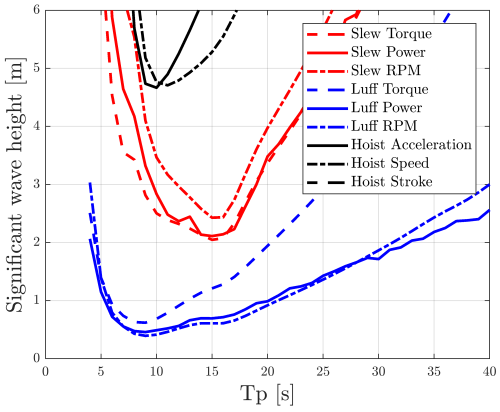

(d) Workability of the PMOC for design case 1 for which the capacity of the drive system for the luffing motion has been doubled.

Figure 4.39: Workability graphs for the Pedestal Mounted Offshore Crane in design case 1 with different modifications of the drive system.

Reducing the gearing ratio

In the reference situation it can be seen that the limiting property of the drive system is the power of the E-motors. Also, it has already been explained that the required power is a function of both the velocity and the acceleration of the luffing motion. Because the luffing motion is not designed to be quick, and has to generate a large torque to hold up the load, the gearing ratio between the luffing motion and the rotations of the E-motor is large. It was already explained that a reduction of the number of falls will lead to an increased wire diameter and larger sheaves however, the transmission ratio of the gearbox that is mounted to the E-motor can be reduced. By doing this, it is expected that the contribution of the gravitational torque to the total torque requirement will increase because this load will not change and a reduced gearing ratio will lead to an increase in torque. However, the changes of the dynamic torque are more interesting and might lead to an improved performance of the crane.

A reduction of the transmission ratio between the luffing motion and the rotations of the E-motor will increase the inertia of the rotating boom motion at the motor shaft, but also reduce the required acceleration of the E-motor. Because the inertia balance of the luffing motion consists mainly of motor inertia, the increase of the boom inertia is not very large compared to the total inertia for luffing. The total torque at the shaft of the E-motor is a combination of both the gravitational loads and the dynamic loads and whether this increases or decreases has to do with these balances. Also, a reduction of the transmission ratio will decrease the required RPM of the E-motor which is a limiting factor as well. Depending on the increase or decrease of the total torque, the total power requirement is expected to decrease because of the lower angular velocities

at the E-motor.
A reduction of the total transmission of the luffing motion of 2 was used to investigate its impact of which the result is displayed in figure 4.39b. From this graph it can be seen that the luffing motion is not limited by the power and maximum speed anymore for the lower wave periods, but the maximum torque has become a limiting factor. Also, it can be seen that the total performance of the luffing motion has increased. For larger reductions of the gearing ratio, the maximum torque will increase further because of the gravitational loads and the total performance is not expected to increase. Also, the reduction of the gearing ratio had a positive effect on the maximum speed and the maximum power did not change significantly. Because the total torque increases and the speed decreases, not much improvement was made with respect to the maximum power capacity. Also, the non-linear relation of the power of the system with the wave height requires the power to increase quadratically with the wave height.

Reducing the inertia of the E-motor
The boomhoist drive that controls the luffing motion is placed within the cranehouse and the E-motors that are currently used, have a cooling system with which air is forced through the E-motor. The cooling system of an E-motor is very important because one of the factors that limits the performance of the E-motor is heat generation. Therefore, smaller E-motors can be used for the same power output when they are equipped with better cooling systems. This is interesting for a possible modification of the drive system because when a smaller E-motor can be used, the inertia of the E-motor will be smaller as well and from previous result it was already shown that the inertia of the E-motor has a large impact on the performance of the luffing motion.
The E-motors that are used for boomhoist drives already have a cooling system and when the cooling has to be improved, two options are possible. Either the air that is blown through the E-motor is cooled to lower temperatures, or water-cooling systems are used. To illustrate the impact on the drive system, specifications of water cooled E-motors are used in the model for the PMOC where a reduction of the motor inertia of 50% was used. The reduction of 50% followed from specification sheets of different manufacturers [7], [20].
In figure 4.39c it can be seen that the reduced inertia lead to a better performance of the drive system when the torque and power limit are concerned. In this configuration the maximum speed is the limiting factor. However, it can be seen that the performance of this configuration is still not anywhere near the target significant wave height of 3 meters.

Increase the capacity of the drive system
A third, and final modification of the drive system that is considered is an increase of the installed capacity of the drive system. For this, E-motors are used that have twice the capacity as the original E-motors. Not only will the available torque of the drive system increase but also the available power. Whereas this seems to be a good solution, also the inertia of the E-motor increases and this will reduce the performance of the system. To determine the impact of such a modification, a workability was calculated which is shown in figure 4.39d. In this figure it can be seen that the performance of the system increases only slightly. The torque limit is improved but the additional performance by the power is limited from which it can be said that simply increasing the installed capacity of the drive system by using more/or larger E-motors will have a small impact on the total performance of the crane system.

5

Crane stiffness

For the feasibility of motion compensation, it is to be investigated whether the possible deformations by gravitational loads of the crane have influence on the motion compensating performance of the crane. Also, the natural frequencies of the crane are evaluated and the impact of dynamic motion amplification on the motion compensating performance is elaborated on. With a crane fixed to a moving vessel, the natural frequencies of the crane should not be close to any of the periodic vessel motions to avoid resonance.

Within the offshore industry, crane vessels have been in use for a long time and Huisman is experienced in the design of offshore cranes that can also be operated at sea. Generally, large cranes are not used in high waves and heavy lifting operations can only be performed in mild wave conditions. For larger waves, such as H_{sig} = 3m, the load will start to swing too much to continue the operation. Therefore the crane does not have to be designed to sustain the loads that would be experienced in high waves. For this reason, static strength requirements are generally used in the design process.
In a conventional design process, the crane is designed for a specific SWL at which the crane must satisfy certain load requirements. These load requirements include loads at inclination, swinging loads, external loads and also dynamic loads from a so-called dynamic impact factor. This impact factor originates from the impact on the crane when a load is suddenly lifted from the deck. For many of these requirements, the existing assessment mainly focuses on the stresses that take place in different parts of the crane. These may not exceed the yield stress of the material where a specific safety factor is included that is demanded by classification authorities. Another aspect of the boom that is part of the conventional design process is an assessment of the buckling limit. Buckling may occur even when stresses are below limits, while the buckling stability is depending on the stiffness of the boom. However, for the wind turbine maintenance crane, it is expected that even when the boom is sufficiently strong according to the conventional design method, dynamic amplification may occur by resonance.

The analysis of the crane stiffness is divided into three parts.

- A boom is selected and modified to suit the purposes of this operation and the boom stiffness is determined from a FEM model. (section 5.1)
- Deflections of the boom by gravitational loads are calculated for limiting situations during the motion compensation cycle. (section 5.2)
- The natural frequencies of the cranes are calculated with simplified models by the use of a modal analysis and the dynamic response of the crane is elaborated on. (section 5.3)

The calculations that are performed in this chapter are specifically focused on the PMOC and HBC. Because the design of the MCCC is not specified in detail, it is difficult to calculate maximum stresses and natural frequencies for this crane concept. However, in the discussion at the end of this chapter, results and findings are expanded to the MCCC.

5.1. Boom strength & stiffness

For the motion compensated PMOC, an initial boom of a 600mt PMOC is used and this boom is elongated from 88 to 120 meters so that it fits the purpose of a wind turbine maintenance crane. To do so, the same initial crane design is used as in section 2.7. For the motion compensated HBC, the same initial boom is used and it is elongated from 88 to 132 meters.

At first, it is verified whether the boom is strong enough for the new load conditions and therefore different load cases are simulated. For all of them, the maximum stresses in the boom are calculated with the use of a FEM analysis (Finite Element Model) that has been developed by Huisman. Also, the buckling limit is checked to have at least a safety factor of 2 which is generally used for crane designs within Huisman. Afterwards, the boom stiffness is calculated which will be used to calculate the deflections of the crane tip as a result of the gravitational load. Also, the stiffness of the boom is used to determine the natural frequencies of the crane system. For the strength calculations, a load of 240 mt is used, which was selected in operational context. The crane positions, and load conditions, that are used to check the strength of the boom are displayed in table 5.1.

Crane position	1	2	3	4	
Boom angle [°]	83	73	64	5	
Load [tonne]	240	240	240	0	
Load case	1	2		3	4
Hoist factor	1.1	1.1		1.1	1.1
Heel [°]	0	5	Sidelead [°]	1	5
Trim [°]	0	5	Offlead [°]	1	5

Table 5.1: Crane positions and load conditions that are used to check the maximum stresses in the boom.

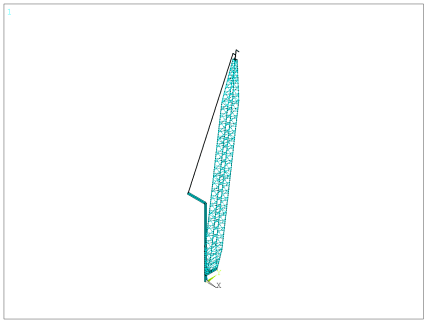

Figure 5.1: FEM model for the boom strength calculations of crane position 1.

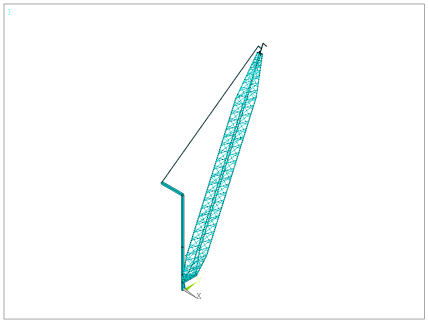

Figure 5.2: FEM model for the boom strength calculations of crane position 2.

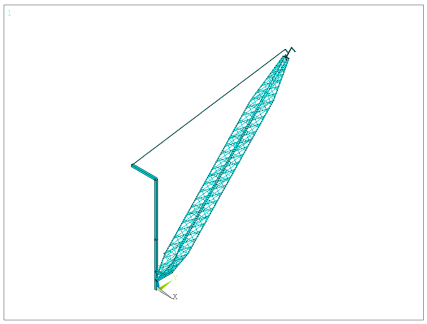

Figure 5.3: FEM model for the boom strength calculations of crane position 3.

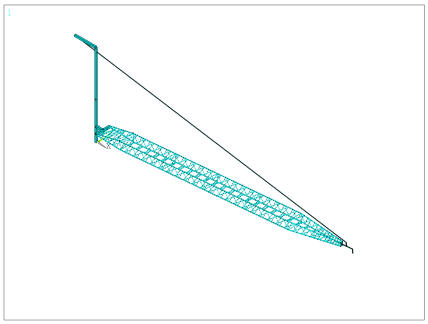

Figure 5.4: FEM model for the boom strength calculations of crane position 4.

The crane positions from table 5.1 follow from the design cases for which the crane concepts are evaluated. In design case 1, the initial boom angle of the crane is 73° for the PMOC and 78° for the HBC and MCCC. While compensating, the boom angle changes and for this reason two additional crane positions are used with boom angles of 83° and 68° to cover the range in which the boom will operate. Finally, crane position 4 simulates the case when the boom is lowered into transit position. Although the load cases for heel and trim will impose the largest loads on the boom, sidelead and offlead load cases are also included because they are used to determine the stiffness of the boom.

Strength of the boom
After performing a FEM analysis in ANSYS for the combinations of table 5.1, maximum stresses throughout the entire boom are obtained. The wall thickness of the chords of the original boom has been increased to satisfy the design requirements. From all combinations in table 5.1, load case 2 for crane position 1 results in the highest stresses in the PMOC boom. The top chords of the boom turn out to be the limiting factor. The material that is used for the boom is S690 which is a steel that has a yield limit of 690 MPa, A non-linear FEM model with load factors is used and therefore a safety factor of 1.1 can be used for the yield strength of the steel. The maximum stress that follows from all load cases is 620 MPa which is within margin of the limit of $\frac{690}{1.1} = 627MPa$. Although the load condition in which the maximum stresses take place (5° heel and 5° trim) is not a load condition that is expected during the motion compensation cycle, the boom must be sufficiently strong in case the motion compensating system fails. The buckling limit is evaluated with the FEM model as well by calculating the maximum buckling load at which the boom will fail and compare this with the resulting loads from the different load cases. For all load cases a safety factor of more than 3 was calculated which is sufficient because within Huisman, the minimum safety factor used for buckling of the boom of a crane is 2.

For the HBC boom, the FEM model of the elongated boom of 132 meters is used at which a rigid element is connected to the top of the boom to simulate the knuckle (figure 5.5). The rigid element that represents the knuckle has a length that is chosen such, that it generates the same torsional moment around the mainboom as the knuckle would do. By doing this, no stresses in the knuckle itself are calculated. The motivation to do this analysis is to check whether the mainboom is sufficiently strong to sustain the additional torsional moment, that is a result of the knuckle and the specific design of the knuckle itself is not focused on. The torsional moment is mainly absorbed by the braces in the boom and from the FEM results, the maximum stresses in the braces are found to be much larger than for the boom of the PMOC. The wall thicknesses of some parts of the PMOC boom have been increased in order to obtain a boom design in which the stresses do not exceed maximum stress including safety factor. Also, the buckling loads were found to be within limits.

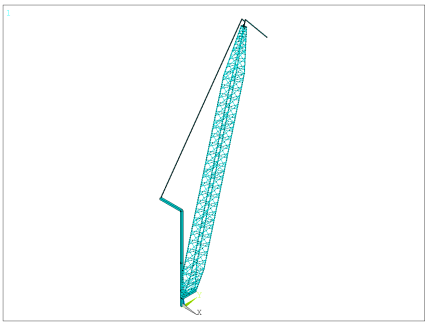

Figure 5.5: FEM model of the HBC with a rigid beam element to simulate the torsional moment as a result of the knuckle.

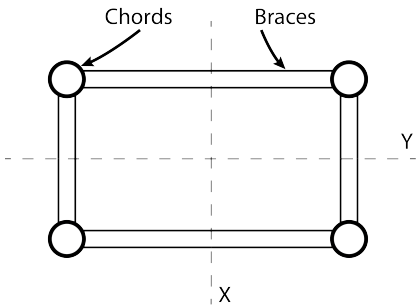

Figure 5.6: Schematic illustration of the cross section of the boom with the definition of its moments of inertia.

After checking the static strength of the boom, its stiffness is determined. The stiffnesses of the boom are calculated so that they can be used in the modal analysis of the crane. In the modal analysis of the crane, the natural frequencies of the crane are evaluated to assess the dynamic response (section 5.3). In figure 5.6, a cross section of the middle of the boom is illustrated with the definition of the local X- and Y-axis. In this illustration, the Y-direction corresponds to the transverse displacement of the boom. The moments of inertia around the X- and Y-direction are calculated with the results of the FEM models that have been used to check whether the boom is sufficiently strong.

Moments of inertia of the boom

In figure 5.6, the cross section of the boom is illustrated and the moments of inertia around the X- and Y-axis are calculated. At first, the moment of inertia around the X-axis is calculated with the use of a clamped beam model (figure 5.7). By creating load cases for 1- and 5 degrees sidelead and extracting the maximum transverse tip displacement (δ_{tip}) from the FEM calculations, the moment of inertia around the X-axis (I_{xx}) can be determined. On purpose, sidelead angles are used and not heel angles because the force by sidelead (F_{side}) can be approximated by a force vector at the tip of the boom and no transverse gravitational loads on the boom have to be incorporated. However, during motion compensation, heel and trim angles are more realistic because the boom will experience the load of its own weight when it is not perfectly vertical. Therefore, heel and trim conditions are used for the deflections by gravitational loads in section 5.2.
The transverse moment of inertia I_{xx} of the boom is calculated with equation 5.2. In equation 5.2, a boom length L_{boom} of 120 meters is used together with an E-modulus for steel of 210 GPa. The values displayed in table 5.2 are valid for crane position 2, which corresponds to the initial crane position of design case 1. An illustration of the clamped beam model is displayed in figure 5.7.

$$F_{side} = sin(\angle_{sidelead}) \cdot 9.81 \cdot m_{load} \tag{5.1}$$

$$I_{xx} = \frac{F_{side} \cdot L_{boom}^3}{3 \cdot E \cdot \delta_{tip}} \tag{5.2}$$

$$\tag{5.3}$$

PMOC Horizontal plane		
Sidelead [°]	1	5
Y-Deflection (δ_{tip}) [mm]	173	863
F_{side} [kN]	41.1	205
I_{xx} [m^4]	0.65	0.65

Table 5.2: Deflections of the PMOC crane tip in the horizontal plane by sidelead and the moment of inertia of the boom around the X-axis for crane position 2.

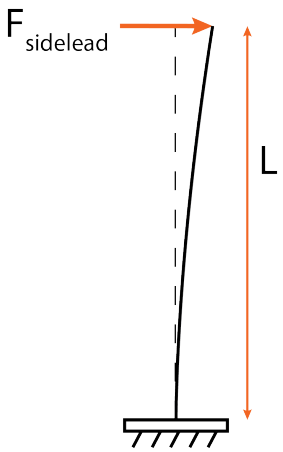

Figure 5.7: Schematic representation of the clamped boom for which the moment of inertia I_{xx} is calculated with the use of the sidelead force.

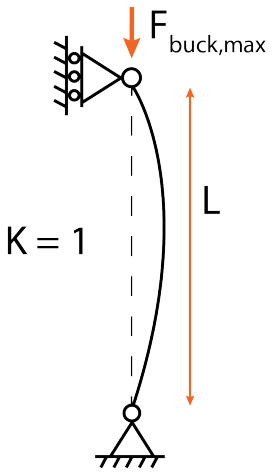

Figure 5.8: Schematic representation of the hinged boom for which the moment of inertia I_{yy} is calculated with the use of the buckling force.

For the modal analysis, the moment of inertia around the y-axis of the boom (I_{yy}) is required as well. The approach that was used to calculate I_{xx} cannot be used to calculate I_{yy} because the forces by offlead are mainly absorbed by the boomhoist. To calculate I_{yy}, the maximum buckling force of the boom is used. The FEM model that has been used to determine the stresses in the boom can also be used to calculate the maximum

allowable buckling force of the boom ($F_{buck,max}$). From the maximum buckling load of the FEM analysis, the moment of inertia around the y-direction can be approximated by using Euler's formula for buckling of slender structures (equation 5.4). In equation 5.4, the maximum buckling force is used together with the E-modulus of steel, the length of the boom and the column effective length factor (K). A K-factor of 1 is used for the buckling of the boom along the y-axis which corresponds to a beam that is supported by a pinned hinge at both ends of the boom, see figure 5.8.

$$F_{buck,max} = \frac{\Pi^2 \cdot E \cdot I_{yy}}{(K \cdot L_{buck})^2} \tag{5.4}$$

For the HBC boom, the exact same approach has been used to determine I_{xx} and I_{yy} of the mainboom. By doing this, the moments of inertia of the mainboom are calculated. In the dynamic analysis, the other components of the HBC such as the knuckle will be modelled as rigid beams while the flexibility of these parts of the crane is expected to be of minor influence because of their shorter lengths. The parameters calculated for I_{xx} and I_{yy} are summarized in table 5.3.

Structural parameters of boom	$I_{xx}[m^4]$	$F_{buck,max}[kN]$	$L_{buck}[m]$	$I_{yy}[m^4]$
PMOC	0.65	32826	120	0.23
HBC	0.55	29117	132	0.26

Table 5.3: Structural parameters of the boom that are calculated from the FEM results.

5.2. Deflections by gravitational loads

During the motion compensation cycle, the gravitational loads on the boom are constantly changing. Whereas the compensating motions module uses a rigid boom to calculate the compensating motions of the crane, in real practice the boom will elastically deform. To determine whether the deflections of the boom during the motion compensating cycle are of significance, these are calculated. For this, the loads on the boom are used which follow from the heel and trim angles that are calculated in the compensating motions module.
For H_{sig} = 3m and T_p = 8s, maximum expected deflections of the tip are calculated in the local reference frame on the tip of the boom. In table 5.4 the tip deflections for design cases 1 to 4 of the PMOC are displayed. The stiffness in the local X- and Z-direction are mainly a result of the stiffness of the boomhoist whereas the stiffness in Y-direction is mostly dependent on the stiffness of the boom itself. The results that are shown for the X-direction and Z-direction of the different design cases are offsets from the static deformation for zero heel and zero trim.

PMOC		DC 1	DC 2	DC 3	DC 4
Heel angle [°]	0	0.97	2.47	2.47	0.54
Trim angle [°]	0	2.52	1.10	1.10	2.645
X-direction [mm]	1015	130	57	129	136
Y-direction [mm]	2	213	544	544	119
Z-direction [mm]	-375	-43	-19	-180	-45

Table 5.4: Tip deflections of the PMOC by elastic deformation due to gravitational loads for a significant wave height of 3 meters. The initial crane positions of the design cases have been used and the deflections are offsets from the initial crane position.

The heel and trim angles used in this calculation are based on a 30-min maximum with a probability of exceedance of 10%. It is important to note, that these heel and trim angles must not be used for the strength calculations of the boom, because the probability that these will be exceeded during the lifetime of the crane is high.

For the HBC, the boom is loaded differently when the vessel rolls or pitches. When the vertical plane of the crane and the vertical plane of the global coordinate system are not aligned perfectly, the gravitational load will induce a torsional moment in the boom. This torsional moment is dependent on the position of the crane and also the heel and trim angles of the vessel. Just as for the PMOC, the tip displacements are calculated for heel and trim angles that can be expected for H_{sig} = 3m and T_p = 8s. The actual tip displacements have been extracted from the FEM calculations which use the input of the heel and trim angles, these are displayed in table 5.5. Again, the results that are shown for the X-direction and Z-direction of the different design cases are offsets from the static deformation for zero heel and zero trim. The rotations that are presented are rotations in the local axis system at the base of the crane and also represent offsets with respect to zero heel and trim.

HBC		DC 1	DC 2	DC 3	DC 4
Heel angle [°]	0	0.97	2.47	2.47	0.54
Trim angle [°]	0	2.52	1.10	1.10	2.645
X-direction [mm]	1133	209	94	189	219
Y-direction [mm]	13	443	1137	1137	244
Z-direction [mm]	-663	-34	-16	-120	-36
X-rotation [°]	6.3e-3	0.017	0.057	0.27	3.4e-3
Y-rotation [°]	1.891	-0.115	-0.058	-0.229	0.112
Z-rotation [°]	0.023	0.894	2.383	2.372	0.481

Table 5.5: Tip deflections by elastic deformation of the HBC for a significant wave height of 3 meters for which the initial crane positions of the design cases have been used.

From tables 5.4 and 5.5 it can be seen that the deflections of the boom tip are small for the X- and Z-direction (< 0.3m). However, for relatively small heel and trim angles, the displacements by deformations of the boom in the Y-direction are too large to be neglected.

In order to include the deflections by gravitational loads in the motion compensation system, multiple options can be considered. A first option would be to use the sensors that are already present in a general crane design to determine the loads on the crane. By applying these loads on a FEM model of the crane, the expected deformations of the crane can be estimated. By including these estimated deflections in the control loop, the motion compensation system can compensate for the static tip displacements. However, difficulties could be encountered when the measured data is not accurate. Also, it is very difficult to make a computer model that is similar to the actual crane after it has been build.
A more accurate option would be to actively monitor the deflections of the crane tip with sensors and linking the measured deflections to the control system. In the wind energy industry, companies use Fiber Brag grating to measure the deflections of wind turbine blades while these are in operation [33]. This measuring method uses an optical fibre that reflects particular wavelengths and transmits all others [11]. Within this study, no extended research was done into the application of this measuring system on cranes but it is suggested that for measuring the deflections of the crane tip, it can be useful.

5.3. Dynamic Response

To assess the dynamic response of the wind turbine maintenance crane, its natural frequencies are calculated with a modal analysis in ANSYS. To determine these natural frequencies, the horizontal plane, and vertical plane of the crane are separated in the analysis because they have different stiffnesses from which different natural frequencies will follow.
For the vertical plane, many parts of the crane can be modelled by springs that are connected in series where the weakest link dominates the behaviour of the system. For this reason, very stiff elements that are linked in series with less stiff elements are excluded from the model without significantly influencing the outcome of the analysis. Also, the boom will be modelled as a flexible beam element which will influence the natural frequencies of the crane.
In the horizontal plane, the crane is modelled by a flexible beam element that represents the boom, in combination with a spring element to represent the restoring force of the boomhoist.
The most flexible components within a crane are the mainhoist, boomhoist and the boom itself. Some of the elements that are excluded from the analysis are the stiffness of the cranehouse, pedestal, slew bearing and drivetrain. The models that are developed in ANSYS have been validated by analytic models which can be found in appendix H.

5.3.1. Vertical plane

The natural frequencies in the vertical plane are calculated with the use of simplified crane models. The simplified models for the PMOC and HBC are illustrated in figures 5.9 and 5.10. In figure 5.9, it can be seen that the PMOC has two degrees of freedom (when the flexibility of the boom is disregarded), one is the rotation of the boom (ϕ_1) and the other one is the vertical displacement of the load (u). The load (M_2) is modelled as a point mass without rotational inertia (M_2) and the boom is modelled as a flexible beam with a distributed mass. The boom is supported by a hinge which represents the pivot of the boom. Different springs are included in the model which represent the boomhoist (K_1), and the mainhoist (K_2). The boomhoist is supported by a rotational hinge as well which represents the top of the cranehouse and the mainhoist has a minor offset from the tip of the boom which simulates the sheave by which the mainhoist is lowered. For the model of the HBC, an additional degree of freedom is added which is the rotation of the knuckle around the tip of the mainboom (ϕ_2). Also, a knucklehoist is added to control the knuckle motion (K_3).

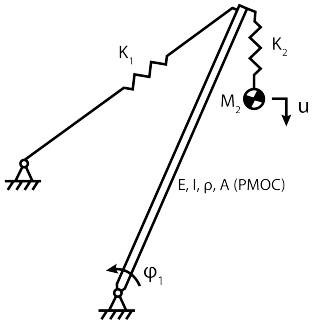

Figure 5.9: Simplified dynamic model of the PMOC.

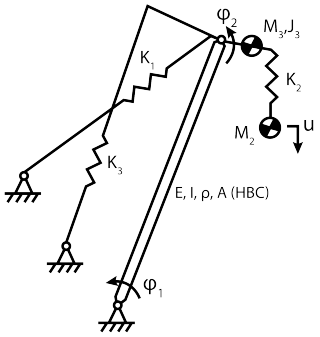

Figure 5.10: Simplified dynamic model of the HBC.

At first, the stiffness of the luffing motion (K_1) is estimated. To determine the stiffness of the different components that influence the luffing motion, an assembly of different spring elements can be made which will be used as K_1 in the model. In figure 5.11 the different components that influence the stiffness of the luffing motion are shown. These components are all in series as the rotational motion of the E-motor at the boomhoist drum will eventually rotate the boom. However, the stiffness of all components that are between the E-motor and the top of the cranehouse have a small influence on the total boomhoist stiffness. The reason for this is the fact that their contribution is increased by the squared number of falls which makes these stiffnesses very large with respect to the boomhoist stiffness. To explain this, figure 5.11 is used.
It can be seen that the force in the boomhoist wire between the E-motor and the cranehead ($F_{bh,2}$) is the total force of the boomhoist assembly ($F_{bh,1}$), but then reduced by the number of falls (equation 5.5). Also,

the displacement of the boomhoist wire between the E-motor and the cranehead ($\Delta L_{bh,2}$), is increased by the number of falls when compared to a displacement of the boomhoist assembly ($\Delta L_{bh,1}$) as can be seen in equation 5.6. Whereas the stiffness of a spring is the force divided by the displacement, the stiffness of the components between the E-motor and the cranehead are increased with the number of falls squared when the total boomhoist stiffness is calculated. This makes the total stiffness of the components between E-motor and cranehead very large and it has been calculated that the contribution of the return wire from the cranehead to the drum contributes for <2 % of the total stiffness of the boomhoist for these crane models. Therefore, only the stiffness of the boomhoist assembly is used for the stiffness of the luffing motion.
The stiffness of the boomhoist wire is calculated with equation 5.7 and because the number of falls in the boomhoist will act as parallel springs, the stiffness of the boomhoist assembly is the wire stiffness multiplied with the number of falls (equation 5.8). The same holds for the knucklehoist and the mainhoist and all three are calculated with the use of the parameters in table 5.6. For the steel wire, a reduced E-modulus is used and the reason for is the fill factor of the rope diameter and the helical force distribution within the wire rope. Huisman tests indicated that an E-modulus of 85 GPa is a representative value which is also used in this model. The total stiffnesses of the springs that are used in the dynamic analysis are displayed in table 5.12.

$$F_{bh,1} = \frac{F_{bh,2}}{falls_{bh}} \tag{5.5}$$

$$\Delta L_{bh,1} = \Delta L_{bh,2} \cdot falls_{bh} \tag{5.6}$$

$$K_{wire} = \frac{E \cdot A}{L} = \frac{D^2 \cdot \pi \cdot E}{4 \cdot L} \tag{5.7}$$

$$K_{assembly} = K_{wire} \cdot falls_{bh} \tag{5.8}$$

Parameters for spring stiffness	No. falls [-]	D [mm]	L [m]	E [GPa]
Boomhoist PMOC	15	50	92	85
Boomhoist HBC	18	50	101	85
Knucklehoist HBC	9	50	118	85
Mainhoist PMOC & HBC	10	50	15	85

Table 5.6: Parameters used to calculate the stiffness of the different springs in the dynamic crane models.

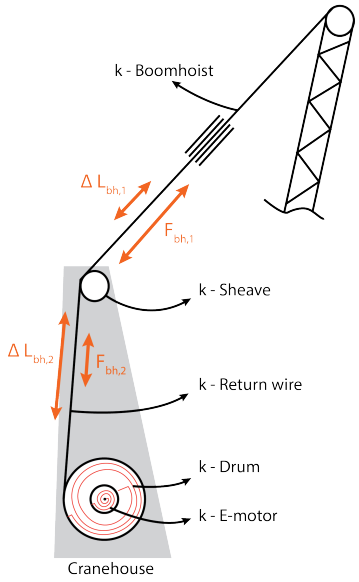

Figure 5.11: Springs in series for the boomhoist stiffness.

Component	Type	Stiffness [kN/m]
Boomhoist PMOC	Wire	1814
Total luffmotion PMOC	Assembly	27211
Boomhoist HBC	Wire	1652
Total luffmotion HBC	Assembly	29744
Mainhoist	Wire	11126
Total mainhoist	Assembly	111264
Knucklehoist	Wire	1414
Total knuckle motion	Assembly	12729

Figure 5.12: Stiffnesses of the springs that are used in the simplified crane models for the dynamic response.

Not only the springs of the dynamic models displayed in figure 5.9 and 5.10 are to be approximated by the crane data. Also the beam that is used in this dynamic model must have properties that represent the actual boom. In section 5.1, the moments of inertia of the boom have already been calculated and in this section these are used for the dynamic models of the cranes. Instead of incorporating the complex lattice structure of the boom in the dynamic model, an equivalent steel beam has been used. The width and height of the rectangular beam element are scaled, so that the beam has the correct moments of inertia around the X-axis and Y-axis of the cross section. Although the moment of inertia around the X-axis of the cross section is not of relevance for the vertical plane, it is calculated to use it in the model for the horizontal plane. With equations 5.9 and 5.10, the width and height of the cross section are determined and from the cross section and the length of the beam element, its volume is calculated. To give the beam element the mass of the boom, the weight of the boom is divided by the volume of the beam element by which the density of the beam element is obtained (equation 5.11). This is done for the beam element that represents the boom of the PMOC in figure 5.9 and also for the beam element that represents the boom of the HBC in figure 5.10. The knuckle of the HBC is modelled as a rigid beam.

$$I_{xx} = \frac{b \cdot h^3}{12} \tag{5.9}$$

$$I_{yy} = \frac{h \cdot b^3}{12} \tag{5.10}$$

$$\rho_{beam} = \frac{M_{boom}}{b \cdot h \cdot L_{boom}} \tag{5.11}$$

Properties used for the dynamic crane models	$I_{xx}[m^4]$	$I_{yy}[m^4]$	$b[m]$	$h[m]$	$\rho[kg/m^3]$
PMOC	0.65	0.23	1.90	1.13	890
HBC	0.55	0.26	1.76	1.21	849

Table 5.7: Properties used for the dynamic crane models.

5.3.2. Horizontal plane

In the horizontal plane, the dynamic response is mainly dependent on the transverse stiffness of the boom and also a contribution of the boomhoist is to be incorporated. For these models, a flexible beam is used as well and for this, the properties are used that were already calculated in section 5.1. The beam is clamped at the bottom which is a result of the pivot connection with the crane. The models that are used for the PMOC and HBC are different because the HBC has an additional mass at the tip of the mainboom which is the mass of the knuckle (M_k). The models used for the dynamic analysis in the horizontal plane are displayed in figures 5.13 5.14.

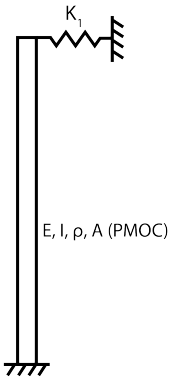

Figure 5.13: Simplified dynamic model of the PMOC in the horizontal plane.

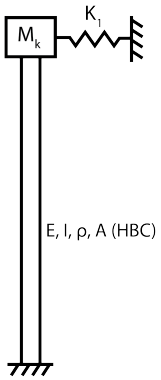

Figure 5.14: Simplified dynamic model of the HBC in the horizontal plane.

The contribution of the boomhoist to the transverse stiffness of the boom (K_1) in figures 5.13 and 5.14 is approximated by a linear spring. To determine the spring constant of this spring, the total force in the boomhoist of both cranes is calculated for a static loading condition in which only gravitational loads are considered. The boomhoist force is calculated with equation 4.11 from chapter 4. The spring stiffness that is calculated for the horizontal restoring component of the PMOC boomhoist is 38.1 kN/m and that of the HBC boomhoist is 42 kN/m. For the HBC, the knucklehoist will contribute to the transverse stiffness as well which adds an additional 19.6 kN/m to the horizontal spring of the model in figure 5.14.

5.3.3. Modal analysis

To determine the eigenfrequencies of the simplified crane models, a modal analysis is performed in ANSYS. Natural frequencies are determined in the vertical 2D plane of the crane, and in the horizontal plane where the boom is loaded sideways. With the use of ANSYS, the natural frequencies of the system are determined and in parallel an analytic model is set-up to verify the results of the computer analysis (see Appendix H). These analytical models use a rigid beam for the equations of motion and to validate the ANSYS models, the stiffness of the beam elements was increased by which the same results were found for the ANSYS- and analytical models. In the ANSYS models with the flexible beam, the stiffness of the mainhoist, boomhoist and knucklehoist are used from the previous section together with the properties of the equivalent steel beam.

First the natural frequencies and modes shapes that are found from the modal analysis will be described. Afterward the impact of these natural frequencies on the motion compensating performance of the crane will be discussed.

Vertical plane

Because the PMOC model contains a flexible beam element, a lot of natural frequencies can be calculated but for the dynamic response of the crane only the lowest natural frequencies are of interest. The lowest natural frequency is found at 0.43 Hz and the corresponding mode shape is plotted in figure 5.15. The mode shapes that are displayed follow from the ANSYS analysis but for clear images these were re-drawn. The actual ANSYS plots can be found in appendix K. In figure 5.15 it can be seen that the flexibility of the boomhoist is the factor that is responsible for the low natural frequency of the crane. Also, the flexibility of the boom, which shows the first mode shape of a hinged beam, contributes to the low natural frequency. To prove this, the same model has been solved for a rigid beam by which a first natural frequency for the total system of 0.57 Hz was obtained. From this is can be said that the flexibility of the boom is important to include in the dynamic model of the vertical plane of the crane.
The second natural frequency that followed from the ANSYS analysis is shown in figure 5.16. The second natural frequency was found at 0.90 Hz, at which the boom rotates around the pivot. The main difference with the first natural frequency can be explained by the mode shape of the boom. Still the boomhoist is the most flexible element from the system but the second mode shape of the beam leads to a larger natural frequency.
The third natural frequency was found at 2.31 Hz at which the boom resonates without the influence of the boomhoist. The mode shape for this natural frequency is plotted in figure 5.17

Figure 5.15: First natural frequency of the PMOC at 0.43 Hz and its corresponding mode shape.

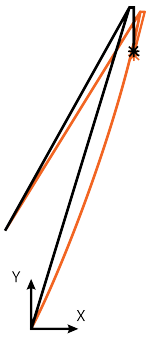

Figure 5.16: Second natural frequency of the PMOC at 0.90 Hz and its corresponding mode shape.

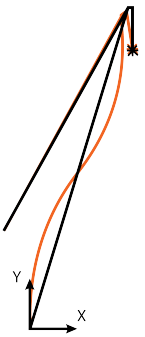

Figure 5.17: Third natural frequency of the PMOC at 2.31 Hz and its corresponding mode shape.

For the HBC, natural frequencies are calculated as well with the use of the dynamic model that was elaborated on earlier. The first natural frequency that is found from the modal analysis is 0.31 Hz. In figure 5.18 the deformed shape for this first natural frequency is plotted in which one can see that the stiffness of the boomhoist is the most flexible element. It is interesting to see that the first natural frequency of the HBC is much lower than that of the PMOC. The boom of both cranes is almost similar and the boomhoist of the HBC is stiffer than that of the PMOC which can be seen in table 5.12. Still the natural frequency at which the boomhoist is flexing is smaller and this is explained by the additional mass of the knuckle at the tip of the mainboom which contributes to a larger moment of inertia around the pivot. Because of this additional mass, the dynamic response of the luffing motion is worse.
The second natural frequency is found at 0.63 Hz at which the boom is oscilating in a higher mode shape. In figure 5.19, this second mode shape is plotted.
The third natural frequency is found at 0.90 Hz and at this frequency, the knuckle rotates around the tip of the mainboom. The stiffness of the knucklehoist is responsible for this and by increasing the stiffness of the kucklehoist, this natural frequency can be increased.

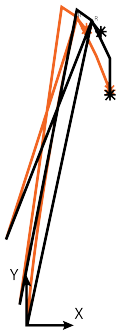

Figure 5.18: First natural frequency of the HBC at 0.31 Hz and its corresponding mode shape.

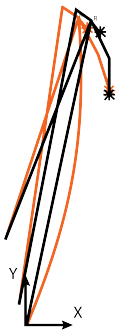

Figure 5.19: Second natural frequency of the HBC at 0.63 Hz and its corresponding mode shape.

Figure 5.20: Third natural frequency of the HBC at 0.90 Hz and its corresponding mode shape.

Horizontal plane
For the horizontal plane model of the PMOC, a lowest natural frequency of 0.36 Hz was found from the modal analysis. The accompanying mode shape is displayed in figure 5.21 and corresponds to the first mode shape of a clamped beam. It was found that the influence of the boomhoist is not very large, the lowest natural frequency without incorporating the effect of the boomhoist is 0.34 Hz.
The second natural frequency of the PMOC crane in the horizontal plane is 2.1 Hz. The mode shape of this second natural frequency is displayed in figure 5.22 but for the influence of the dynamic response on the motion compensation system, these higher mode shapes are not very important. The third natural frequency was found at 5.9 Hz and its mode shape is displayed in figure 5.23.

Figure 5.21: First natural frequency of the PMOC at 0.36 Hz and its corresponding mode shape.

Figure 5.22: Second natural frequency of the PMOC at 2.1 Hz and its corresponding mode shape.

Figure 5.23: Third natural frequency of the PMOC at 5.9 Hz and its corresponding mode shape.

For the HBC, the additional mass at the tip of the mainboom will negatively influence the natural frequencies of the crane in the horizontal plane. Because of this additional mass, the natural frequencies will be lower and from the modal analysis, a lowest natural frequency of 0.27 Hz was calculated. The mode shape corresponding to the lowest natural frequency is the same as for the horizontal plane of the PMOC and the mode shape plot including the natural frequency of the HBC is displayed in figure 5.24.
The second and third natural frequency of the HBC in the horizontal plane are 1.7 Hz and 5.1 Hz. The mode shapes corresponding to these higher natural frequencies are displayed in figures 5.25 and 5.26.

Figure 5.24: First natural frequency of the HBC at 0.27 Hz and its corresponding mode shape.

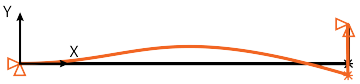

Figure 5.25: Second natural frequency of the HBC at 1.7 Hz and its corresponding mode shape.

Figure 5.26: Third natural frequency of the HBC at 5.1 Hz and its corresponding mode shape.

Impact on the motion compensating performance

In figure 5.27 a schematized representation of the vessel - crane - load system is displayed. A spring mass system is used to illustrate the influence the motion compensation system on the crane motions. The goal of the motion compensation system is to minimize the motions of the load, U_2 in figure 5.27. The motions of the vessel (U_1) are to be compensated by the motion compensation system. However, because the compensating motions are to be realized by the crane, which has its own stiffness, the natural frequencies of the crane will be limiting the compensating performance of the motion compensation system. Therefore, the natural frequencies of the crane must not be close to the frequencies of the compensating motions.

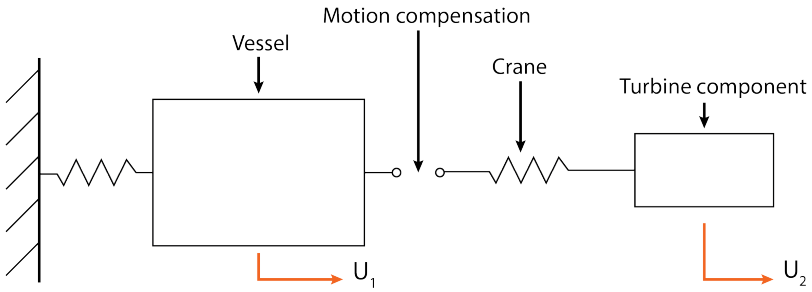

Figure 5.27: Schematized representation of vessel - crane - load system.

At the natural frequencies of the crane, the system resonates and the motion amplitudes are amplified. Depending on the damping in the system, frequencies that are close to the natural frequency will also experience an amplification by the dynamic response. To be able to calculate the dynamic response of the system, the damping in the system is to be estimated. For steel structures, a damping of 2 percent of the critical damping is generally used, this is also stated by Stevenson [30]. Within Huisman Equipment a damping value of 2 percent is used regularly for dynamic analyses.
When the damping is known, the amplification factor for relative frequencies can be determined for a simplification to a single mass-spring-damper system which is displayed in figure 5.28. For a derivation of the transfer function please see appendix H. In this figure, the fraction of the natural frequency is plotted versus the amplification factor of the system. Because the natural frequencies of the system are not very close to each other, this simplification holds for the lowest natural frequency that is found.
For motion compensation, the influence of dynamic motions of the crane is difficult to compensate for. For

this reason, a maximum amplification factor of 10 % is used. This means that the motions of the tip will be increased with 10%. To sketch an example, a maximum amplitude of 5 meters along the local y-axis of the tip is initiated by the slewing motion. When a dynamic amplification of 10% is concerned, the actual displacement of the tip along the y-direction by the dynamic response of the system will be 5.5 meters.
From figure 5.28 it can be seen that a maximum dynamic amplification of 10% can be expected at a fraction of 0.3 from the natural frequency (horizontal green line).

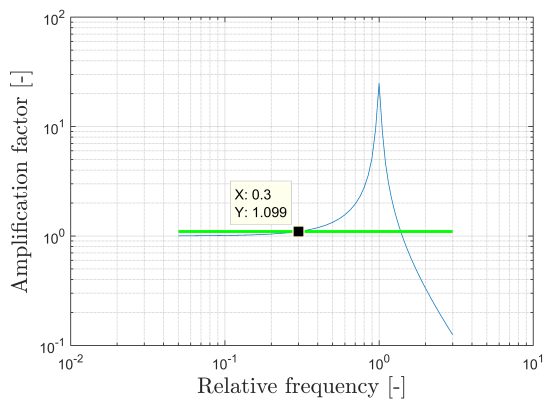

Figure 5.28: Dynamic amplification factor of a single mass spring damper system versus the relative frequency for a damping of 2%.

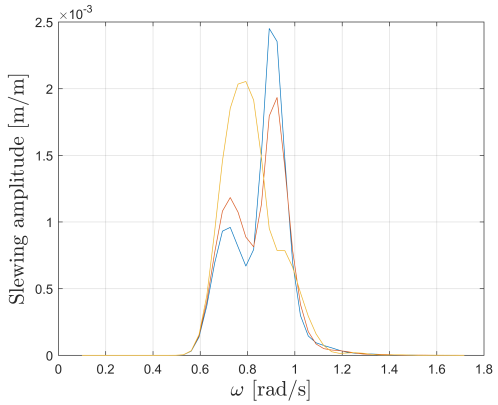

Figure 5.29: Response spectrum of the slewing amplitude of the PMOC for a wave spectrum with a peak period of 7 seconds.

Now that the fraction of the natural frequency at which the system is amplifying the motions too much is known, the minimum natural frequency of different components of the system can be determined. For this, the response spectra of the compensating crane motions are used. From these response spectra, the highest frequencies at which energy is present in the spectrum are determined, and according to the previous assumption, the natural frequency should be 3.3 (1/0.3) times higher than this frequency. As the response spectrum is dependent on the wave spectrum, a wave spectrum with a peak period of 7 seconds is used which was the lowest peak period that followed from the fetch calculations in section 3.1.1. From the response spectra for different design conditions, and different crane types, it can be concluded that there can be energy in the response spectrum up to wave frequencies of 1.4 rad/s (0.22 Hz) (see figure 5.29). This means that the natural frequencies of the crane system should be higher than $\approx 0.72 Hz$. This holds for all different crane motions, because every degree of freedom of the vessel is coupled to every crane motion and therefore energy is found up to 1.4 rad/s for all crane motions. Notice must be made that this frequency is very much reliant on the vessels RAOs and for other vessels, different design frequencies are expected. When this frequency limit of 0.7 Hz is compared to natural frequencies that follow from previous crane designed that are designed for strength, 0.7 Hz already is relatively low. For previous crane designs, the natural frequencies of the crane are usually around 1 Hz.

The natural frequencies of the different crane types that already have been calculated can be compared to the 0.7 Hz that was obtained as 'target natural frequency'. In table 5.8 an overview of all the calculated natural frequencies of the crane is shown and it can be seen that all of these are lower than 0.7 Hz. Although section 5.1 indicated that the boom is strong enough when the maximum stresses and buckling limit are concerned. The dynamic response of the crane shows that the stiffness of the designs is too low to prevent large dynamic amplification of the motions at the crane tip. The stiffness of the cranes will have to be increased in order to be feasible for motion compensation and this can be realized by multiple adjustments. To increase the stiffness of the boomhoist and knucklehoist, additional falls can be used, however, this will directly decrease the workability performance. The transverse stiffness of the boom can be increased by using a different boom structure such as an A-frame most likely increasing the weight of the boom which will also influence the workability. Unfortunately, this thesis does not include an assessment on these modifications but further research should prove whether the stiffness of the crane can be increased to eliminate the dynamic amplifications of the structure for which the motion compensation system has to compensate.

Natural frequencies of the crane	First [Hz]	Second [Hz]	Third [Hz]
PMOC vertical	0.43	0.90	2.31
PMOC horizontal	0.36	2.1	5.9
HBC vertical	0.31	0.63	0.9
HBC horizontal	0.27	1.7	5.1

Table 5.8: Natural frequencies of the PMOC and HBC that are calculated with the modal analysis.

5.4. Results & discussion

The goal of this chapter is to asses the effect of the crane stiffness on the motion compensating performance of the crane. By using an existing boom and re-sizing this boom to fit the purpose of a motion compensated crane, a representative basis for analysis was created. The original boom was designed for a SWL of 600mt whilst the new boom is only loaded with 240mt. A FEM analysis has been performed for different crane positions and load conditions to check whether the boom is strong enough. For all load conditions used, the stresses in the boom are lower than the steel's yield limit including safety factor and the buckling limit is within safety limits.
After defining a boom that is valid for the operation according to a normal design approach, the stiffness effects on motion compensation can be quantified. Both the deflections by gravitational load, and the dynamic response have influence on the compensation system. From the deflections of the boom by gravitational loads it was shown that the resulting deflections of the crane tip are not small enough to neglect. Even for this relatively small load and stable vessel, the deflections of the boom will distort the motion compensation system when not accounted for. Also, it was found that the transverse deflection of the boom by sidelead is much larger than the forward- and vertical tip deflection. The motion compensation must therefore compensate for the additional displacement of the crane tip by elastic deformation due to gravitational loads.

The goal of the dynamic response analysis of the boom was to determine the natural frequencies of the crane and estimate their influence on the compensation performance. The natural frequencies are determined in the vertical and horizontal plane of the crane because the boom has different stiffnesses in these planes. The transfer function for the dynamic response of the system is determined for 2% critical damping and a maximum amplification factor by dynamic effects of 10% is assumed. The maximum frequency in the crane response spectra at which energy is present is used to determine a design value of 0.7 Hz for the natural frequencies of the crane.

In the vertical plane, the natural frequencies of the cranes are significantly lower than the 0.7 Hz limit. For the PMOC, a lowest natural frequency of 0.43 Hz was found. The lower natural frequencies are mainly caused by the limited stiffness of the boomhoist. The relatively small boomhoist stiffness is a result of scaling the cranes which requires a much longer boomhoist. The boomhoist fulfills the static strength requirements in which it has to hold the load of 240 mt but in the dynamic response it turns out to be very flexible. Although the boomhoist of the HBC is stiffer by having three more falls, the natural frequency of the boom rotating around the pivot (0.31 Hz) is even lower than for the PMOC. This is explained by the additional mass of the knuckle at the tip of the mainboom. Also for the MCCC, this problem will arise because of the extra weight of the skid-table at the tip of the boom. Even though the MCCC wil not compensate with the boomhoist, the motions of the crane will be periodic with the vessel motions and therefore the boomhoist of the MCCC will also need to be stiff enough to prevent dynamic amplifications.
In the horizontal plane, the first natural frequency of the boom for the PMOC is found at 0.36 Hz. The influence of the boomhoist on the natural frequency of the boom in transverse direction is found to be small (<5%) and the natural frequency of the HBC in the horizontal plane (0.27 Hz) is lower than that of the PMOC. Again, this is a result of the additional mass of the knuckle at the tip of the mainboom and this will also be the case for the MCCC. Therefore, the further design of the MCCC should focus on increasing the stiffness of the crane and minimizing the masses of the system.

By combining the results of this chapter it can be said that the natural frequencies of the crane, that follow from the existing design method, are too low to prevent the crane from large dynamic motion amplifications. Therefore, the crane designs following from this design method are not feasible for motion compensation. Also, it was shown that a target natural frequency can be determined from the response spectrum when a maximum dynamic amplification factor is selected. By doing this, a required crane stiffness can be determined for which the dynamic amplifications will be within limits. However, an increased crane stiffness will most likely lead to heavier crane components. Heavier crane components can reduce the workability performance of the crane and therefore, an iteration through the different modules of this study is suggested to iterate towards a feasible design.

6

Safety analysis

To ensure safe offshore operations, classification societies have been called into service who specify technical standards. The main goal of classification societies is to ensure safety and to obtain their approval, a construction or operation must meet up to these standards. Because motion compensation of an offshore crane is a relatively new development, there is little guidance by the classification societies. For Huisman it is important to include safety aspects and their importance into the design cycle from the beginning. In this module, an FMEA (Failure Mode and Effect Analysis) is performed, focused on the motion compensation system of the crane. Because the design concepts used are not very specific and detailed, this chapter focuses on the possible consequences of general failures, disregarding each possible component failure.

6.1. Failure modes

To generate structure among specific risks and consequences, failure modes are categorized into four categories. Failure modes that could occur for all crane concepts comprise the main category and three other categories contain failures that are focused on specific crane designs. The FMEA addresses Risk Priority Numbers (RPN) to every event. The RPN is used for prioritization in addressing the mitigation of failure modes. The RPN follows from a multiplication of the Severity, Occurence and Detectability. The severity is assessed by the seriousness of the failure mode to the user and operation in terms of safety and damage. The occurrence assesses the likelihood that a particular failure takes place. The detectability assesses the likelihood that one of the control systems or the operator detect the failure.
Specific failures that would follow from a subsystem failure analysis, are not included because these are not specifically related to motion compensation. This means that for example a failure of the slewing system can be defined and its effect on the motion compensation system is discussed, but no elaborate explanation is given on which specific part of the slewing system has failed.

SEVERITY (S) Assessment of the seriousness of the effect(s) of the failure mode to the user.			OCCURENCE (O) Assessment of the likelihood that a particular cause will mitigate and result in the failure mode.		DETECTABILITY (D) Assessment of the likelihood that the current controls will detect the cause of the failure.		
Safety	**Damage**	**Ranking**	**Frequency**	**Ranking**			**Ranking**
No injury	No or minor damage	2	Less than once per 20 year	2	Almost certain	Detection through shut off or alarm or meter reading	2
Small injury	Moderate structural mechanical damage	4	Once per 2 years - once per 20 years	4	High	Detection via indirect measurement	4
Lost time injury	Severe structural mechanical damage of single component	6	Once per year - once per 2 years	6	Mean	Detection via time based condition monitoring	6
Large irreversible injuries	Severe structural mechanical damage	8	Once per 3 months - once per year	8	Low	Detection via specific maintenance inspection / monitoring	8
(Multiple) Casualties	Loss of machinery, Catastrophic	10	More than once per 3 months	10	Impossible	Detection not possible	10
RISK PRIORITY NUMBER (RPN) Risk priority number is used for prioritization in addressing the mitigation of failure modes. Multiplying the rankings of the three criteria gives the RPN: **RPN = S x O x D**							

Figure 6.1: Factors for assessing the severity of failure modes.

6.2. General failures

For the general failures that are identified in the FMEA, a clear distinction can be made between mechanical-, environmental- and control failures. For these three categories, the failure modes with the highest RPN ratings are discussed in further detail. All other risks that are identified in the FMEA can be found in appendix J. Figure 6.2 presents an overview of the different categories that are used.

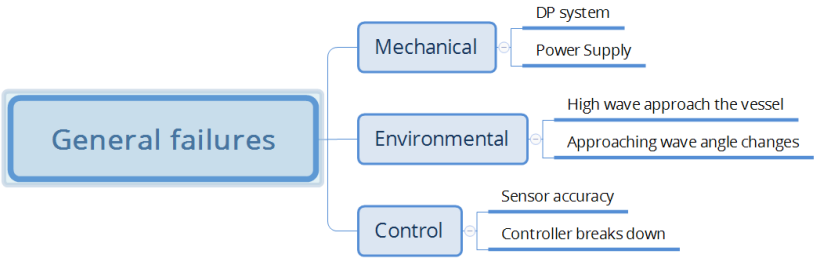

Figure 6.2: Failure mode categories for which the FMEA was performed.

6.2.1. Mechanical failures

DP System

The working principle of motion compensation is very much reliant on the DP system of the vessel. The crane is designed to compensate for the vessel induced motions, but only for a fixed initial crane position. The accuracy and offsets of the DP system will have to be incorporated in the control system of the motion compensated crane but for DP failure, the crane will not be able to keep the load at its initial position because it runs out of reach. At first, the offset of the DP system could be compensated for but when the vessel drifts the crane simply cannot maintain the position of the load. When this happens, the PMOC and HBC have an advantage over the MCCC as their possibility to extend their reach will be larger in the first place. When an active coupling of the slewing and luffing system of the MCCC would be realized its disadvantage would be neutralized.

The effect of a DP failure is the same for all crane concepts, positioning of the load will fail but the load will not start to swing. Notice is to be made that the vessel should always be positioned below winds to prevent the possible risk of drifting towards the structure. When a DP-failure is detected the load should be moved away from the structure to prevent collision. A specific event is to be highlighted, which is the case where the turbine blade or gearbox is being connected to the wind turbine. When the vessel drifts while the load is suspended in the crane and also connected to the structure, there is a risk of excessive loads on the crane structure which can result in severe structural damage if not acted upon accordingly. In such a case, an AOPS (Automatic Overload Protection System) should prevent excessive crane loads. The working principle and application of an AOPS is discussed in section 6.4.

Power supply

In case of a total or limited power supply failure, the motion compensation system will not be able to operate. For a limited power supply failure the performance of the crane will be reduced but it would still be able to operate in lower significant wave heights. A total black-out is one of the most dangerous failure modes. Within Huisman, the drives for the boomhoist and mainhoist are designed to be fail-safe. This means that the brake is automatically applied and has to be lifted actively. For a black-out the brakes will be applied automatically. The slew drive of a motion compensated crane should be designed with the same philosophy. When the compensation system of either of the crane types is locked by the brakes, the motions of the vessel cannot be compensated for and also, the load cannot be moved away from the structure. Result is that the load will start to swing and might crash into the crane or the structure leading to serious structural damage and falling objects. When the operation is in the stage of attaching the load to the structure while it is still held by the crane, the crane could be excessively loaded leading to crane failure. A mitigation strategy for a total blackout would be to position the vessel downwind of the turbine so that it will float away from the structure automatically. Also, back-up generators which use a separate electrical network could be installed to provide emergency power that can be used to move the load away from the structure.

6.2.2. Environmental failures

High waves approach the vessel

During the compensation cycle, the height of the waves approaching the vessel is uncertain. In previous sections of the report, a 30 minute period of operation is used with a probability of exceedance of 10%. Depending on the failure mode that is concerned, different probabilities of exceedance can be used. The local effect (situation) of the event 'high waves approaching the vessel' is a temporary reduction of the accuracy of the position control. For extreme waves, the drive system may be overloaded leading to specific component failure. Multiple global effects (consequence) can be identified for this event. The compensation mechanism can run into its limits leading to a minor swinging motion of the load. When the load is attached to the structure at the moment of high waves approaching the vessel, the global effect is more severe because the load cannot be moved away from the structure. Depending on the stage of the operation the mainhoist can pay-out wire to prevent a snap load. The most critical stage of the operation is when is in position within the structure but not safely connected yet. At this stage the mainhoist cannot pay-out wire as the load will drop. In this case the load must be moved away from the structure immediately and a collision with the structure is very likely. Measures to reduce the likelihood of this event at this stage in the operation can be found in the form of wave radar prediction. As described in section 4.6, the use of radar can help predicting optimal weather windows for critical stages in the operation.
Another global effect of this event is the fact that the AHC can be limited to its maximum stroke. In this case, the vertical compensation is limited and the AHC cylinder crashes into its stop, imposing a large dynamic impact on both the load and the crane. However, the design of the AHC cylinder can be altered to reduce shock-effects and the pressure of the passive part of the AHC can be increased to prevent the AHC cylinder from reaching its limit.

Approaching wave angle changes

During the operation at sea, wave and current conditions can constantly change. When the wave angle changes and the heading of the vessel is restricted by the current speed and DP capability, the vessel motions can increase significantly. While the crane design is calculated for maximum wave headings of 30°, the drive system will run into its limitations as result of the larger vessel motions. In this case, the positioning accuracy is reduced and the load can start to swing. When the operator observes load swing, he can decide to move the load away from the structure to prevent collision with either the crane or the structure.

6.2.3. Control system failures

Sensor accuracies

When positioning sensors such as remote MRU's would fail, it would be immediately clear to the operator that the system is not able to keep in position and the load can be moved away from the structure. Another scenario, when the sensors would generate a certain bias which can be unnoticed by the operator or control system, could lead to a more hazardous situation. In this case the operation might be continued with a system that is not functioning properly and the accuracy of the compensation system is reduced. To prevent such a failure, critical measuring systems such as the crane tip's position should be redundant.

Controller breaks down

When a part within the controller loop breaks down, such as the PLC, drive or invertor, the actuator control is lost. By the fail-safe design the brake will be applied, the degree of freedom for which this happens is locked in position and cannot move. The load will start to swing because vessel motions cannot be compensated for anymore and the load can collide with the tower or the crane itself. In such a situation, the remaining degrees of freedom of the crane should be used to move the load away from the structure and terminate the operation in a safe manner.

6.3. Concept specific failures

PMOC failures

Concept specific failures for the PMOC include the failures of the slewing and luffing system as these are used for the motion compensation. For the slewing motion, multiple failures modes are identified. The event with the lowest RPN is an E-motor, gearbox of pinion failure. When one of these fails, two scenarios can be present. Either the slewing system is still able to slew by the other E-motors, or the slewing motion is locked in position. When the slewing system can still move, its compensating performance is decreased and mi-

nor swinging motions can be expected for large wave heights while the load will be moved away from the structure. For lower wave heights the operation can continue. However, when the entire slewing system is locked, compensating performance is lost and the load must be moved away from both the structure and the boom so that a collision is prevented. This can be done with the luffing motion and mainhoist, as well as the thrusters of the vessel.

For the luffing motion, the same events can take place as with the slewing motion although a failure of one of the E-motors has a larger impact. Also, a broken boomhoist wire is one of the failure modes of the luffing system. When this happens, the boom cannot be held up anymore and it will turn over. This would lead to catastrophic damage and possible casualties. The detectability of this event is very difficult because the life-time usage of a steel wire rope is difficult to estimate. Causes for failure can be wire rope fatigue, or overload of the wire ropes loading capacity.

HBC failures
The HBC design will have the same failure modes as the PMOC and in addition, the knuckle mechanism could fail. Again two separate cases with respect to the drive of the knuckle mechanism are concerned of which the first is a single E-motor or gearbox failure. In this event the knuckle would still be able to operate at reduced performance. For a total drive failure, the knuckle mechanism would be fixed in position and only the mainboom could be used for motion compensation. In this case the risk of colliding the load with the structure or crane is smaller than for the PMOC. Also, when the boomhoist would break, the boom will not top over as the boom will be held up by the mainhoist and knucklehoist when the lower block is caught in the block catcher.

MCCC failures
For the MCCC concept, failure modes for the X-compensation and Y-compensation are determined which both have the same general lay-out for their drive systems and therefore no distinction is made between these 2 mechanisms.
The X-compensation and Y-compensation are actuated by winches in the same way this works for the boomhoist. Multiple guidance sheaves will be used and the winch will be actuated by 2 E-motors. Therefore, the drive system for these compensating mechanisms is almost equal to that of the boomhoist and the failure modes that are identified in the FMEA are a drivetrain failure and broken wire. The consequences of a drivetrain failure are a possible collision between the load and the crane, or structure, before the load can be moved away. For a scenario in which one of the wire breaks, the ability to control the suspension point of the mainhoist from the skid-table is lost and the load swing is amplified by transnational movements in the frame.

6.4. AOPS & MOPS

For cranes used at sea, an AOPS (Automatic Overload Protection System) is a very common safety feature. Usually this system is installed on the mainhoist to prevent the crane from loads that are higher than the design limits of the crane and appear so quickly that the operator would never be fast enough. The AOPS will be activated when overload is detected and automatically be de-activated when the load is reduced. When the AOPS is activated, it will automatically pay-out wire to reduce the load on the crane while keeping tension in the wire to prevent the load from dropping. At sea, the AOPS will be operational in all configurations and shall be designed such that crane damage is prevented.
A MOPS (Manual Overload Protection System) works in the same way as the AOPS but it is activated manually. In the event of power failure, the MOPS can be activated manually as well whereas the AOPS will be disabled.

In the design of a motion compensated crane, AOPS systems would be required for all degrees of freedom. When the load is attached to the structure while it is also still suspended in the crane, a high wave that exceeds the motion compensation limitations would lead to a high force on the structure and the crane. In such an event, an AOPS should prevent the crane from being overloaded. In the MCCC, this AOPS could be installed on the compensating mechanisms of the skid-table without influencing the rest of the cranes drive system. For the PMOC and HBC, this system would have to be installed on the slewing and luffing motion.

6.5. Results & discussion

Within a safety analysis, an endless amount of failure modes can be considered. For the early stage that the motion compensating system design is in, a safety analysis is performed to provide input for the process that must lead to the optimal crane design. The different failure modes have been split into three categories from which the failure modes with the highest RPN are elaborated upon. From the FMEA it follows that a failure of the power supply from the vessel would lead the most hazardous situation. In such an event the crane would be locked in position as a result of the fail-safe design of the cranes drive systems. For a normal operation this would not directly impose large consequences, but for motion compensation this induces a large potential danger. During installation procedures, the vessel should be positioned downwinds to reduce risk of collision and back-up generators that are connected by a second power supply should be installed to be able to move the crane away from the structure in an event of power failure.

A positioning failure has little effect on the system when the load is not critically close to the structure. AOPS systems are suggested for all compensating degrees of freedom of the crane because the critical stage at which the load is coupled to the structure and still connected to the crane through the mainhoist could lead to excessive crane damage and possible failing objects. This is essential to obtain a feasible wind turbine maintenance crane because otherwise the risk to overload the crane would be too large.

7

Conclusions & Recommendations

7.1. Conclusions

In this thesis report, the mechanical feasibility of motion compensation of an offshore crane for wind turbine maintenance is investigated. To do so, different factors influencing the feasibility for motion compensation have been identified and investigated within the different chapters.

From the operational context of wind turbine maintenance it can be concluded that a minimum lifting height of 135 meters is required to obtain a maintenance crane that is suited for most offshore wind turbines. The initial crane positions that are used in order to assess the performance of motion compensation, are not only limited by a minimum clearance between the vessel and the structure but also by a maximum boom angle that can be present during motion compensation for stability reasons. It was found that a significant wave height of 3 meters should be used as a design target for the workability of the motion compensated crane in order to produce a design that can compete with the workability of a jack-up, based on maximum wind speeds of the operation.

To assess the feasibility of motion compensation for offshore cranes, the required compensating crane motions have to be determined. Results have shown this can be done in the frequency domain by coupling the crane geometry to the RAOs of the vessel. By doing this, maximum expected compensating crane motions for different sea states can quickly be estimated. However only after coupling the compensating crane motions to the drive system, an optimal lifting position can be selected. To calculate these maximum expected values, a duration of the operation of 30 minutes followed from the operational context and a probability of exceedance of 10% has been used. It was found that the probability of exceedance must not be large because one single wave exceeding the design limit can be compensated for by a control system, though multiple successive waves will lead to an increasing positioning error.
The maxima that are calculated in the frequency domain do not contain phase information and it was found that this leads to conservative estimates when the power of the crane motions is calculated. Therefore, time domain calculations in which phase delays can be accounted for must be used to determine the power for the compensating motions. Convergence studies for the spectral resolution and the number of simulations were performed to obtain statistically proven results. These results showed that a percentual offset of the maximum expected values from the time domain remains after many simulations, although this is expected to convergence.

It was found that the limiting mechanism of the crane can be identified by plotting different properties of the drive system in a workability graph. In the workability calculations, the crane is modelled as a rigid structure and stroke, torque, speed and power limitations are incorporated. For the PMOC it can be concluded that the luffing motion is the limiting factor for all design cases which limits its workability to H_{sig} = 0.8m. By increasing the capacity of the drive system, only minor improvements could be realized as a result of the increased inertia of the drivetrain which has a large impact on the workability performance. Even though the HBC performs slightly better than the PMOC, the performance of the MCCC is much better than both other cranes which is explained by the decoupling of the gravitational loads from the compensating motions. It

was found that for a design in which the MCCC is equipped with only half of the power used for the luffing motion of the PMOC and HBC, its workability almost reached H_{sig} = 3m. By this it can be concluded that the MCCC offers the highest potential for a feasible crane design when the workability of the crane is concerned.

By determining the stiffness of the crane, it was found that the deflections of the crane tip by gravitational loads have to be incorporated in the motion compensation control. Also, the natural frequencies of the crane were calculated in a modal analysis to assess the dynamic response of the structure to the compensating motions. It was found that the natural frequencies of the cranes coincide with frequencies at which energy is present in the response spectrum of the compensating crane motions. Also, it was found that from the response spectra of the compensating motions, a minimum natural frequency of the crane can be determined for a maximum allowable dynamic amplification of the crane motions which will depend on the crane concept. For this, 2% of the critical damping of the structure was used. Whereas the current design method of an offshore crane focuses on maximum stresses in the boom and the buckling limit of the boom, it can be concluded that the required stiffness for a motion compensated maintenance crane can be determined from the response spectrum of the compensating motions and the allowable dynamic amplification of the motions.
The risk assessment indicated that the phase of the operation at which the turbine component is both connected to the turbine structure, and suspended by the crane, is the most critical phase of the operation. The statistical maxima of the compensating motions will be exceeded during the lifetime of the crane and therefore the crane is to be equipped with protection for overloading.

All together, the mechanical feasibility of 3D motion compensation is assessed by comparing three different crane types. From the workability performance of the different concepts it can be said that the MCCC offers the best potential for motion compensation and from a drive system point of view a feasible design can be obtained in which a workability of approximately H_{sig} = 3m can be realized. However, for all three cranes, the stiffness that follows from the original design method is too low to avoid large dynamic motion amplifications at resonance by which the concepts are considered not feasible. Therefore, the design of the maintenance crane should focus on stiffness as well as strength and for future designs, this study's methodology can be used to determine its feasibility.

7.2. Recommendations

Increase the stiffness of the crane designs and reconsider workability output.
Opportunities must be investigated by which the stiffness of the crane can be increased in order to increase the natural frequencies of the crane. For the new design, workability estimates should be reconsidered because the inertia and drive system of the crane will be different. By iterating through the steps that are used in this research, the design will evolve by which the feasibility of a motion compensated wind turbine maintenance crane can be assessed in more detail.

Time domain simulations for crane motions.
The FD calculations that are used within this study offer a good basis for estimating the requirements of the drive system of the crane which is needed to assess its feasibility. However, the phase difference between different crane motions could not be accounted for because maximum expected estimates were used. In the time domain, these phase differences can be accounted for which will increase the accuracy of the calculations and also bring the opportunity to determine the total torque and power usage of the crane. At the same time, a control system for the motion compensation system of the crane must be designed which can be incorporated in the TD analysis of the crane motions.

Perform a dynamic simulation of the compensation cycle.
In this study, natural frequencies of the crane are calculated and amplification factors are determined. The actual displacements of the tip during the motion compensation cycle as a result of the stiffness of the crane were not obtained and it is recommended to do this with a dynamic simulation of a crane model. In this dynamic simulation, the control strategy should be implemented such that the actual crane response can be simulated and the additional compensating motions for the structural deformations can be included in the drive requirements. For this, the crane motions for a motion compensation cycle can be used which follows from time domain simulations.

Bibliography

[1] Bargemaster. 3D Motion Compensated Crane BM-T40. URL https://www.barge-master.com/products/bm-t40. Accessed: 2017-09-01.

[2] Huisman Equipment B.V. Products - Cranes, . URL https://www.huismanequipment.com/en/products/cranes. Accessed: 2017-09-01.

[3] Ulstein Equipment B.V. Ulstein Colibri, . URL https://ulstein.com/equipment/ulstein-colibri. Accessed: 2017-09-01.

[4] Det Norske Veritas AS (DNV). Recommended Practice DNV-RP-C205, Environmental Conditions and Environmental Loads. Technical report, DNV, April 2007.

[5] Det Norske Veritas AS (DNV). Recommended Practice DNV-RP-H102, Modelling and Analysis of Marine Operations. Technical report, DNV, April 2011.

[6] Det Norske Veritas AS (DNV). Offshore standard DNV-RP-C205, Transit and Positioning of Offshore Units. Technical report, DNV, February 2012.

[7] Wolfer Elektromschinenfabrik Osnabruck GmbH. Product - sheet Three phase low voltage squirrel cage motors. URL http://www.woelfer-motoren.com/. Accessed: 2017-07-15.

[8] J. M. Godhaven. Adaptive Tuning of Heave Filter in Motion Sensor. In *OCEANS '98 Conference Proceedings*, volume 1, pages 174–178 vol.1, Sep 1998. doi: 10.1109/OCEANS.1998.725731.

[9] D-F. Feder H. Vorhölter, H. Hatecke. Design Study of Floating Crane Vessel for Lifting Operations in the Offshore Wind Industry. Technical report, Germany: Joint Research Project HoOK, 2015.

[10] K. H. Henriksen. MacGregor Three Axis compensated Crane for Wind turbine Services. Technical report, MacGregor, September 2014.

[11] K. O. Hill and G. Meltz. Fiber Bragg grating technology fundamentals and overview. *Journal of Lightwave Technology*, 15(8):1263–1276, Aug 1997. ISSN 0733-8724.

[12] L. H. Holthuijsen. *Waves in Oceanic and Coastal Water*. Camebridge University Press, digitally printed version 2009 edition, 2007.

[13] G. Hundleby and K. Freeman. Unleashing Europe's Offshore Wind Potential. Technical report, WindEurope - BVG Associates, 2017.

[14] Offshore Wind Industry. The World's Biggest Wind Turbine Gearbox, September 2016. http://www.offshorewindindustry.com/news/worlds-biggest-wind-turbine-gearbox.

[15] P. Naaijen H. van den Boom J. Dannenberg, K. Hessner and K. Reichert. The On Board wave and Motion Estimator OWME. *International Society of Offshore and Polar Engineers*, June 2010. The Twentieth International Offshore and Polar Engineering Conference, 20-25 June, Beijing, China.

[16] D-P. Molenaar Th. J. Mulder S. Hoonings G. Etna J. Koch F. Gerner J. van der Tempel, D. Cerda Salzmann. Der Ampelmann - Safe and easy access to Offshore Wind Turbines. *Duwind*, 2014.

[17] T. A. Johansen, T. I. Fossen, S. I. Sagatun, and F. G. Nielsen. Wave Synchronizing Crane Control during Water Entry in Offshore Moonpool Operations - Experimental Results. *IEEE Journal of Oceanic Engineering*, 28(4):720–728, Oct 2003. ISSN 0364-9059.

[18] J.M.J. Journee and W.W. Massie. *Offshore Hydromechanics*. Delft University of Technology, first edition edition, 2001.

[19] S. Küchler, T. Mahl, J. Neupert, K. Schneider, and O. Sawodny. Active Control for an Offshore Crane Using Prediction of the Vessel Motion. *IEEE ASME Transactions on Mechatronics*, 16(2):297–309, April 2011. ISSN 1083-4435.

[20] Dynamometer Equipment (Ching) Co. Limited. Product - sheet, Water Cooled Asychronous Motor. URL `http://www.dynoequip.com/`. Accessed: 2017-10-14.

[21] High Wind N.V. The Boom Lock. URL `http://www.high-wind.eu/boomlock/`. Accessed: 2017-09-01.

[22] 4C Offshore. Global Offshore Wind Speeds. Technical report, 4C Offshore, 2017.

[23] G. Parker, M. Graziano, F. Leban, J. Green, and J. D. Bird. Reducing Crane Payload Swing Using A Rider Block Tagline Control System. *OCEANS 2007 - Europe*, pages 1–5, June 2007.

[24] I. Pineda. Wind in power - 2015 European statistics. Technical report, The European Wind Energy Association, 2016.

[25] Siemens Wind Power. Fact sheet - B75 Rotor Blade, March 2014.

[26] K. Peng S. Ragunathan, D. Frakes and W. Singhose. Filtering Effects on Input-shaped Command Signals for Effective Crane Control. *IEEE International Conference on Control and Automation*, pages 1091–1101, December 2011.

[27] S. Sawyer and M. Dyrholm. Global Wind Report - Annual Market Update. Technical report, Global Wind Energy Council, 2016.

[28] H. Zhang S.B. van Albada, G.D. Van Albada H.P. Hildre. A Novel Approach to Anti-sway Control for Marine Shipboard Cranes. Technical report, Faculty of Maritime Technology and Operation Aalesund University College, 2015.

[29] Statoil. New energy solutions - Hywind project. URL `https://www.statoil.com/en/what-we-do/new-energy-solutions.html`. Accessed: 2017-10-11.

[30] J.D Stevenson. Structural Damping Values as a Function of Dynamic Response Stress and Deformation Levels. *Nuclear Engineering and Design*, 60(2):211 – 237, 1980. ISSN 0029-5493.

[31] E. Skjong T.A. Johansen V.W. Henriksen, A.G. Røine. Three-axis Motion Compensated Crane Head Control. *IFAC-Papers Online*, 49(23):159 – 166, 2016. ISSN 2405-8963. 10th IFAC Conference on Control Applications in Marine SystemsCAMS 2016.

[32] M. Whitby MHI Vestas Offshore Wind. V164-8.0 MW breaks world record for wind energy production. Technical report, MHI Vestas Offshore Wind, 2015.

[33] X. Zhoa. Research on wind turbine blade monitoring based on fbg strain sensors. *Power and Energy Engineering Conference 2010*, 2010.

A

Conventions and terminology

PMOC

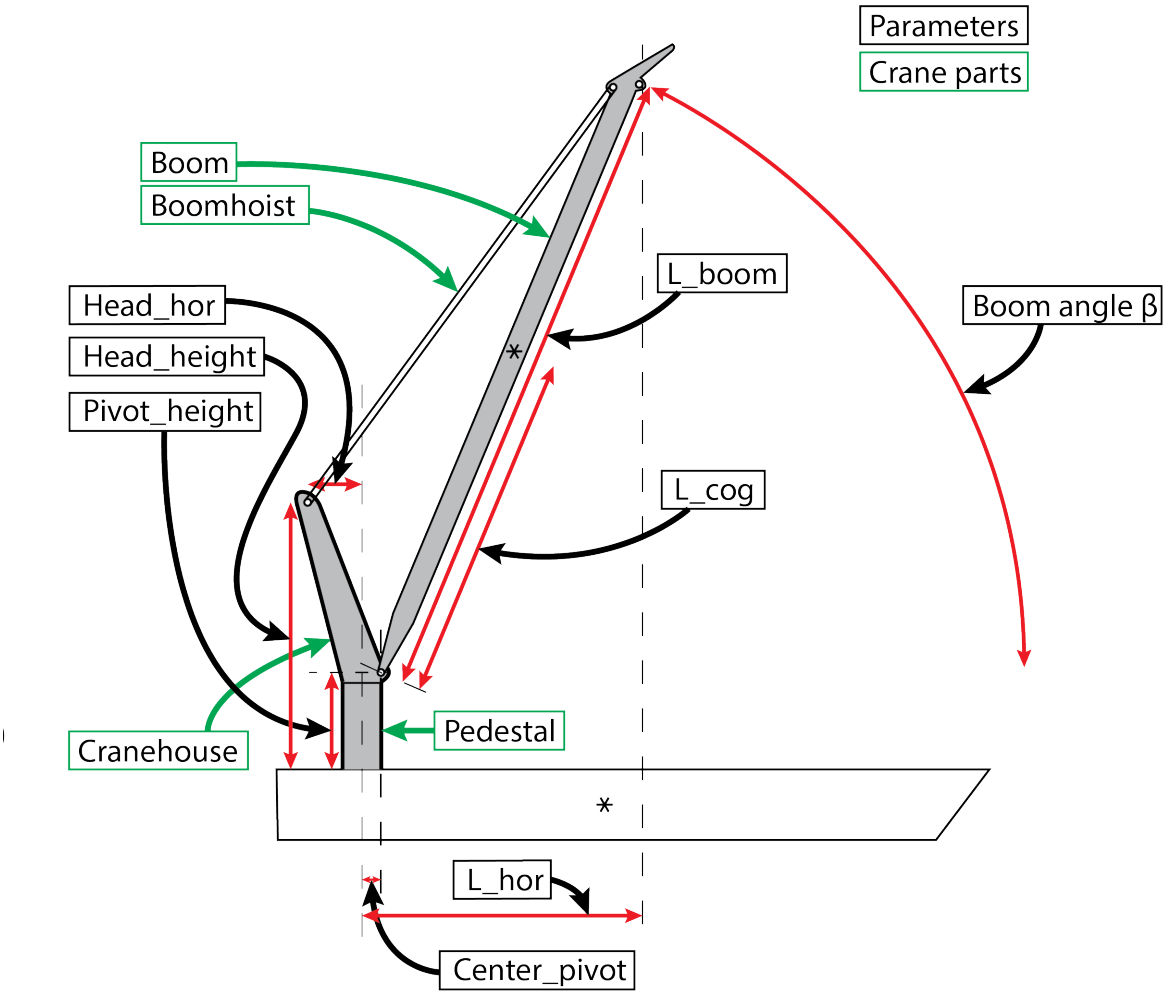

Figure A.1: Side view of a PMOC with conventions.

HBC

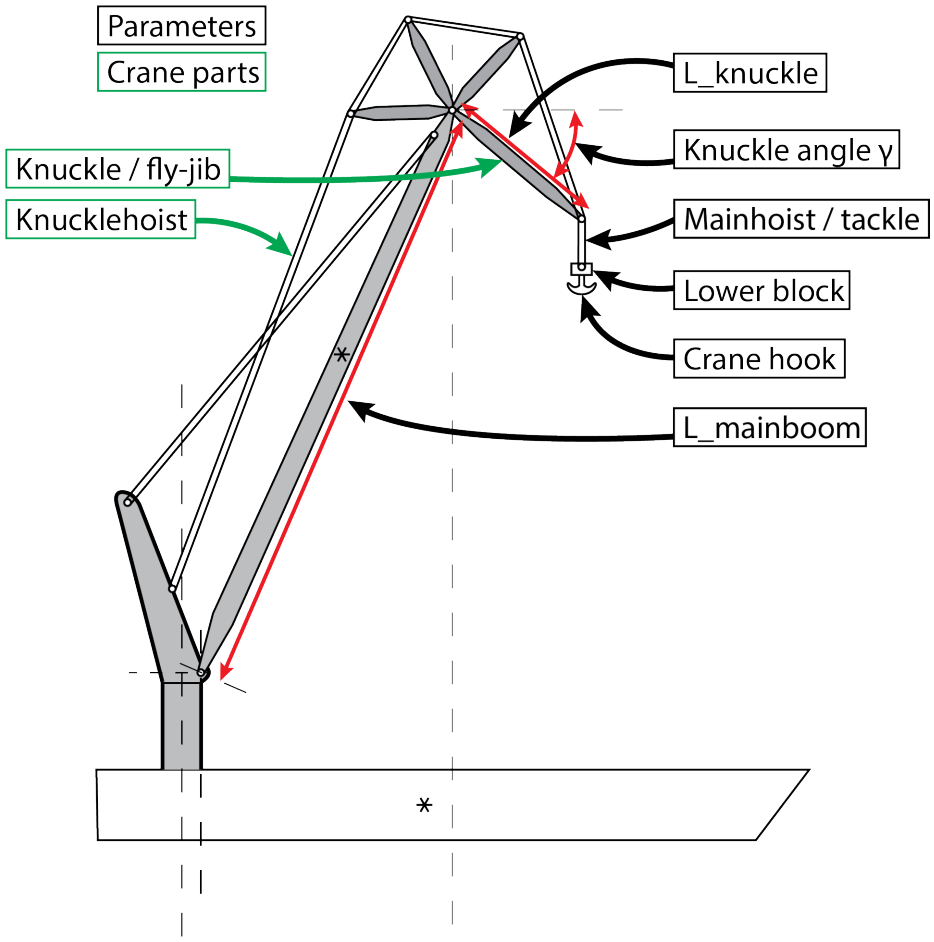

Figure A.2: Side view of a HBC with conventions.

Boom

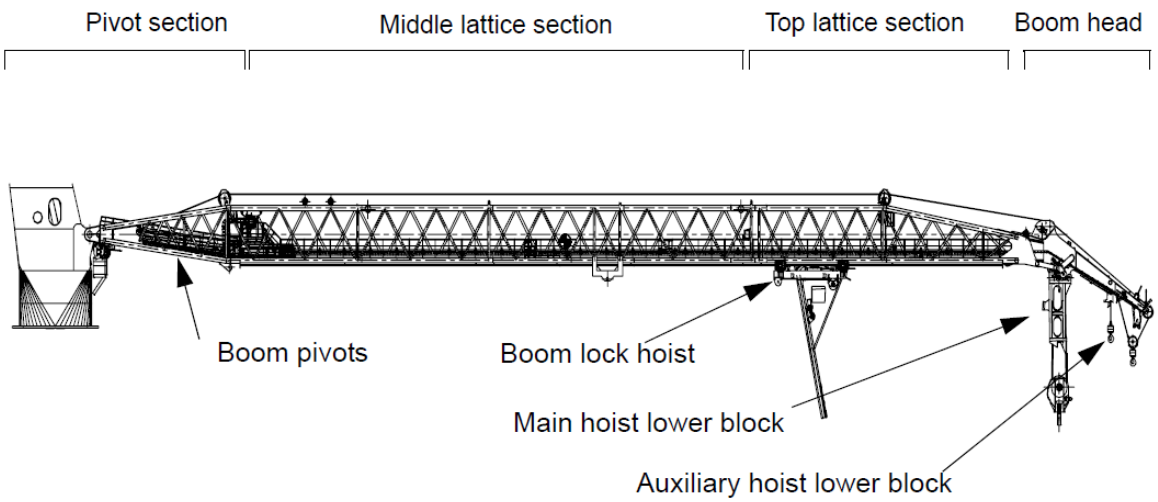

Figure A.3: Side view of the boom from a 600mt WTIC.

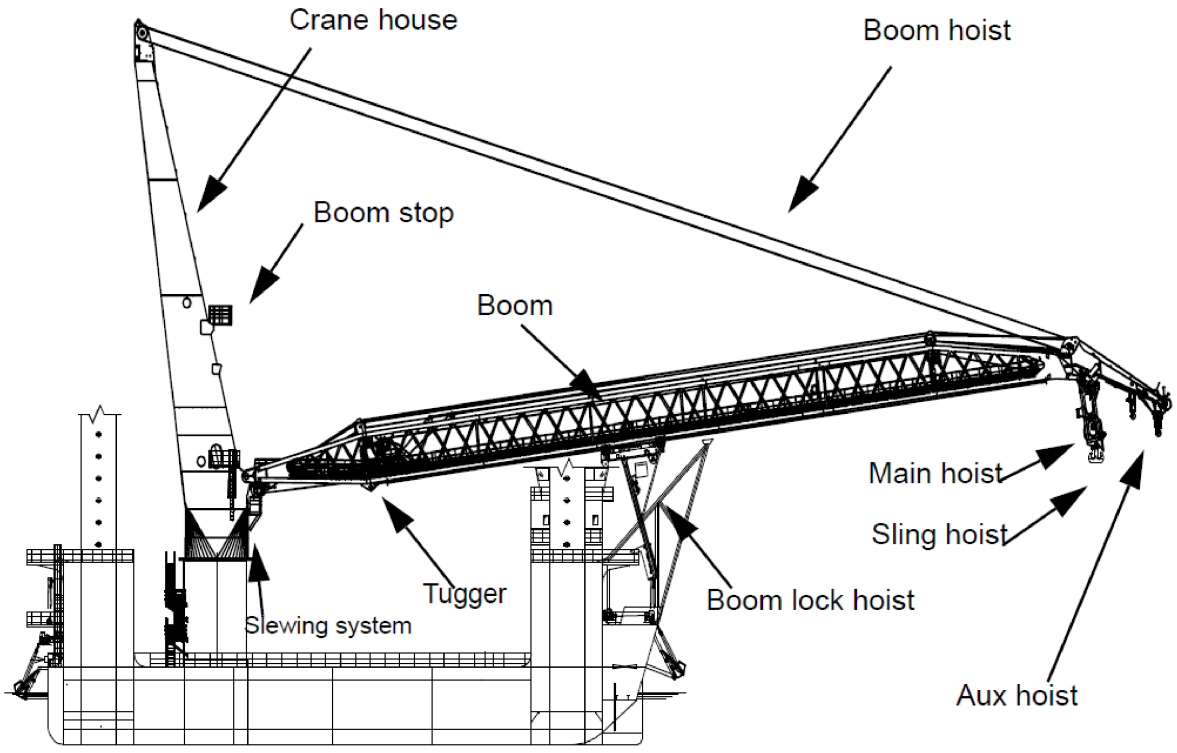

Figure A.4: Overview of crane terminology by parts.

Slew Drive

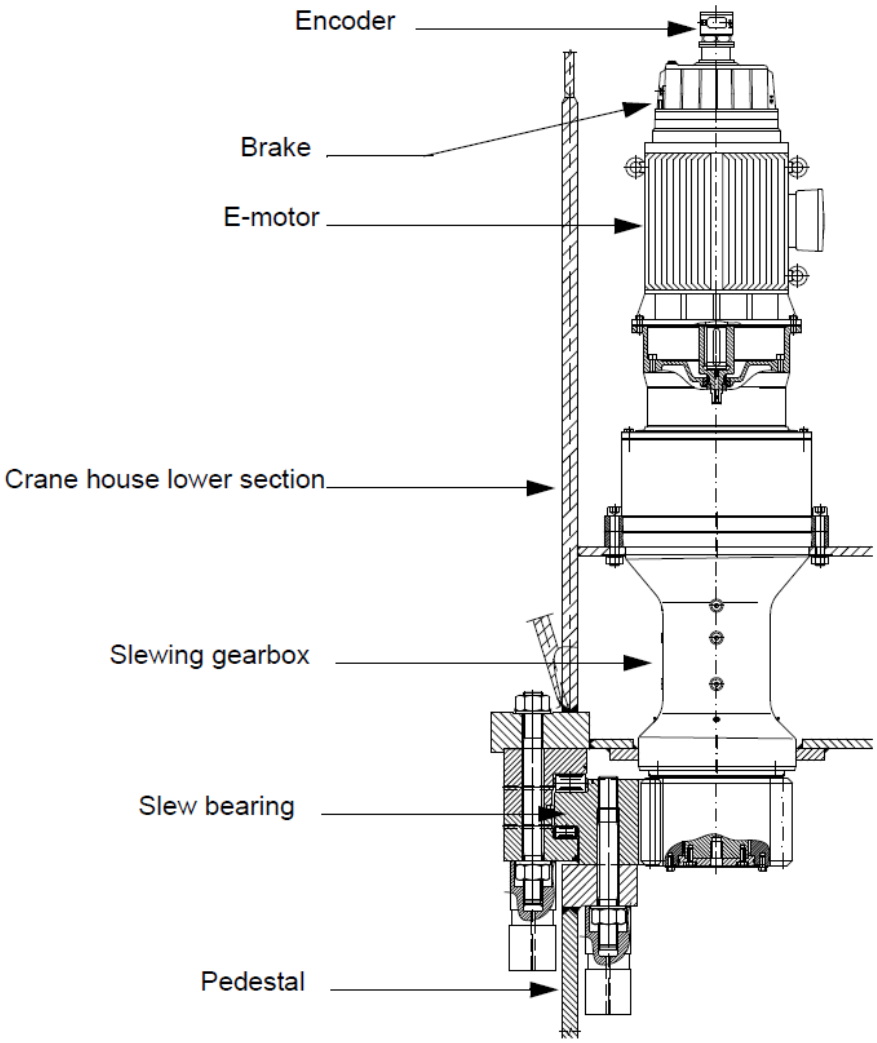

Figure A.5: Overview of components of a slew drive.

B

Wave conditions

The wave elevation is described by:

$$\zeta(t) = \sum_{n=1}^{N} \zeta_{an} \cdot cos(k_n x - \omega_n t + \epsilon_n) \tag{B.1}$$

$$\zeta_{an} = wave\ amplitude\ component\ (m)$$
$$\omega_n = wave\ number\ component\ (rad/s)$$
$$k_n = wave\ number\ component\ (rad/m)$$
$$\epsilon_n = random\ phase\ angle\ component\ (rad)$$

The wave amplitude ζ_{an} can be expressed in a wave spectrum $S_\zeta(\omega_n)$ (equation B.2). When $\Delta\omega \rightarrow 0$, the wave energy spectrum $S_\zeta(\omega_n)$ is defined by equation B.3.

$$S_\zeta(\omega_n) \cdot \Delta\omega = \sum_{\omega_n}^{\omega_n+\Delta\omega} \frac{1}{2}\zeta_{an}^2 \tag{B.2}$$

$$S_\zeta(\omega_n) \cdot d\omega = \frac{1}{2}\zeta_{an}^2 \tag{B.3}$$

Within this research, the mean JONSWAP wave spectrum for fetch-limited situations in deep water is used for all calculations [12]. Although it is arguable whether the deep water assumption fully covers the local wave climate for wind turbine areas, it does not change much for the goal of this research. The JONSWAP wave spectrum is defined by:

$$S_\zeta(\omega) = \frac{\alpha \cdot g^2 \cdot \gamma^a}{\omega^5} \cdot exp(-\frac{5}{4}(\frac{\omega_p^4}{\omega^4})) \tag{B.4}$$

For the formulation of the JONSWAP spectrum in equation B.4, a gamma factor of 3.3 was used. Additional equations used to formulate the wave spectrum are:

$$\alpha = \frac{5}{16} \cdot \frac{{H_{sig}}^2 \cdot {\omega_p}^4}{g^2} \cdot (1 - 0.287 \cdot ln(\gamma)) \tag{B.5}$$

$$\omega_p = \frac{1}{T_p} \cdot 2 \cdot \Pi \tag{B.6}$$

$$a = exp(\frac{-(\omega - \omega_p)^2}{2 \cdot W^2 \cdot {\omega_p}^2} \tag{B.7}$$

$$\tag{B.8}$$

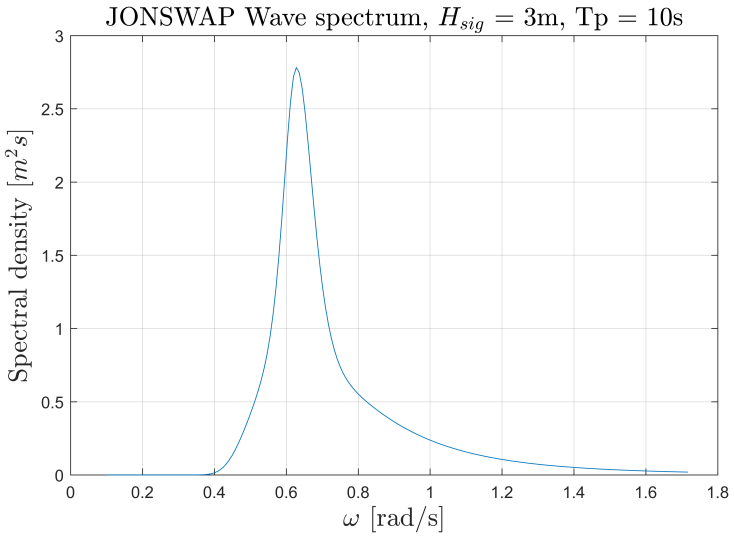

Figure B.1: The JONSWAP spectrum for H_{sig} = 3m, Tp = 10s and γ=3.3.

Wave spectrum parameters	
γ	3.3
W for ($\omega < \omega_p$)	0.07
W for ($\omega > \omega_p$)	0.09
g	9.81

Table B.1: Parameters used to calculate the wave spectrum.

In the wave model that is used, the phases of each frequency component of the wave spectrum are described by a uniform distribution. The phases are distributed between 0 and 2 Π.

C

Vessel specifications

The RAOs of the vessel are calculated for a specific frequency range, so that they can be multiplied with the corresponding amplitudes (at the same wave frequency) in the wave energy spectrum. For the vessel concerned in this study, the RAOs are calculated for 50 different frequencies ranging from 0.1 rad/s to 1.717 rad/s. In figure C.1, the RAOs of all six degrees of freedom from the vessel (Jumbo Fairplayer) are displayed. No tables with the exact data were included in the report as this information is sensitive information that Huisman does not want to distribute.

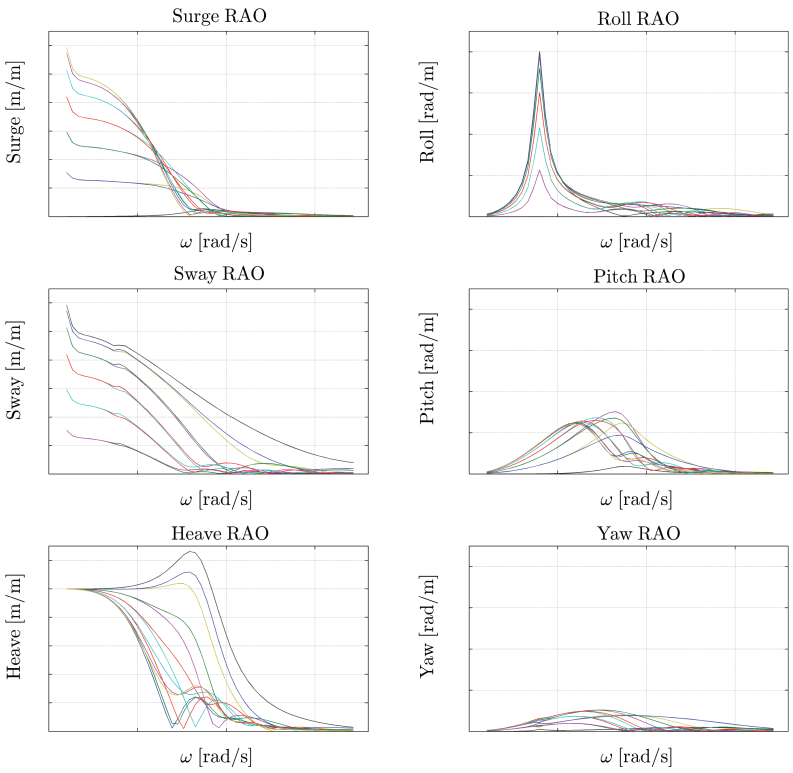

Figure C.1: The RAOs of the Jumbo Javelin construction vessel for its six degrees of freedom. The coloured lines represent different headings with a total range of 0-180 degrees and interval steps of 15 degrees.

D

Specifications of the crane concepts

Crane drive system				
Slewing system	PMOC	HBC		
Torque	764	764		Nm
Power	120	120		KW
Max. motor speed	3000	3000		RPM
# Motors	4	6		
Luffing system	PMOC	HBC		
Torque	2387	2387		Nm
Power	300	300		KW
Max. motor speed	3000	3000		RPM
# Motors	2	2		
# Falls	15	18		
Knuckle system		HBC		
Knuckle system		HBC		
Torque		2387		Nm
Power		370		KW
Max. motor speed		3000		RPM
# Motors		2		
# Falls		9		
Skid table system			MCCC	
Torque-x,y			1719	Nm
Power-x,y			180	KW
Max. motor speed x,y			3000	RPM
# Motors x,y			2	
Heave system	PMOC	HBC	MCCC	
Stroke	8	8	8	m
Speed	2.5	2.5	2.5	m/s
Acceleration	1.6	1.6	1.6	m/s^2

Table D.1: Properties of the drive systems of the different crane concepts.

Crane structural properties				
	PMOC	HBC	MCCC	[-]
Boom length	120	132	120	m
Knuckle length		18		m
Skid-table X			18	m
Skid-table Y			12	m
Boom weight	220	250		tonne
Knuckle weight		50		tonne

Table D.2: Structural properties of the different crane concepts.

E

Moment arm of boomhoist and knuckle hoist

Because the boomhoist is guided by the crane head, the moment arm of the boomhoist around the pivot is changing with the boom angle of the crane. The mass of the boom generates inertia when the boom is rotated around the pivot and because the position of the boom is controlled by the boomhoist winch, the inertia of the boom around the pivot has to be translated to the drum of the boomhoist. To do so, the moment arm of the boomhoist must be known. Figures E.1 and E.2 illustrate a schematized representation of the situation where the coordinates of A, B and C correspond to the location of the pivot, tip and cranehead respectively. To determine the length of 'r', it is important whether the angle at C is smaller or larger than 90 degrees. In the model, the dot product is used to determine the angle between the vector from pivot to cranehead and from pivot to boomtip. Equations E.1 to E.6 are used to determine 'r' from figure E.1. Equations E.7 and E.8 are used for figure E.2.

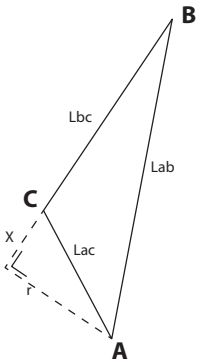

Figure E.1: With a large boom angle, the angle at corner A is larger smaller 90 degrees.

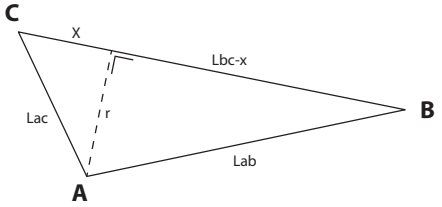

Figure E.2: When the boom is relatively horizontal, the angle at corner A becomes larger than 90 degrees

$$x^2 + r^2 = L_{AC}^2 \tag{E.1}$$

$$(L_{BC} + x^2) + r^2 = LAB^2 \tag{E.2}$$

$$x^2 - (L_{BC} + x)^2 = L_{AC}^2 - L_{AB}^2 \tag{E.3}$$

$$-2 \cdot L_{BC} \cdot x = L_{AC}^2 - L_{AB}^2 + L_{BC}^2 \tag{E.4}$$

$$x = \frac{L_{AB}^2 - L_{AC}^2 - L_{BC}^2}{2 \cdot L_{BC}} \tag{E.5}$$

$$r = \sqrt{(L_{AC}^2 - x^2)} \qquad (figureE.1) \tag{E.6}$$

$$x = \frac{L_{AC}^2 - L_{AB}^2 + L_{BC}^2}{2 \cdot L_{BC}} \tag{E.7}$$

$$r = \sqrt{(L_{AC}^2 - x^2)} \qquad (figureE.2) \tag{E.8}$$

F

Model validation

Vessel motions

The model that is built to determine the drive requirements that follow from the compensating motions of the crane is validated in two parts. One part of the validation focuses on the calculated compensating motions, and the other part focuses on the drive calculations that follow from these motions.

The first part is used to check whether the vessel motions are calculated correctly. The tip displacements are a result of the vessel motions and a comparison is made between the obtained results from the analytic Matlab model, an Orcaflex TD simulation, and a calculation sheet in excel that is used within Huisman to determine crane tip motions by irregular waves. The vessel RAOs are defined in the COG of the vessel and a relative tip position is used with respect to the CoG. For all three calculation models, the input data is the same. The vessel RAOs in the center of gravity, the tip location and the wave conditions are used as input. For this validation check, the same RAOs are used as in the report of which plots can be found in appendix C. A tip location of (3.33 -27.24 134.76) in the global reference frame is used which corresponds to the tip location in design condition 1. A one-dimensional JONSWAP wave spectrum with a significant wave height of 3 meters is used and the input parameters into the different models are specified in table F.1. The maximum expected tip displacements for a 3-hour period are calculated and compared. The probability of exceedance is set to 63% and a heading of 30°offset with bow wave conditions is used.

The maximum expected tip displacements resulting from Matlab-, Orcaflex and Excel calculations are plotted in figure F.1. The order of columns per displacement direction is Matlab-Orcaflex-Excel. Also, in figure F.2 the relative error between Matlab and Orcaflex, and Matlab and Excel is plotted. For both the X- and Y-direction, the relative error is very small (< 1.5 %) for all calculations. For the Z-direction the differences between Matlab and Excel are also small (< 2 %), but between Matlab and Orcaflex a difference of 7% is calculated. It is not clear why this error is so large but it is expected that an error was made in the Orcaflex model with the definition of the position of the CoG, leading to an offset in the heave direction.

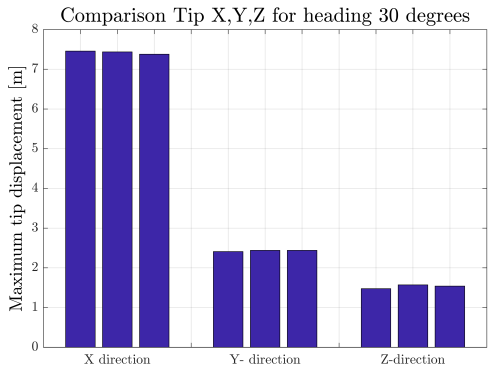

Figure F.1: Tip displacements calculated by Matlab, Orcaflex and Excel.

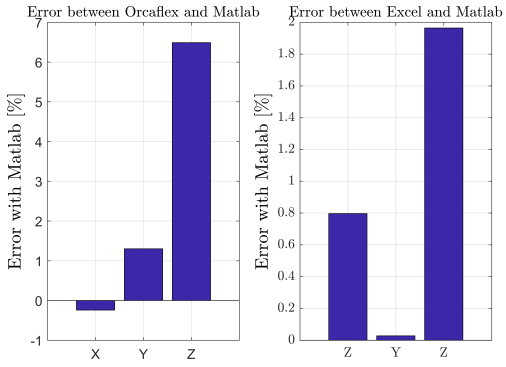

Figure F.2: Relative error between Matlab and Orcaflex, and Matlab and Excel.

Wave spectrum parameters		
Hsig	3	[m]
Tp	10	[s]
ω	0.1 : 1.717	$[rad/s]$
$\Delta\omega$	0.033	$[rad/s]$
γ	3.3	
σ	0.07 ($\omega < \omega_p$)	
σ	0.09 ($\omega > \omega_p$)	
Phase	Uniformly distributed	

Table F.1: Parameters used for the Jonswap wave spectrum.

Drive system

The workabilities that are calculated in the chapter 4 follow from the compensating motions of the crane. Therefore, the compensating motion function as input for the calculations of the drive system and now that the compensating motions are validated, the calculations of the drive system are validated. To do so, parameters for the crane motions are selected as input, while the validation of both system was split in two parts. A maximum acceleration (a_{slew}) has been used to calculate the associated dynamic torque that is required for the crane motion.
A check is performed on the model for the PMOC. The total slewing torque consists of a gravitational part and a dynamic part. For this check, parameters of design case 1 are used, just as for the check of the compensating motions.

The maximum dynamic torque of the slewing motion for design case 1 is 763 Nm per engine according to the model output. A hand calculation is performed to verify this result. The following information is used as input for the calculation, this is the same information that is present in the Matlab model:
- Max. slewing acceleration (a_{slew}): 0.0358 rad/s^2
- Slewing inertia at the motor shaft ($I_{m,s}$): 25.2978 kg/m^2
- Total slewing transmission ($i_{total,s}$): 2958
- Slewing efficiency ($\eta_{slew,total}$): 87.8 %
- Number of slewmotors ($slewmotors$): 4

To calculate the total torque required for this slewing acceleration:

$$T_{dyn,slew,total} = I_{m,s} \cdot (a_{slew} \cdot i_{total,s}) \cdot \frac{1}{\eta_{slew,total}} \tag{F.1}$$

$$T_{dyn,slew,total} = 3052\,Nm \tag{F.2}$$

$$T_{dyn,slew,motor} = \frac{T_{dyn,slew,total}}{slewmotors} = \frac{3052}{4} = 763\,Nm \tag{F.3}$$

$$\tag{F.4}$$

The maximum gravitational torque for the slewing motion for design case 1 is 495 Nm according to the model output. The gravitational slewing torque is a result of the sidelead angle, and the weight of the boom. The maximum expected sidelead angle follows from the motions module and for design case 1 this is 2.11 °. The following information is used as input for the calculation, this is the same information that is present in the Matlab model:
- Max. sidelead angle ($\angle_{side}$): 2.11 °
- Mass of the load (M_{load}): 240 mt
- Mass of the boom (M_{boom}): 220 mt
- Moment arm load CoG and slew axis ($L_{hor,load}$): 38.5 m
- Moment arm boom CoG and slew axis ($L_{hor,boom}$): 21 m
- Slewing transmission ($i_{total,s}$): 2958
- Slewing efficiency ($\eta_{slew,total}$): 87.8 %
- Number of slewmotors ($slewmotors$): 4

To calculate the total torque induced by the sidelead:

$$T_{grav,slew,total} = \frac{9.81 \cdot sin(\angle_{side}) \cdot (M_{load} \cdot L_{hor,load} + M_{boom} \cdot L_{hor,boom})}{i_{total,s}} \cdot \frac{1}{\eta_{slew,total}} \tag{F.5}$$

$$T_{grav,slew,total} = 1837Nm \tag{F.6}$$

$$T_{grav,slew,motor} = \frac{T_{grav,slew,total}}{slewmotors} = \frac{1183}{4} = 495Nm \tag{F.7}$$

(F.8)

Crane motions - cumulative linearization error

By use of the small angle approximation in the motions module, an error with the exact solution is introduced. Because this method is used in multiple parts of the research, the total cumulative error by the approximation is assessed. The simplification that is used with the small error approximation is the following:

$$sin(\phi) \approx \phi$$
$$cos(\phi) \approx 1.0 \qquad angles\ in\ radians$$

The approximation is used in:
- Translation from vessel COG to crane-tip
- Translation from crane-tip to crane motions

The x-z plane is observed, in which the x-axis corresponds to aligned with the length of the vessel, and the z-axis is the vertical axis in the global reference frame. When the slew angle of the crane is set to 0, a pitching motion of the vessel will lead to a rotation of the boom, and change in tackle length as described by the transformation matrices in chapter 3.2. By linearizing, an error is introduced between the approximated rotation of the boom to compensate and the exact rotation of the boom to compensate. The main question is however, how large is the effect of this linearization on the total tip displacement after the boom is rotated, and how can this be minimized. The general error of the assumption sin(theta)=theta is plotted in figure F.3.

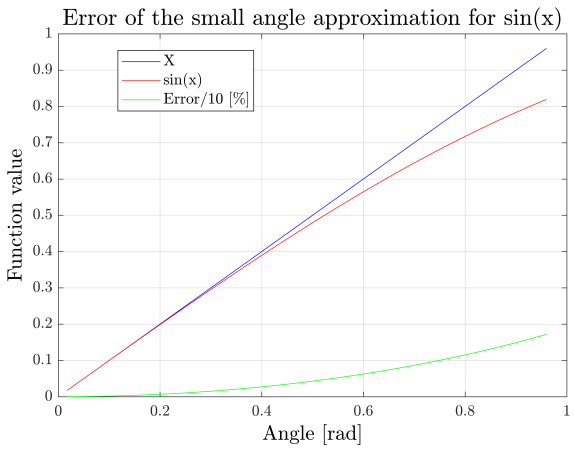

Figure F.3: Error of the small angle approximation for $sin(\theta)$.

Because the linearization error works both ways, from the COG to the tip, and from the tip to the pivot, the distance between the COG and the pivot is critical for the total error of the change in boom angle. Therefore, the error would be zero if the pivot and COG would be located at the exact same position. Also, because the assumption for sin(theta)=theta is used in combination with the vertical distance to the tip for the horizontal displacement, the initial angle of the boom has effect on the error. For lower boom angles, the horizontal displacement of the boom will be less accurate and then the vertical displacement of the tip becomes more accurate.
For larger pitching angles, the error increases non-linearly. When the vessel motions are concerned, a pitching angle with an amplitude of 3 °is already quite significant when a large ship is concerned.
The displacements of the tip by the vessel rotations are:

$$\Delta X_{real} = cos(\angle_{Tip} - 3°) \cdot L_{tip} - cos(\angle_{Tip}) \cdot L_{Tip} \tag{F.9}$$

$$\Delta X_{approx} = V_{tip} \cdot 3° \cdot \frac{2 \cdot \pi}{360°} \tag{F.10}$$

$$\Delta Y_{real} = sin(\angle_{Tip} - 3°) \cdot L_{tip} - sin(\angle_{Tip}) \cdot L_{Tip} \tag{F.11}$$

$$\Delta Y_{approx} = -H_{tip} \cdot 3° \cdot \frac{2 \cdot \pi}{360°} \tag{F.12}$$

$$\tag{F.13}$$

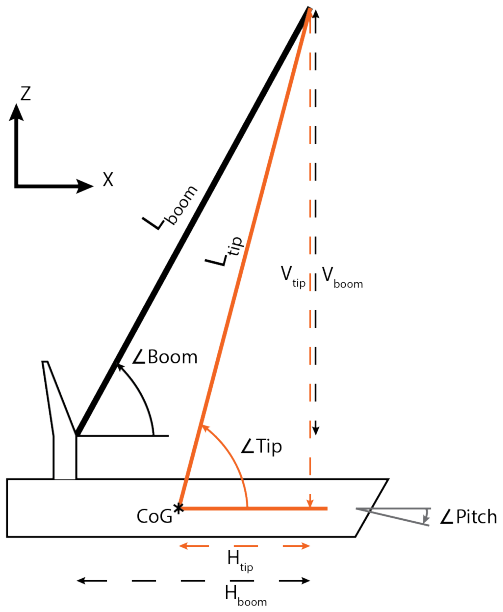

Figure F.4: Vessel with PMOC and the parameters used in the different formulas.

For changing boom angles, the error between the calculated rotation of the boom and the exact rotation of the boom to compensate for the horizontal motions, is calculated with equations F.14 and F.15. From the error of the boom angle, the error of the tip position is calculated as well. Because the boom is more vertical than horizontal, the boom rotation is calculated by the horizontal tip displacement. For this reason, the error becomes much larger for smaller boom angles. For a more horizontal boom, the boom rotation should be estimated by vertical tip displacement. The increase in error is shown in figure F.6 which also shows that for a boom angle of 70°, the error of the tip position by 3°vessel pitch is less than 1%.

$$\Delta\angle_{boom,approx} = \frac{\Delta X_{approx}}{V_{boom}} \tag{F.14}$$

$$\Delta\angle_{boom,real} = \angle_{boom} - acos(\frac{cos(\angle_{boom} \cdot L_{boom} + \Delta X_{real})}{L_{boom}}) \tag{F.15}$$

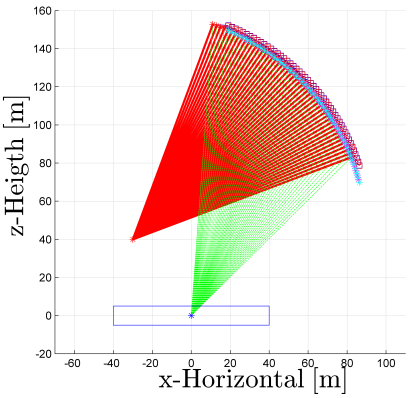

Figure F.5: For boom angles between 20 and 70 degrees, the position of the tip by the rotation of the vessel is plotted and the boom position after it compensates for the x displacement at the tip.

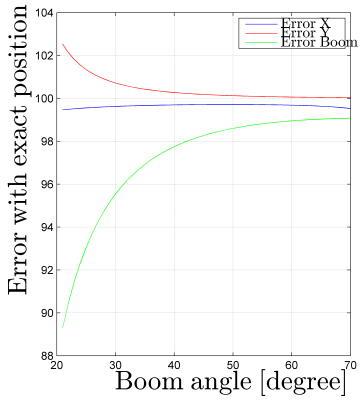

Figure F.6: The error between the exact tip location and the real tip location after compensating the with the boom. The boom angle to compensate is calculated by the small angle displacement of the x direction at the tip.

G

Power calculations in the Frequency Domain

During this research, an attempt was made with which it was tried to directly estimate the power of the crane motions from frequency domain calculations including the phase delay between the velocity of the crane motions and the acceleration of the crane motions. Two methods have been tried and within this appendix, these are elaborated on shortly.

Convolution
To obtain the power of the crane motions, the torque and velocity of the motion have to be multiplied in the time domain. In general, a multiplication in the time domain is the same as a convolution in the frequency domain. A convolution is performed on the response spectra for the torque and velocity of one of the crane motions. By doing this, the response spectra of the power for this crane motion would be obtained. When performing a convolution on two amplitude and phase spectra, a resulting amplitude spectrum for the power can be obtained after the use of trigonometric identities. Because a multiplication of two spectra is in fact multiplying cosine waves, cosine squared terms present itself which can be rewritten to sum- and difference frequencies using equation G.4. When sum- and difference frequencies are formed, different energy terms are defined for overlapping frequencies. These energies are present at the same frequency, and at first thought it would be logical to add these to obtain a 2-dimensional power spectrum. This is the point at which the calculation methods fails, because these energies cannot be added while their phases are different. The multiplication of for example ω_5 and ω_6 will lead to a sum frequency ω_{11}. Also, the multiplication of ω_3 and ω_8 will lead to the same sum frequency, ω_{11}. Because both are dependent on different initial frequencies, their phases will be different and the amplitudes at ω_{11} cannot be added.

$$T(t) = \sum_{n=1}^{N} A_{n\ torque} \cdot cos(\omega_n t\ +\ \phi_{n\ torque}) \tag{G.1}$$

$$V(t) = \sum_{n=1}^{N} A_{n\ velocity} \cdot cos(\omega_n t\ +\ \phi_{n\ velocity}) \tag{G.2}$$

$$T_1 \cdot cos(\omega_1 \cdot t + \phi_{T,1}) \cdot T_2 \cdot cos(\omega_2 \cdot t + \phi_{T,2}) = T_1 \cdot T_2 \cdot cos(\omega_1 \cdot t + \phi_{T,1}) \cdot cos(\omega_2 \cdot t + \phi_{T,2}) \tag{G.3}$$

$$A \cdot B \cdot cos(\omega_1 \cdot t) \cdot cos(\omega_2 \cdot t) = \frac{A \cdot B}{2} \cdot (cos(\omega_1 - \omega_2) \cdot t + (\phi_1 - \phi_2)) \tag{G.4}$$

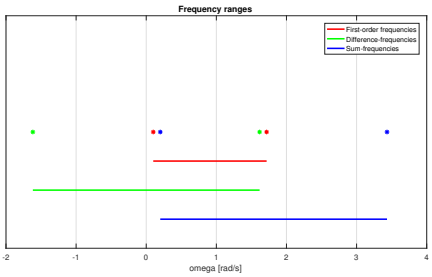

Figure G.1: The ranges of the initial frequencies, sum-frequencies and difference-frequencies that follow from the multiplication of two spectra.

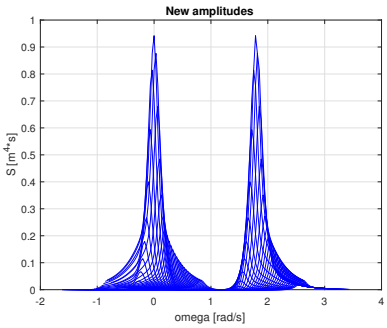

Figure G.2: Amplitudes for all sum- and difference frequencies for a wave spectrum, plotted on the same frequency axis.

Analogy with second order wave drift forces

In another attempt, the analogy with second order wave drift forces is used. The second order wave drift forces are calculated in the frequency domain by the use of Quadratic Transfer Functions (QTF), see equation G.9, where a convolution is to be used that is described by the parameter μ. Also, the mean wave drift force in irregular waves can be determined in the frequency domain by the use of QTF's from which the mean power could be calculated, equation G.8. The mean second order wave drift force is a result of the multiplication of cosines which generates an average. Instead of using the response spectrum of the torque and the velocity, it has been tried to determine a power QTF that is constructed with the use of the RAOs of the torque and velocity of a specific motion.

$$P = Real(\hat{T} \cdot \hat{V}) \tag{G.5}$$

$$Q = Imag(\hat{T} \cdot \hat{V}) \tag{G.6}$$

$$T = sqrt(P^2 + Q^2) \tag{G.7}$$

$$F^{(2)}_{mean} = \sum_{n=1}^{N} \zeta^{(1)^2} \cdot P_{ii} = 2 \cdot \int_0^{\infty} S_\zeta(\omega) \cdot P(\omega, \omega) \cdot d\omega \tag{G.8}$$

$$S_F(\mu) = 8 \cdot \int_0^{\infty} S_\zeta(\omega + \mu) \cdot S_\zeta(\omega) \cdot |T(\omega + \mu, \omega)|^2 \cdot d\omega \qquad where\ \mu = \omega_1 - \omega_2 \tag{G.9}$$

(G.10)

The transfer function is determined from the complex torque and velocity RAOs which include the phase information. By equation G.7 the transfer matrix is calculated which is used in equation G.9 in the convolution with the wave spectrum $S_\zeta(\omega)$. It was tried to determine the 'power' spectrum, just as the spectrum for second order wave drift forces can be determined. From this power spectrum, a significant maximum, and also, maximum expected value is calculated. As stated, these values did not mach the results from the calculations in the time domain. Therefore, time domain calculations are used to determine the power requirements of the crane.

H

Analytic dynamic models

To calculate the natural frequencies of the crane for different motions, simplified models of the crane are used in two different planes. These simplified models are described in section 5.3 where they are used in a model analysis in ANSYS. In order to validate whether the modal analysis is performed correctly, an analytic dynamic model has been set-up by which the same eigenfrequencies are calculated. For the purpose of this validation, a simplified version of the ANSYS models is used. In the ANSYS models, the exact position of the CoG's are used, also the attachment point of the boomhoist is not exactly at the tip of the boom, sheaves are included that create an offset of the lowering point. For the validation, these details are not included and input parameters are not related to the design cases.

Vertical plane

PMOC

General parameters are formulated which function as input for both the ANSYS model and the analytic model for validation purposes. The following input is used where the parameter notations are explained in figure H.1.

- $L_1 = 41.7$ $[m]$
- $L_2 = 88$ $[m]$
- $L_3 = 30$ $[m]$
- $L_4 = 27$ $[m]$
- $K_1 = 3.34e7$ $[N/m]$
- $K_2 = 8.34e7$ $[N/m]$
- $M_1 = 216e3$ $[Kg]$
- $M_2 = 240e3$ $[Kg]$

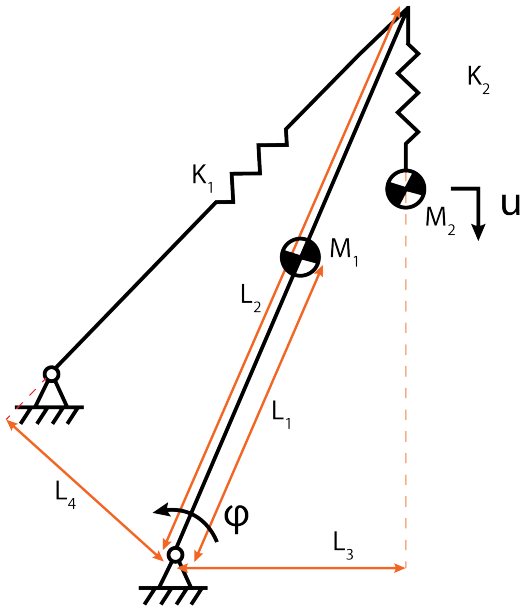

Figure H.1: Illustration of the analytic dynamic model that was used to validate the ANSYS calculations of the PMOC, with the parameter notations.

The equations of motion are formulated as follows:

$$I_1 \cdot \ddot{\phi} = -\phi \cdot K_2 \cdot L_3^2 - \phi \cdot K_1 \cdot L_4^2 - K_2 \cdot u \cdot L_3 \qquad (EOM1) \tag{H.1}$$

$$M_2 \cdot \ddot{u} = -K_2 \cdot u - \phi \cdot K_2 \cdot L_3 \qquad (EOM2) \tag{H.2}$$

$$I_1 = M_1 \cdot L_1^2 \tag{H.3}$$

The equations of motion are written in matrix form:

$$M \cdot \ddot{u} + K \cdot u = 0 \tag{H.4}$$

$$M = \begin{bmatrix} I_1 & 0 \\ 0 & M_2 \end{bmatrix} \tag{H.5}$$

$$\ddot{u} = \begin{bmatrix} \ddot{\phi} & 0 \\ 0 & \ddot{u} \end{bmatrix} \tag{H.6}$$

$$k = \begin{bmatrix} K_1 \cdot {L_4}^2 + K_2 \cdot {L_3}^2 & K_2 \cdot L_3 \\ K_2 \cdot L_3 & K_2 \end{bmatrix} \tag{H.7}$$

$$u = \begin{bmatrix} \phi & 0 \\ 0 & u \end{bmatrix} \tag{H.8}$$

$$det(-\omega_i \cdot \mathbf{M} + \mathbf{K}) = 0 \tag{H.9}$$

By substituting the Mass and Stiffness matrix into equation H.9 and solving for omega, the natural frequencies are calculated. The resulting natural frequencies for the two modes in which one of the springs is excited at its natural frequency are:

$$\omega_1 = 0.9968\ [Hz]$$
$$\omega_2 = 3.8139\ [Hz]$$

The exact same model is configured in ANSYS. The same properties for the springs are used and the distance between all nodes corresponds to that of the analytical model. A "Modal Analysis" is performed by ANSYS, which calculates all eigenfrequencies and eigenmodes wihtin a pre-defined range. The results are shown in

figure H.2 and figure H.3. The eigenfrequencies for the two modes are exactly the same as those that follow from the analytical model.

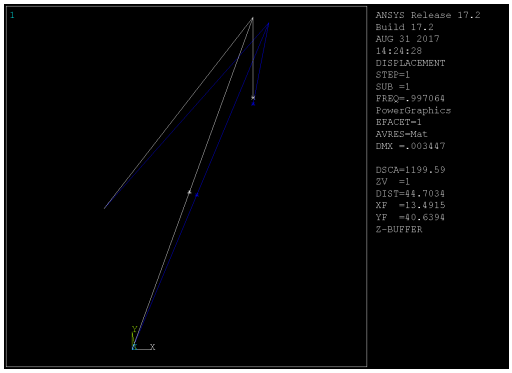

Figure H.2: ANSYS output for the first natural frequency of the PMOC at 0.99 Hz where the boomhoist is excited at its natural frequency.

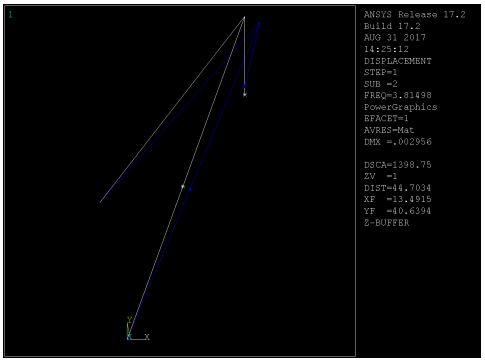

Figure H.3: ANSYS output for the second natrual frequency of the PMOC at 3.81 Hz where the mainhoist is excited at its natural frequency.

HBC

For the Hybrid boom crane, an analytic model is used for validation purposes as well. The parameters used for validation are listed below for which the notation is explained in figure H.4:

- $L_1 = 15.5\ [m]$
- $L_2 = 26.0\ [m]$
- $L_3 = 2.3\ [m]$
- $L_4 = 17.0\ [m]$
- $L_5 = 7.7\ [m]$
- $L_6 = 7.7\ [m]$
- $L_7 = 6.8\ [m]$
- $L_8 = 2.4\ [m]$
- $L_9 = 2.6\ [m]$
- $L_10 = 4.0\ [m]$
- $L_11 = 14.4\ [m]$
- $L_12 = 23.3\ [m]$
- $M_1 = 173e3\ [Kg]$
- $M_2 = 160e3\ [Kg]$
- $M_3 = 65e3\ [Kg]$
- $K_1 = 7.14e7\ [N/m]$
- $K_2 = 9.15e6\ [N/m]$
- $K_3 = 4.65e7\ [N/m]$

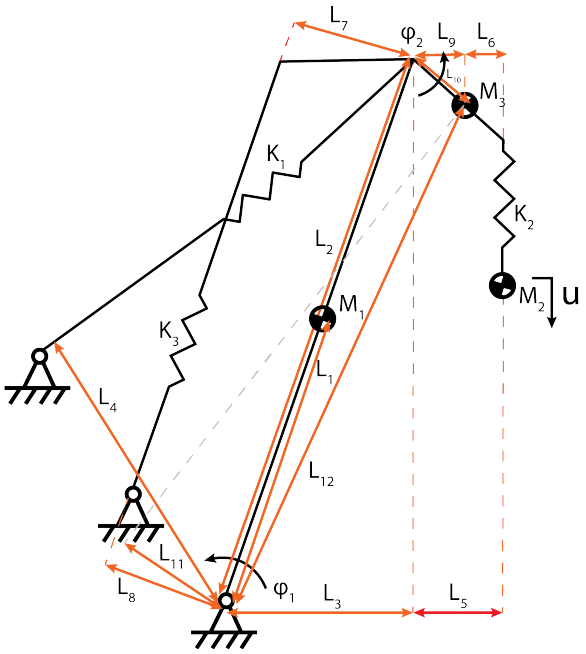

Figure H.4: Illustration of the analytic dynamic model that was used to validate the ANSYS calculations of the HBC, with the parameter notations.

The equations of motion are formulated and re-written to matrix form:

$$M \cdot \ddot{u} + K \cdot u = 0 \tag{H.10}$$

$$M = \begin{bmatrix} I_1 + M_3 \cdot L_1 2 & 0 & -M_2 \cdot L_{10} \cdot L_{11} \\ 0 & M_2 & 0 \\ -M_2 \cdot L_{10} \cdot L_{11} & 0 & I_3 \end{bmatrix} \tag{H.11}$$

$$\ddot{u} = \begin{bmatrix} \ddot{\phi_1} & 0 & 0 \\ 0 & \ddot{u_1} & 0 \\ 0 & 0 & \ddot{\phi_2} \end{bmatrix} \tag{H.12}$$

$$K = \begin{bmatrix} K_1 \cdot {L_4}^2 + K_2 \cdot (L_3 + L_5)^2 + K_3 \cdot L_8 & K_2 \cdot (L_3 + L_5) & K_2 \cdot L_6 \cdot (L_3 + L_5) + K_3 \cdot L_7 \cdot L_8 \\ K_2 \cdot (L_3 + L_5) & K_2 & K_2 \cdot L_6 \\ K_2 \cdot (L_3 + L_5) + K_3 \cdot L_7 \cdot L_8 & K_2 \cdot L_6 & K_2 \cdot {L_6}^2 + K_3 \cdot {L_7}^2 \end{bmatrix} \tag{H.13}$$

$$u = \begin{bmatrix} \phi_1 & 0 & 0 \\ 0 & u_1 & 0 \\ 0 & 0 & \phi_2 \end{bmatrix} \tag{H.14}$$

The resulting natural frequencies for the three modes in which one of the springs is excited at its natural frequency are:

$$\omega_1 = 1.0614[Hz]$$
$$\omega_2 = 2.5074[Hz]$$
$$\omega_3 = 9.2509[Hz]$$

For the HBC, the eigenfrequencies calculated by the 'modal analysis' in ANSYS also match those calculated with the analytic modal. In figures H.5, H.6 and H.7 the ANSYS output is displayed.

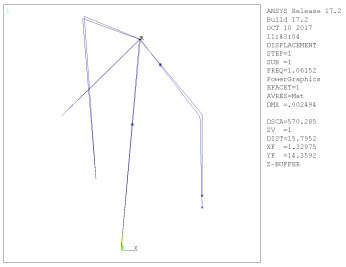

Figure H.5: ANSYS output for the first natural frequency of the HBC at 1.06 Hz.

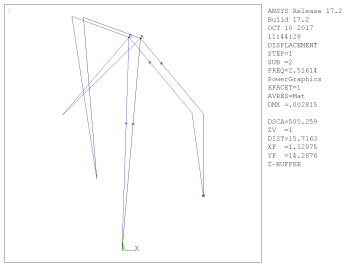

Figure H.6: ANSYS output for the second natural frequency of the HBC at 2.51 Hz.

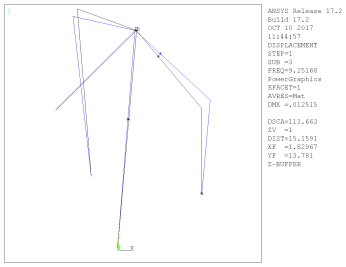

Figure H.7: ANSYS output for the third natural frequency of the HBC at 9.25 Hz.

Dynamic response curve

The response curve for a single mass-spring-damper system is derived by the following equation:

$$m \cdot \ddot{y} = k \cdot (u - y) + c \cdot (\dot{u} - \dot{y}) \tag{H.15}$$

$$m \cdot \ddot{y} + c \cdot \dot{y} + k \cdot y = k \cdot u + c \cdot \dot{u} \tag{H.16}$$

$$s^2 \cdot m \cdot Y + c \cdot s \cdot Y + k \cdot Y = k \cdot u + s \cdot c \cdot U \tag{H.17}$$

$$(m \cdot s^2 + c \cdot s + k) \cdot Y = (s \cdot c + k) \cdot U \tag{H.18}$$

$$\frac{Y}{U} = \frac{s \cdot c + k}{m^2 + c + k} \tag{H.19}$$

Validation of Time Domain calculations

In this section, the time domain calculations will be verified. For a JONSWAP wave spectrum, time domain representations of the surface elevation are made with the same method that is used for the power calculations. From these time representation, the maximum expected wave height is determined and it is verified whether this matches with the calculated value from the frequency domain.

As was described earlier, the significant wave height of a wave spectrum can be estimated in the frequency domain by integrating the area below the wave spectrum (equations 3.5 and 3.6). With the significant wave height, the maximum expected wave height of a specific duration can be determined with a certain probability of exceedance with the use of equations 3.7 to 3.10. Now that time series are generated from the wave spectrum, the same significant wave height, and maximum expected wave height should follow from the results of the time series. To verify whether this is true, one specific wave spectrum is used and for this wave spectrum the significant wave height and maximum expected wave height are calculated in the frequency domain.

Frequency domain
A wave spectrum is used with a significant wave height of 3 meters and a (most probable) maximum wave height is estimated for a 3-hour duration with a probability of exceedance of 63%. The spectrum that is used is plotted in figure I.1. The most probable maximum expected wave height for this spectrum is 5.6 meters.

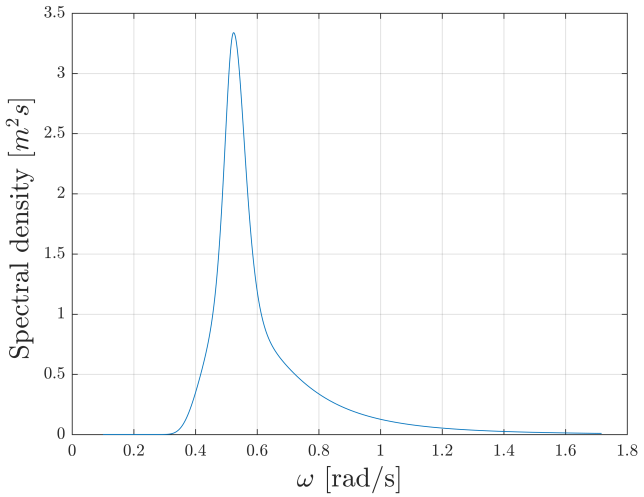

Figure I.1: Wave spectrum that is used for the validation of the FD and TD calculations. H_{sig} is 3 meters, and T_p is 12 seconds.

Time domain
Now that the wave spectrum is selected, time domain representations of the sea surface elevation are produced. The data that is known when a time series is produced, is the sea surface elevation at every moment in time of the simulation. However, the data of the sea surface elevation does not directly about the wave heights of the time signal and therefore, a zero-crossing wave record analysis is performed. In figure I.2, it is illustrated how the wave heights are calculated. With the use of a script that detects the change in positive to negative surface elevation, the starting point and finishing point of every individual wave can be detected and when these are known, the wave height can be calculated. Also, the periods of every individual wave are calculated.

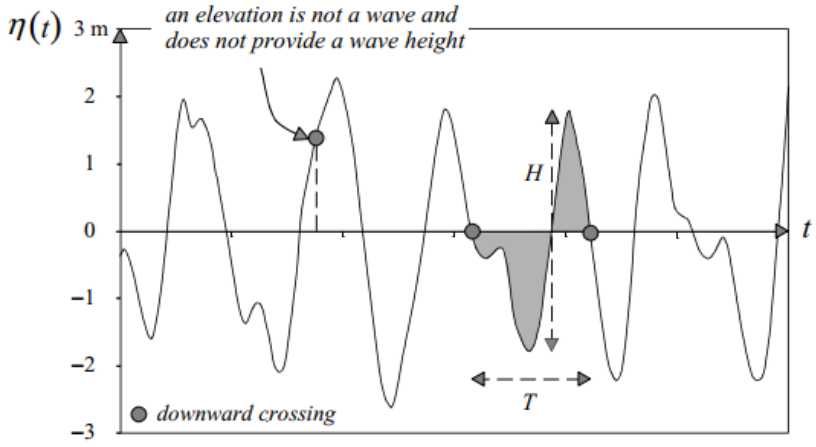

Figure I.2: The definition of wave height and wave period in a time record of the surface elevation (the wave is defined with downward zero-crossings).

Now that the specific data of all the waves in the time record is obtained, the statistical properties of the most probable maximum can be used. At first, all individual waves are sorted from high to low. The highest wave from the time record is in fact the maximum wave height with a zero probability of exceedance. However, for the most probable maximum, the wave is to be selected that has a 63 % probability of exceedance. When the wave with a probability of exceedance of 63 % is found, it should correspond to the maximum expected wave height that is calculated in the frequency domain.

This method is applied to the same wave spectrum as the one with which the frequency domain estimates are determined. 500 different time representations are made in the time domain and from this data a maximum expected wave height of 5.3 was found which can be seen in figure I.3. It is interesting to see that these two values do not correspond. Therefore, different checks are used to find the cause of this difference.

At first the variance of the surface elevation of the time signal is checked. The variance of the time signal should correspond to the variance that can be calculated from the spectrum in the frequency domain. In the frequency domain, the variance of the wave spectrum is calculated by the area under the spectrum which is 0.56 for the wave spectrum that is used for this validation.
From the different time series that are generated, the variances are calculated as well. When the variance that is calculated from the time signals is compared to the variance from the frequency domain it can be said that these correspond very well. In figure I.4, the variance from 500 different time signals are plotted and the variance from the frequency domain is plotted with the blue line.

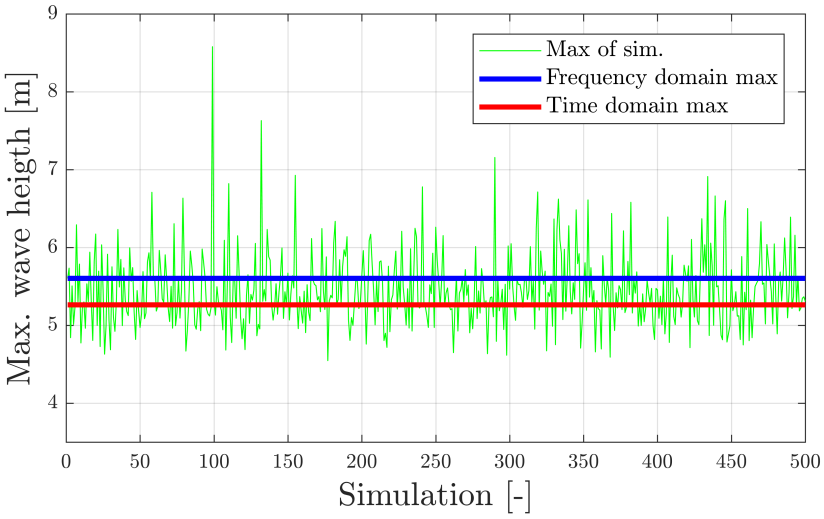

Figure I.3: Maximum wave heights of the time signals for 500 simulations. The green line represents the maximum wave height from each time simulation. The red line indicates the 63% probability of exceedance of the time signal wave heights and the blue line is the most probable maximum from the frequency domain.

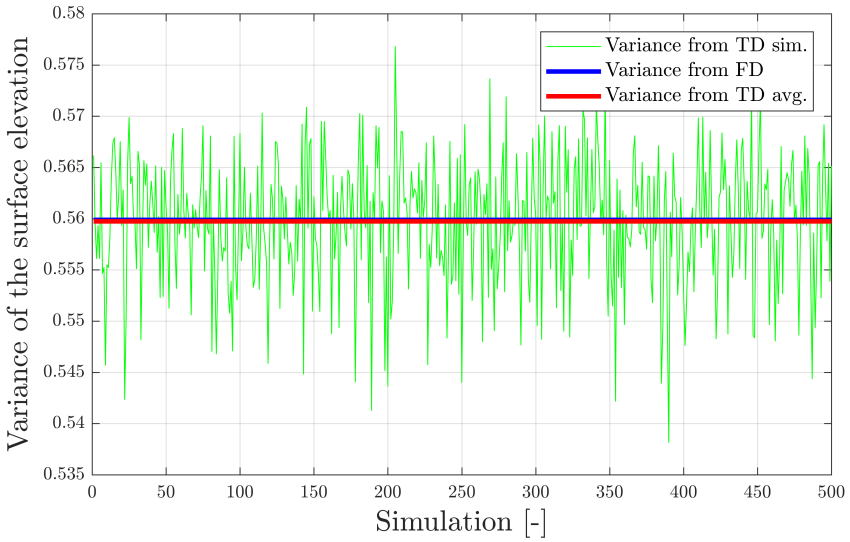

Figure I.4: Variance of the surface elevation from the individual time simulations in green. The variance that is calculated from the frequency domain is plotted in blue and the average of the time signal variances is plotted in red.

Also, the significant wave height from the spectrum, and the time series is compared. Again, for the frequency domain, the significant wave height is calculated with the zero-th order spectral moment. For the time series, at first the zero-crossing analysis is used and after this, the wave heights are sorted again. From the total number of wave height, the highest one-third is selected, and from this selection, the mean value should be the significant wave height of the time record. For all the simulations, this significant wave height is plotted versus the significant wave height from the frequency domain. In the left graph of figure I.5 it can be seen that the significant wave heights that follow from the zero crossing analysis of the time domain simulations is lower than that of the frequency domain. However, in the right graph of figure I.5, the significant wave height is plotted which is calculated with the variance from the time signals and this corresponds to the frequency domain estimate very well. Although the variance of the time signals is correct, the estimates of the significant wave height are not, and by this it can be said that an error is made in the zero-crossing wave analysis. This also explains the difference in maximum expected wave heights between the FD analysis and TD analysis which was already shown in figure I.3.

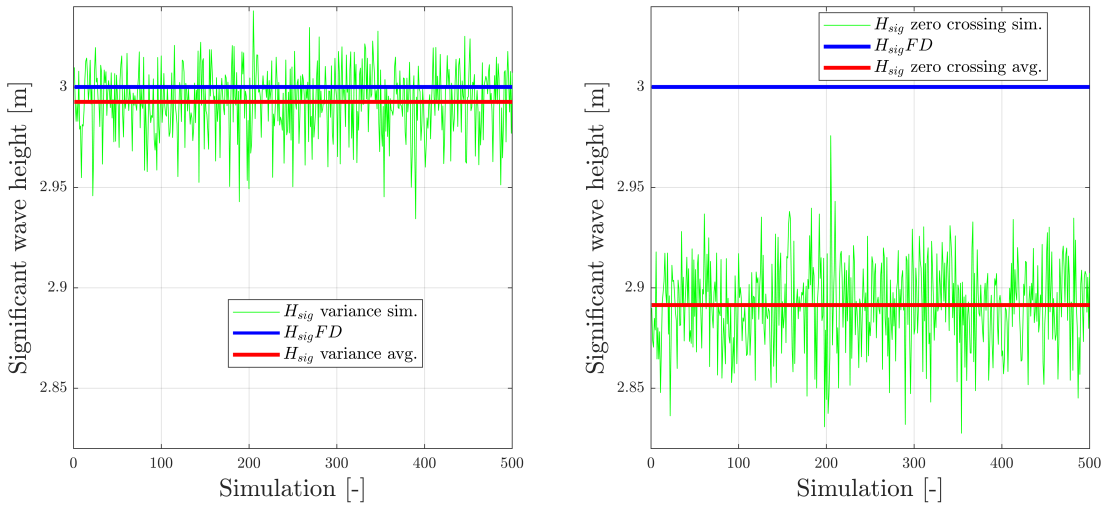

Figure I.5: The significant wave height that is calculated from the zero crossing analysis is plotted in the left graph for all time simulations. Again the blue line represents the FD estimate. In the right graph the significant wave height is plotted which is calculated from the variance of the time simulations.

Plots probability of exceedance In section 4.6, a reference was made to this appendix in which it states that 2 additional plots can be found in the appendix in which the positioning error is calculated for maximum accelerations with a probability of exceedance of 5 % and 20 %. In figure I.6 and I.7, these results are displayed.

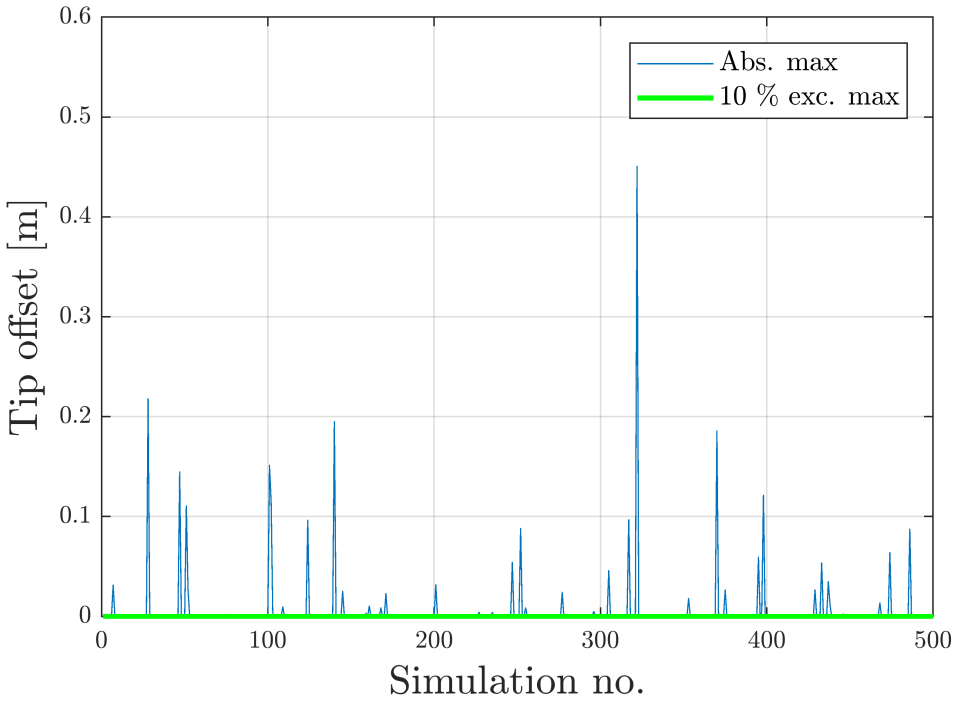

Figure I.6: Positioning error for multiple time simulations when the maximum acceleration is calculated with a probability of exceedance of 5 %.

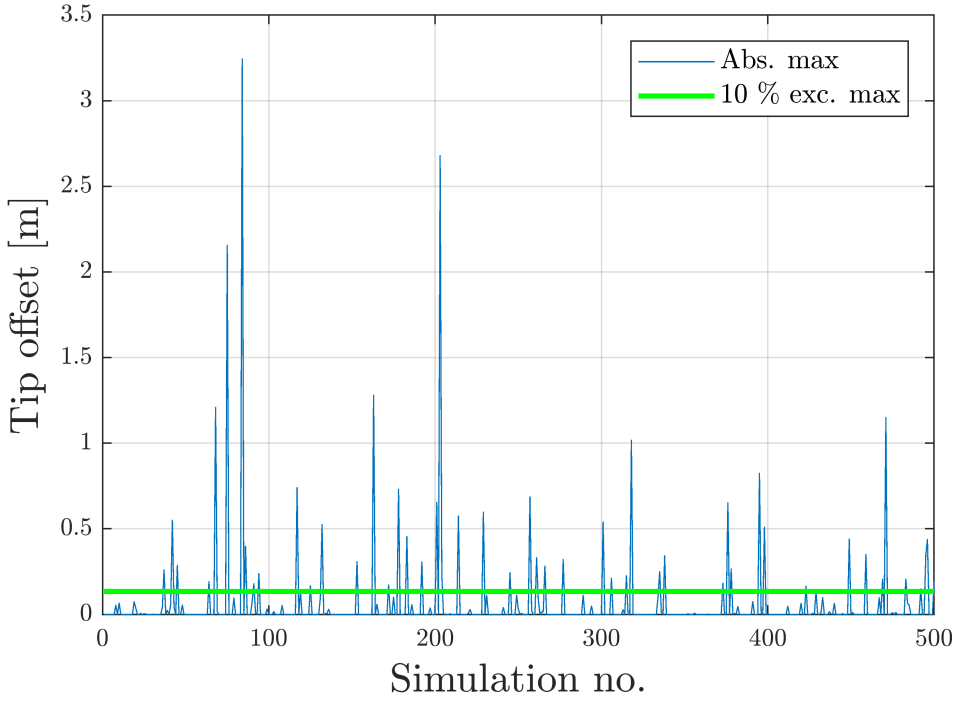

Figure I.7: Positioning error for multiple time simulations when the maximum acceleration is calculated with a probability of exceedance of 20 %.

J

FMEA

Event	Effect local	Effect global	Severity (S)	Occurence (O)	Detectibility (D)	Cause	RPN
General crane failure modes							
DP system fails leading to a collision	Either the vessel will collide with the wind tower structure, or the load will collide with the wind tower structure.	Severe damage to both the vessel and the wind tower, or the crane and the wind tower. Possible dropped objects.	8	2	6	Mechanical failure	96
DP system fails without collision	The compensation mechanism will not be able to maintain position because system runs out of reach.	When load is near the structure, the positioning will be lost and crane moves away from structure, no further damage.	2	2	6	Mechanical failure	24
		When load is attached to structure, crane will be loaded in unconventional manner while mainhoist pays out wire.	4	2	6	Mechanical failure	48
DP system accuracy failure	Sensors in the DP system lead to an offset of the positioning system.	When load is near the structure, the positioning accuracy is reduced, no further damage.	2	4	6	Mechanical failure	48
		When load is attached to structure, crane will be loaded in unconventional manner while mainhoist pays out wire.	4	4	6	Mechanical failure	96
Part of power supply from vessel fails	Crane has limited power available while it is compensating by which the compensation mechanism is suddenly limited.	Load is kept in position but performance is decreased. Minor swinging motions.	4	4	8	Mechanical failure	128
		When load is attached to structure, crane will be loaded in unconventional manner while mainhoist pays out wire.	6	4	8	Mechanical failure	192
Total blackout of crane power supply	Fail-safe brakes within in the crane are activated. Crane is locked in position and cannot move.	Load will start to swing. Can collide with tower or crane itself. Possible dropped objects.	8	4	8	Mechanical failure	256
		When load is attached to structure, and mainhoist is locked. Crane will be overloaded and can collapse. Possible dropped objects.	10	4	8	Mechanical failure	320
Sensor failure within control system.	No measurements. Compensation system is stopped.	Load will start to swing. Can collide with tower or crane itself. Possible dropped objects.	8	4	6	Control system failure	192
Sensor drift within control system	Measurement errors, compensation system still in operation.	Load will start to swing a little, positioning accuracy is reduced.	6	4	6	Control system failure	144
Controller breaks down (PLC, drive or inverter)	Actuator control is lost. Compensation system is shut-down.	Load will start to swing. Can collide with tower or crane itself. Possible dropped objects.	8	4	6	Control system failure	192
		When load is attached to structure, crane will be loaded in unconventional manner while mainhoist pays out wire.	8	4	6	Control system failure	192
Series of high waves approach the vessel.	Positioning accuracy is lost temporarily.	Compensation mechism runs into its limits and load experiences minor swinging motions	2	8	6	Environmental failure	96
		When load is attached to structure, crane will be loaded in an	4	8	6	Environmental failure	192
	AHC can run into its maximum stroke.	High dynamic impact on the load and crane.	8	4	6	Environmental failure	192
Approaching wave angle changes and vessel maitains same heading.	Vessel motions exceed design limits and compensation mechanism runs into its limits.	Load will start to swing. Can collide with tower or crane itself. Possible dropped objects.	6	4	4	Environmental failure	96
		When load is attached to structure, crane will be loaded in unconventional manner while mainhoist pays out wire.	6	4	4	Environmental failure	96

Figure J.1: FMEA part 1/3

Event	Effect local	Effect global	Severity (S)	Occurence (O)	Detectibility (D)	Cause	RPN
Compensation mechanism is not activated when approaching the	Load will start swinging.	Load can collide with the tower or crane itself. Possible dropped objects.	8	4	4	Human error	128
Lifted load exceeds design limit	Compensation mechanism has not enough power to compensate for all motions.	Compensation mechism runs into its limits and load experiences minor swinging motions	4	4	4	Human error	64
		Compensation mechanism can fail by excessive loading leading to a uncontrollable swinging load.	8	4	4	Human error	128
Input of DP system is changed during the operation	Load can still be compensated but its position is not accurate.	Load is moved away from structure.	2	4	4	Human error	32
		Laod is moved towards structure and can collide with the structure. Possible dropped objects.	6	4	4	Human error	96
Accidental de-activation of motion compensation system during operation.	Compensation system is stopped.	Load will start to swing. Can collide with tower or crane itself. Possible dropped objects.	8	4	4	Human error	128
		When load is attached to structure, crane will be loaded in an unconventional maner while mainhoist pays out wire.	8	4	4	Human error	128
Maintenace is performed during opertation leading to a shortcut in	Crane control is lost.	Load will start to swing. Can collide with tower or crane itself. Possible dropped objects.	8	4	4	Human error	128
		When load is attached to structure, and mainhoist is locked.	10	4	4	Human error	160
Operation is executed with a	Load can still be compensated but its position is	Compensation mechism runs into its limits and load	2	4	6	Human error	48
		When load is attached to structure, crane will be loaded in an	4	4	6	Human error	96
Wrong AHC passive vessel pressure.	AHC can run into its maximum stroke.	High dynamic impact on the load and crane.	8	4	4	Human error	128

Figure J.2: FMEA part 2/3

Event	Effect local	Effect global	Severity (S)	Occurence (O)	Detectibility (D)	Cause	RPN
Specific PMOC failures							
Failure of 1 of the E-motors, pinions or gearboxes for slewing without locking the movement of the slewing system.	Compensation capacity of the slewing motion is reduced. Load will experience minor swinging motions when drive system runs into its limits.	Minor swinging motions of the load can be expected. Load is moved away from the structure.	2	6	6	PMOC failure	72
Total failure of slewing system. Crane is locked in position by fail-	Ability for compensation with the slewing motion is lost. Load will start to swing and load can only be	When load is attached to structure, crane will be loaded in an unconventional manner while mainhoist pays out wire. Load will start to swing and can collide with the crane or structure before it is moved away from the structure.	4 6	6 4	6 6	PMOC failure PMOC failure	144 144
Failure of 1 of the E-motors or gearboxes for luffing without locking the movement of the drum.	Compensation capacity of the luffing motion is reduced. Load will experience minor swinging motions when drive system runs into its limits.	When load is attached to structure, crane will be loaded in an unconventional manner while mainhoist pays out wire. When load is attached to structure, crane will be loaded in an unconventional manner while mainhoist pays out wire. Minor swinging motions of the load can be expected. Load is moved away from the structure.	8 2	4 6	6 6	PMOC failure PMOC failure	192 72
Total failure of luffing system. Crane	Ability for compensation with the slewing motion is	When load is attached to structure, crane will be loaded in an unconventional manner while mainhoist pays out wire. Load will start to swing and can collide with the crane or	4 6	6 4	6 6	PMOC failure PMOC failure	144 144
Boomhoist wire breaks by wire rope fatigue.	Boom cannot held up anymore and will turn over together with the load.	When load is attached to structure, crane will be loaded in an unconventional manner while mainhoist pays out wire. Major failure and collision of load and structure is inevitable. Possible dropped objects.	8 10	4 2	6 8	PMOC failure PMOC failure	192 160
Boomhoist wire breaks by overload.	Boom cannot held up anymore and will turn over together with the load.	Major failure and collision of load and structure is inevitable. Possible dropped objects.	10	2	8	PMOC failure	160
Failure of the 'active' part of the AHC.	Accuracy of the vertical compensation is reduced. Operation will most probably be terminated.	No structural damage.	2	4	8	PMOC failure	64
Failure of the 'passive' part of the AHC.	AHC can run into its maximum stroke.	High dynamic impact on the load and crane.	8	6	4	PMOC failure	192

Event	Effect local	Effect global	Severity (S)	Occurence (O)	Detectibility (D)	Cause	RPN
Specific HBC failures	(on top of the PMOC failures)						
Failure of 1 of the E-motors or gearboxes for knuckle without locking the movement of the drum.	Compensation capacity of the knuckle motion is reduced. Load will experience minor swinging motions when drive system runs into its limits.	Minor swinging motions of the load can be expected. Load is moved away from the structure.	2	6	6	HBC failure	72
Total failure of knuckle system. Crane is locked in position by fail-safe brake system	Ability for compensation with the knuckle motion is lost. Luffing motion can accommodate for motion compensation but has limited capacity	When load is attached to structure, crane will be loaded in an unconventional manner while mainhoist pays out wire. Load will start to swing and can collide with the crane or structure before it is moved away from the structure.	4 6	6 4	6 6	HBC failure HBC failure	144 144
Knuckelhoist wire breaks by wire rope fatigue.	Knuckle cannot held up anymore and will turn over together with the load.	When load is attached to structure, crane will be loaded in an unconventional manner while mainhoist pays out wire. Collision of the load with the mainboom is inevitable. Crane will not collapse, possible dropped objects.	8	4	6	HBC failure	192
Knuckelhoist wire breaks by overload.	Knuckle cannot held up anymore and will turn over together with the load.	Collision of the load with the mainboom is inevitable. Crane will not collapse, possible dropped objects.	8	2	8	HBC failure	128
Specific MCCC failures							
Failure of X-table drive mechanism.	Compensation along X-axis is fixed in position and load will start to swing.	Load will start to swing and can collide with the crane or structure before it is moved away from the structure.	6	4	6	MCCC failure	144
Wire for X-table drive breaks.	Compensation along X-axis is unconstrained. Load will move freely in the skid-table.	Load swing is amplified by translational movements in the frame and load will collide with either tower or boom before load is lowered.	8	2	8	MCCC failure	128
Failure of Y-table drive mechanism.	Compensation along Y-axis is fixed in position and load will start to swing	Load will start to swing and can collide with the crane or structure before it is moved away from the structure.	6	4	6	MCCC failure	144
Wire for Y-table drive breaks.	Compensation along Y-axis is unconstrained. Load will move freely in the skid-table.	Load swing is amplified by translational movements in the frame and load will collide with either tower or boom before load is lowered.	8	2	8	MCCC failure	128

Figure J.3: FMEA part 3/3

K

ANSYS plots

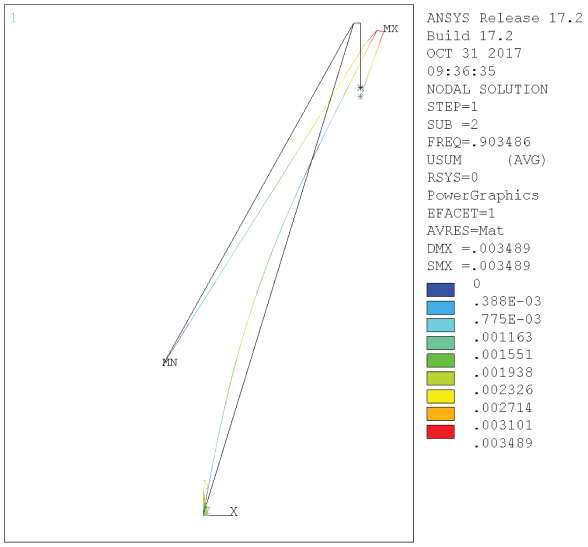

Figure K.1: First natural frequency of the PMOC at 0.43 Hz and its corresponding mode shape.

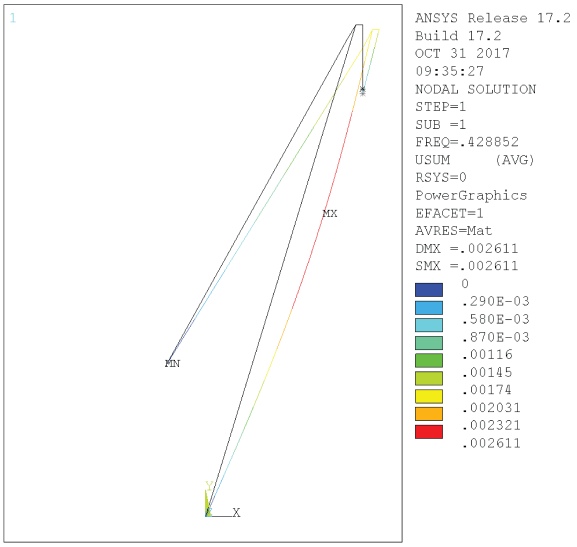

Figure K.2: Second natural frequency of the PMOC at 0.90 Hz and its corresponding mode shape.

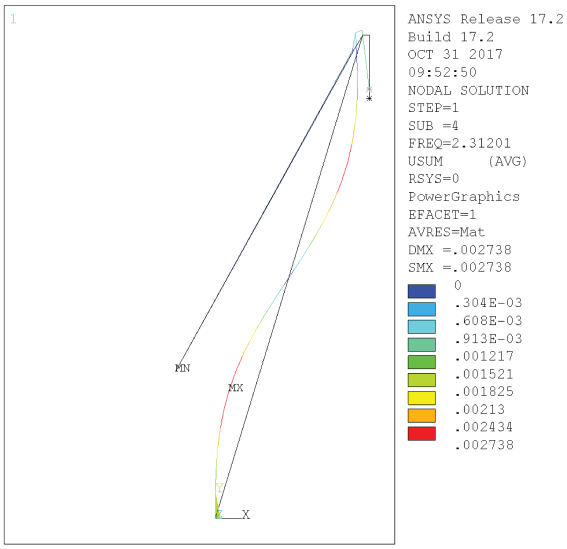

Figure K.3: Third natural frequency of the PMOC at 2.31 Hz and its corresponding mode shape.

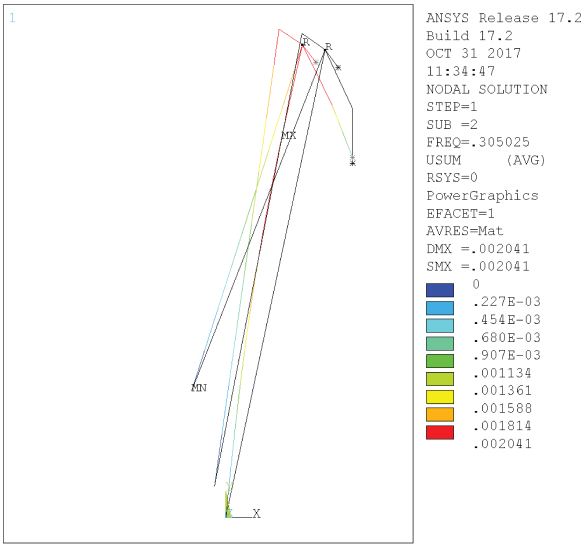

Figure K.4: First natural frequency of the HBC at 0.31 Hz and its corresponding mode shape.

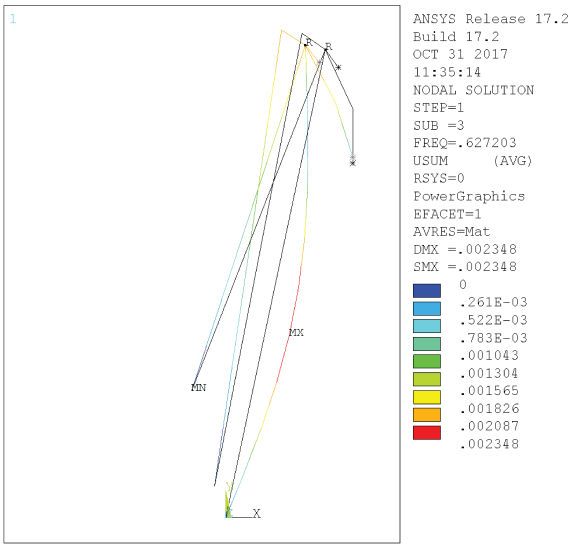

Figure K.5: Second natural frequency of the HBC at 0.63 Hz and its corresponding mode shape.

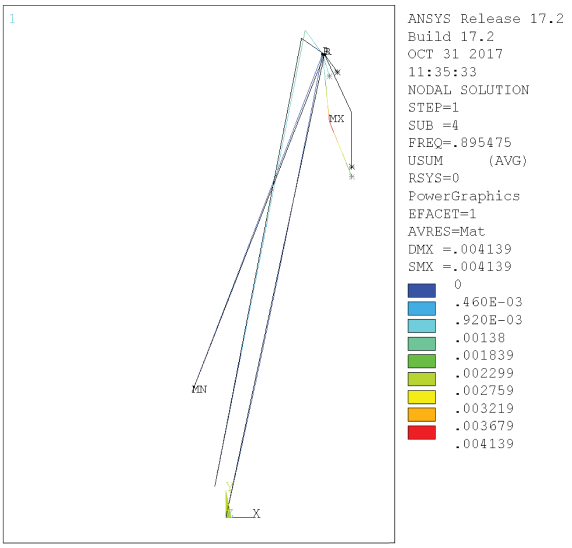

Figure K.6: Third natural frequency of the HBC at 0.90 Hz and its corresponding mode shape.

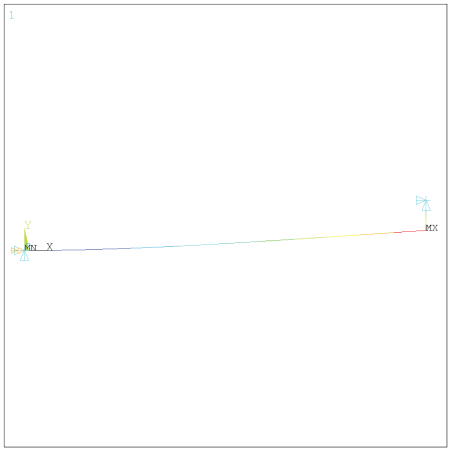

Figure K.7: First natural frequency of the PMOC at 0.36 Hz and its corresponding mode shape.

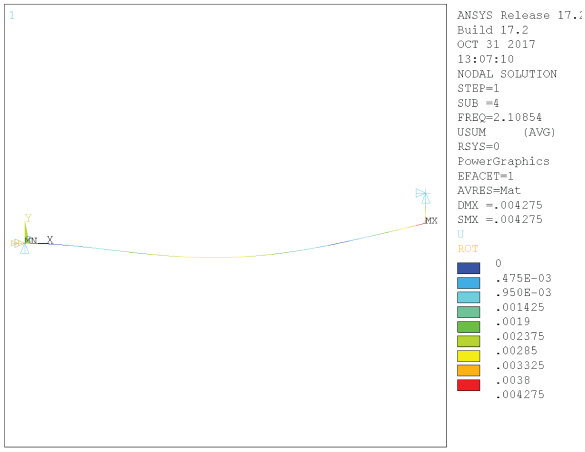

Figure K.8: Second natural frequency of the PMOC at 2.1 Hz and its corresponding mode shape.

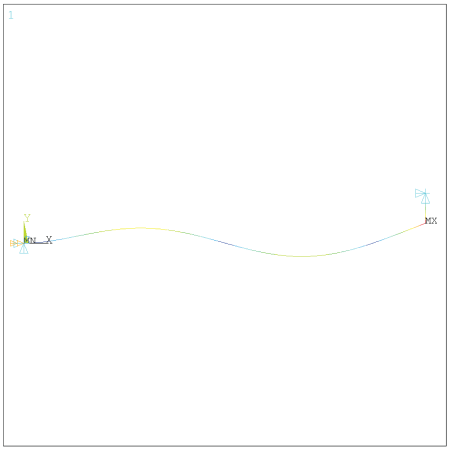

Figure K.9: Third natural frequency of the PMOC at 5.9 Hz and its corresponding mode shape.

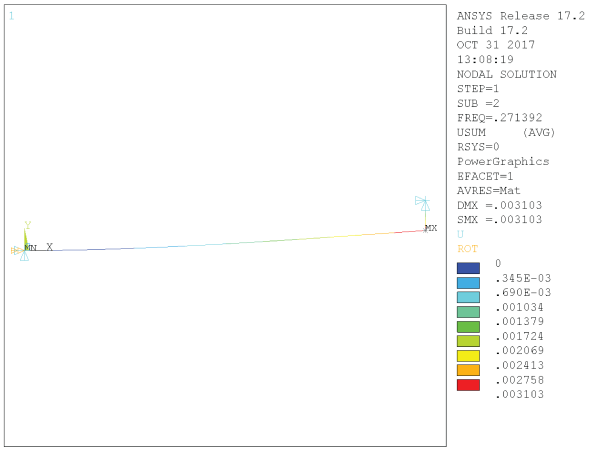

Figure K.10: First natural frequency of the HBC at 0.27 Hz and its corresponding mode shape.

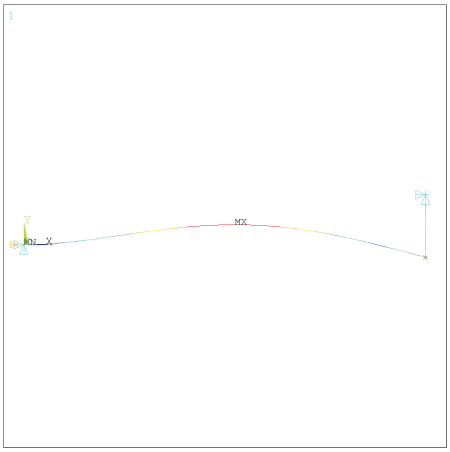

Figure K.11: Second natural frequency of the HBC at 1.7 Hz and its corresponding mode shape.

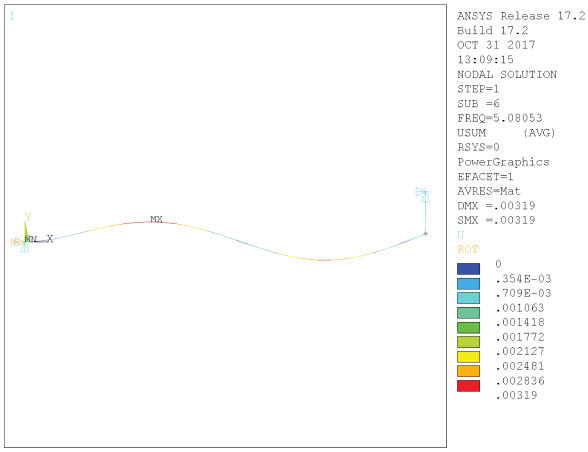

Figure K.12: Third natural frequency of the HBC at 5.1 Hz and its corresponding mode shape.